Thesis for the degree of Doctor of Philosophy

Active Junction Control and Piezoelectric Hybrid Damping for Improving the Acoustic Performance of Lightweight Structures

Jonas Svensson

Department of Civil and Environmental Engineering
Division of Applied Acoustics, Vibroacoustic Group
Chalmers University of Technology
Göteborg, Sweden, 2011

Active Junction Control and Piezoelectric Hybrid Damping for Improving the Acoustic Performance of Lightweight Structures
Jonas Svensson
ISBN 978-91-7385-496-2

Doktorsavhandlingar vid Chalmers tekniska högskola
Ny serie nr 3177 ISSN 0346-718X

Department of Civil and Environmental Engineering
Division of Applied Acoustics, Vibroacoustic Group
Chalmers University of Technology
SE-412 96 Göteborg, Sweden
Telephone + 46 (0) 31-772 1000

Printed by
Chalmers Reproservice
Göteborg, Sweden, 2011

Active Junction Control and Piezoelectric Hybrid Damping for Improving the Acoustic Performance of Lightweight Structures

Jonas Svensson

Department of Civil and Environmental Engineering
Division of Applied Acoustics, Vibroacoustic Group
Chalmers University of Technology

Abstract

Weight reduction is a key factor in lowering the fuel consumption and thereby the greenhouse emissions from vehicles. However, reducing the weight normally results in a deterioration of the acoustic performance. Thus, the purpose of this thesis is to investigate damping treatments for lightweight vehicle panels. Combining active control and passive damping in hybrid control treatments have shown promising. Compared to pure active control, hybrid treatments can have advantages such as reduced control effort or improved fail-safe characteristics. The thesis is dived into two parts, investigating two different concepts for hybrid damping. In the first part of the thesis, a concept of active junction control is developed. Active inputs are used at structural junctions in order to confine vibrational energy to highly dissipative parts of the structure. Theoretical models of beam junctions including active forces and moments are employed to conduct parameter studies. Results show that such an approach can offer advantageous compared to pure active control, e.g. by reducing the control effort. However, it is very sensitive to variations in the properties of the structure. In the second part of this thesis, piezoelectric elements are used for controlling vibrations and/or sound radiation. The piezoelectric element is either shunted by a passive electrical network or by a voltage source in series with a passive electrical network. Analytical models of plates and beams with surface-bonded piezoelectric elements are developed, and experimentally verified. Parameter studies are conducted in order to find the shunt which is optimal under different conditions and control criteria. Results show that for lightly damped structures, passive shunt damping may offer efficient reduction of both the kinetic energy and radiated sound power over a wide frequency range. A properly designed shunt network may also improve the characteristics of an actively driven piezoelectric element, e.g. by reducing the control effort.

Keywords: Active junction control, Hybrid passive-active control, Piezoelectric shunt damping, Sound radiation.

List of publications

This thesis is based on the work contained in the following appended papers, referred to by Roman numerals in the text:

Paper I
Active scattering control of flexural waves at beam junctions: The influence of beam properties on power flow and control effort.
J.L. Svensson, P.B.U. Andersson, J. Scheuren and W. Kropp
Journal of Sound and Vibration (2008) **313**(3-5) p. 418-432.

Paper II
Active control of bending waves at structural junctions using an impedance formulation.
J.L. Svensson, P.B.U. Andersson, J. Scheuren and W. Kropp
Journal of Sound and Vibration (2009) **323**(3-5) p. 555-573.

Paper III
On the design of structural junctions for the purpose of hybrid passive-active vibration control
J.L. Svensson, P.B.U. Andersson and W. Kropp
Journal of Sound and Vibration (2010) **329**(9) p. 1274-1288.

Paper IV
On the design of piezoelectric shunt damping with respect to radiated sound power
J.L. Svensson
Submitted to the Journal of Sound and Vibration, 2010

Paper V
Hybrid active-passive piezoelectric sound- and vibration damping
J.L. Svensson
To be submitted for publication

The following papers are not included in the thesis due to an overlap in content or a content going beyond the scope of this thesis:

- On the design of hybrid active-passive piezoelectric vibration damping
  J. L. Svensson, E. Rustinghi, B. R. Mace
  Proceedings Internoise, Lisbon, Portugal; June 13 - 16, 2010

- Investigation of a hybrid passive-active vibration-control configuration
  J. Svensson, P. Andersson and W. Kropp
  Proceedings of Noise and Vibration: Emerging methods in Oxford, UK; April 5 - 8, 2009

- The influence of material parameters and geometry on an active junction
  J. Svensson, P. Andersson and W. Kropp
  Proceedings of International Congress on Acoustics in Madrid, Spain; September 2 - 7, 2007

- Identification of complex moduli for rubber compounds by minimisation of the error between measured and FE-modelled velocity profiles.
  J. Svensson and P. Andersson
  Proceedings of EuroNoise2006 in Tampere, Finland; May 30 - June 1, 2006

Acknowledgements

This work was financially supported by the Swedish Research Council (Vetenskapsrådet), project: 621-2004-5185, and by the European Commission, grant agreement number: 233764.

First I would like to thank my main supervisor Wolfgang Kropp. Thank you for all the good discussions we have had, all the good advice you have given me and for always helping me to see the "bigger picture". A huge thanks to my assistant supervisor, mentor and friend Patrik Andersson. Thank you, not only for helping me with the research project but also for giving advice, support and guidance during this period. I would also like to thank Adjunct Professor Joachim Scheuren at Chalmers, and Professor Brian Mace and Dr. Emiliano Rustinghi at the ISVR for providing supervision during different periods of my PhD-studies.

I would like to thank all the people who have been at the division during my five years there. You have all contributed to a great atmosphere and a place not only for work but also a lot of fun. Thanks to everyone who have contributed to this thesis, by giving good advice or sharing their knowledge. A special thanks also to my office mate Astrid for coping with me singing along with the music in my headphones, for giving support through the harder periods and for in general making our office a nice place. A special thanks also to Gunilla Skog and Börje Wijk, not only for all the help you have given me with administrative issues or computer problems, but also for pleasant conversations over the morning coffee.

Jag vill tacka min familj för det stöd de givit mig under dessa fem åren. Tack Mor och Far! Tack Syster, Adde och Noah för att jag fått vara del av er familj under stunder som det kännts lite jobbigt, det har betytt så himla mycket. Tack också till familjen NB.

Till sist vill jag tacka min Lisa. Ditt stöd, din uppmuntran och din förmåga att hjälpa mig till perspektiv betyder fantastiskt mycket. Tack för att du finns i mitt liv!

Contents

Chapter 1
Introduction

A key factor in reducing fuel consumption and thereby greenhouse gas emissions from vehicles is weight reduction. However, reducing the weight may severely deteriorate the vehicle quality with respect to sound and vibration. Further, as legislators are constantly increasing the demands on noise emissions the vehicle manufacturers do not only have to maintain current sound and vibration performance of the vehicle with reduced weight, but must actually improve it. Moreover, satisfying sound and vibration properties can be an important selling point for the manufacturers. Since traditional noise and vibration control measures such as heavy walls, damping layers and double walls significantly contribute to the total weight of the vehicle, other treatments, such as active and hybrid, have to be tested and developed.

1.1 Background

The transportation sector is a major contributor to the emission of particles and greenhouse gases such as CO_2 [1, 2] [1]. Therefore, one of the most important tasks of vehicle manufacturers today is to reduce these emissions. Two straightforward ways to do so are to downsize the engine and to reduce the weight of the vehicle. Reducing the weight means that e.g. various vehicle parts will be constructed in lightweight materials. At the same time as the weight is reduced, the vehicle performance cannot be deteriorated. While reducing the mass is important for lowering the fuel consumption, a high structural stiffness is vital for the load-carrying capacity as well as for crash safety reasons. Reducing the weight, while keeping the structural stiffness constant, normally results in lowered attenuation of air- and structure-borne sound. This implies a decrease of passenger comfort due to increased interior sound and vibration level, and an increase of the overall exterior

[1] These citations refer to reports concerning emissions in the United States and Sweden respectively.

noise emissions from the vehicle. The latter have a negative impact on human activities, especially in urban areas as the engine and powertrain are dominant noise sources when accelerating at low speeds. At higher speeds, the tyre/road noise is dominant and reducing the sound radiated by the engine has a negligible effect on the overall noise emissions [3].

The transportation sector is also a major contributor to the overall noise levels in urban areas [4]. Long-term exposure to noise can be the cause of several adverse effects such as sleep disturbance [5, 6], reduced performance of cognitive tasks [4] and cardiovascular effects [4, 7]. This will most likely cause legislators to further increase the demands on noise emissions from vehicles in the future. Therefore, reducing the exterior noise from vehicles is an important task of the manufacturers.

In addition, a pleasant interior vehicle environment with respect to sound and vibration can be an important selling point in today's competitive market. A survey among 1000 people in Italy, presented in "Quattorroute" magazine, reveals the importance to the customer of a satisfying interior noise level. When asked, "What would you be willing to give up to have a cheaper car?" only a mere 3.45 % answered a "well-insulated interior". Furthermore, interior noise levels may be important for safety reasons. Studies have shown that exposure to noise in combination with other stimuli may decrease the driver performance when operating cars [8].

To summarize briefly, there are several reasons why it is vital to direct attention towards reducing and/or controlling the vibration and sound radiation of vehicles. Conventional methods to reduce the interior and exterior sound and vibration levels in vehicles include adding damping materials, heavy walls or double walls, or stiffening the structure. However, although these methods may offer some sound and vibration attenuation, they also have severe disadvantages. Damping materials are normally only sufficiently efficient at high frequencies because of the large wavelengths of low-frequency vibrations. Heavy walls are by definition disadvantageous if one prerequisite is to make the vehicle light-weight. Adding stiffness may result in an increase of radiated sound due to a shift in the critical frequency.

Due to these disadvantages extensive research has been devoted to active and hybrid active-passive sound and vibration control. Active control means introducing a secondary input to reduce or alter the effect from a disturbance. E.g. by the use of an actuator, control vibrations may be introduced in a structure to interact with the original disturbance, thereby reducing the total vibration field. The control vibration is usually obtained by passing a sensor signal through a digital

filter implemented on a digital signal processor (DSP). Due to reasons such as time delay of the DSP unit, active control is normally most efficient in the lower frequency region. Active control therefore offers a satisfying complement to passive damping materials, which are most efficient at high frequencies. Hence by using hybrid treatments, consisting of both active and passive control measures, sound and vibration reduction over a broad frequency range can be achieved. Active and hybrid sound and vibration control has proven to be promising, although practical implementation of such control systems require careful design and may in certain situations be difficult.

1.2 Goals

Based on the possible benefit of combining active and passive sound and vibration control, the overall research question which the work behind this thesis is aimed at investigating can be summarized as follows:

> *How can active and passive methods be combined in order to form efficient hybrid systems for the control of vibration and sound radiation from lightweight structures?*

The scope of this thesis is thus to investigate and compare different concepts of passive, active and hybrid vibration and sound radiation control. The thesis can be divided into two main parts: the first concerns the control of bending waves propagating in beam-like structures; the second concerns piezoelectric transducers mounted to plate-like structures. The stated research question is treated in four topics:

- actively controlling bending waves in structures to cancel the reflection or transmission at structural junctions;
- using the concepts of cancelling bending wave reflection in order to confine wave power to parts of a structure which are treated by passive damping;
- piezoelectric shunt damping in order to reduce the vibration and/or radiated sound power levels from structures;
- hybrid piezoelectric sound and vibration control where the piezoelectric element is not only shunted by a passive electric impedance, but where the possibility of actively controlling the element is also included.

The focus has primarily been on developing conceptual models in order to gain insight into the mechanism and fundamental principles of the damping treatments. Therefore analytical models of beam- and plate-like structures have exclusively been used throughout this thesis. The scope of the thesis has not been to develop an active or hybrid vibration control treatment ready for implementation in a vehicle. This being said, though, some fundamental concepts of piezoelectric shunt damping have also been tested experimentally, both on a simple beam structure and on an actual vehicle structure.

1.3 Outline

Here follows a short summary of the chapters and scientific papers included in this thesis:

Chapter 2 provides the fundamental ideas of active control of bending waves at structural junctions. Some previous literature is presented as well as the mathematical model used for the investigations in this thesis. Two approaches are presented: the first is a model of a junction of two semi-infinite beams, while the second is based on an impedance approach to handle more general junctions. Some key results from *Paper* I and *Paper* II are presented.

In *Chapter 3* the concepts developed in *Chapter 2* are applied to hybrid active-passive vibration control. Bending wave cancellation is used in order to confine all vibrational energy in a structure to parts with high passive damping. Selected results from *Paper* II and *Paper* III are presented.

Chapter 4 presents some concepts of piezoelectric shunt damping. A plate model is used to theoretically investigate piezoelectric shunt damping. The model is used to conduct a parameter study on the efficiency of shunt damping on both structural response and sound radiation. Some key results from *Paper* IV are presented. A beam model, based on the same modelling approach as the plate model, is also presented. The beam model is used in order to verify the modelling approach and is compared against measurements.

Chapter 5 expands the concept presented in *Chapter 4* by also allowing the piezoelectric element to be used as an actuator. The combined effect of a passive shunt network and active driving of the piezoelectric element is investigated. The most important findings from *Paper* V are summarized in *Chapter 5*.

Chapter 6 presents an implementation of some fundamental shunt damping concepts on a vehicle structure. The selected structure is an oil pan. The oil pan has been recognized as a major contributor to the powertrain noise emissions. An approximate model of the resonance peaks of the top plate of the oil pan is constructed, and the potential of shunt damping is estimated. The shunt damping treatment is also experimentally investigated.

Chapter 7 summarizes the results presented in the main body of the thesis and the appended papers. The key findings are highlighted and some prospects for future research are presented.

Appendix A contains mathematical derivations which are not included in the main body or in any of the appended papers.

Appendix B provides some simple examples of applying the impedance approach developed in *Paper* II on deriving the scattering matrices of some typical structural junctions as well as influencing these scattering matrices by the means of active control.

Chapter 2
Active junction control

Active vibration control can be based on various approaches, e.g. wave-based or modal-based. Wave-based control strategies are based on decomposing the vibration field into travelling wave components. Controlling certain waves enables active junctions, e.g. cancelling reflection or transmission of waves past a certain point. This chapter presents some fundamental concepts of active vibration control and some theoretical results based on coupled beams manipulated by active forces or moments.

2.1 Active vibration control

Using secondary, active inputs to control unwanted vibrations in structures is the fundamental idea behind active vibration control. The technique of using a secondary input to interact with a primary disturbance to reduce the total field was proposed for sound propagation as early as 1936 by Lueg [9]. Twenty years later Olson [10] studied control of sound and vibration. He discussed isolating a machine from its foundation by using active control, assuming the machine to be a lumped parameter system. This study is very enthusiastic about the possibilities of active vibration control. Rockwell and Lawther [11] expanded the approach of active vibration control to a distributed parameter structure. They presented a feedback control approach to augment structural damping on a beam. Several textbooks and review articles have been written on the topic of active vibration control. Books such as references [12] and [13] and review articles such as reference [14] give exhaustive overviews of the principles, applications, possibilities and problems of active vibration control.

Active vibration control has found various applications, such as space structures [15], automotive parts [16], power tools [17] and microscopes [18]. An exhaustive review of using of active sound and vibration control for engineering application,is given bin reference [19].

2.2 Travelling wave approaches

The vibration field on a structure can be composed of several different wave types such as extensional waves, bending waves and torsional waves. An active vibration control system based on a wave approach can be used to control or cancel specific waves in a structure. This requires measurement of those waves and since the waves cannot be measured directly they have to be estimated from other measurements. This can e.g. be done by measuring the response at several positions on the structure.

Several investigations have treated cancellation of bending waves propagating in beam-like structures by means of active control. Scheuren [20] presented an experimental investigation of an active reflector. Acceleration measurements at two positions allowed the bending wave amplitude and phase to be estimated. This information was used to drive a control force in order to reflect a bending wave at a certain point. The experimental results revealed that the control force rejected almost all (99.97 %) of the incoming wave power.

Figure 2.1 shows an example of estimating the wave amplitude based on the measurements from two closely spaced accelerometers using the approach of Scheuren. The measurements are done on a 0.4 m long free-free aluminium beam. The beam is excited in one end and two accelerometers spaced by 0.05 m are used to estimate the bending wave in each direction. The figure shows that the measured bending wave amplitude matches the theoretical value quite well above 500 Hz. Under 500 Hz the measurements severely underestimate the wave amplitude. This is partly due to the near-field influencing the measurements at low frequencies. Thus in order to get a better estimate for low frequencies the accelerometers have to be further from the beam boundaries, or more accelerometers are needed.

Halkyard and Mace also presented a study of bending wave cancellation based on multipoint acceleration measurements. A two-point [21] and a three-point wave estimation sensor [22] were developed; the latter sensor could also cope with bending near-fields being present at the measurement point. Although usually multipoint measurements are required, under certain conditions - such as wave propagation in only one direction - it might be sufficient to uses a single sensor [23, 24].

The purpose of the control system can be to cancel the reflection of waves at structural junctions. By cancelling the reflected wave the generation of vibrational modes can be hindered, thus significantly reducing the vibration field on the structure. Tanaka and Kikushima [25] presented a study of cancelling the reflection

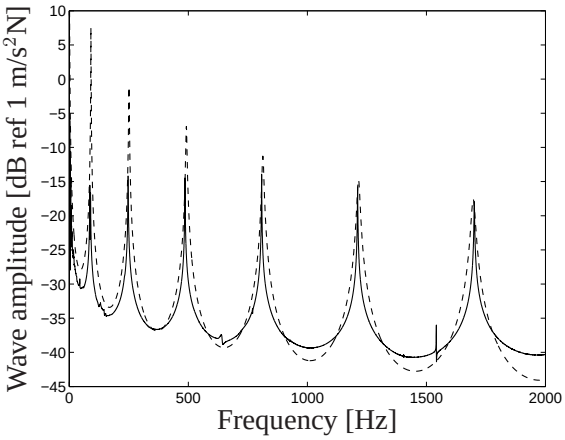

Figure 2.1: The measured and theoretical wave amplitude for positive wave. −: measurement; ·····: theory.

or transmission at a certain point on a beam, and thereby inactivating vibrational modes. Tanaka and Iwamoto[26] presented an approach they referred to as active boundary control, which had the purpose of creating desired boundary conditions at any point on a beam. The approach was used to create vibration-free regions on the beam. Iwamoto et.al [27] developed a feedforward scheme to create vibration-free regions on a plate.

In some situations it may be necessary to control not only a single bending wave but also the near-fields. Mckinnel [28] reported that for low-frequency vibrations, cancelling only the propagating wave may leave a significant residual vibration field caused by the near-fields. Von Flotow and Schafer [29] described a theoretical approach of how to create a matched (anechoic) termination with a matrix that relates deflection and rotation to force and moment, thus considering both waves and near-fields. They report that the matrix which will realize a matched termination is the driving point mobility of a semi-infinite beam. However, they also acknowledged the problem of implementing such a controller due to the difficulty of rotation measurements and moment actuation. Mace [30] also discussed collocated sensing of deflection and rotation together with collocated actuation by force and moment. Another way of controlling all wave types in a structure is to control the power flow. Audrain et al. [31] presented a study with the aim of actively controlling the structural intensity. Five accelerometers served as the basis for a finite-difference scheme to estimate the structural intensity. This controller proved effective in minimising the energy transmission past a certain control point.

Cancelling the reflection or transmission of waves does not necessarily mean a reduction of the vibratory power in the structure. In fact, this may in some cases actually be increased by the actuator injecting power into the structure. Controllers may instead be based on maximizing the absorbed power. Guicking et al. [32] showed that, in theory, a point force on an infinite beam could at the most absorb half the power carried by a single incident bending wave, while a quarter of the power would be reflected and a quarter transmitted. However, at a free end all incident wave power could be absorbed. The latter was also found experimentally by Scheuren [33].

Redman [34] presented an experimental study where a pair of control forces were driven in order to maximize their combined power absorption. Together the forces absorbed almost all the incident power, leaving a residual power which was 36 dB lower than the incident power. An exhaustive theoretical study by Brennan et al. [35] presented several different wave-based control strategies. An important result from this study is that, from a global point of view, it is advantageous to minimize the total power input from both primary and secondary inputs rather than maximising the power absorbed by only the secondary input. Thus, if the total vibrational power of a structure is to be minimized, a controller which has the objective to alter the impedance at the primary force input can perform better than a controller which is designed to absorb vibrational power. Other studies concerning active control at structural junctions, either to influence the scattering properties of the junction or to absorb incoming wave power, include [36, 37, 38, 39].

As mentioned before, the vibration field may be composed of other wave types than bending waves, such as extensional and torsional waves. Thus, the control system may need to consider multiple wave types in order to achieve a significant vibration reduction. Simultaneous control of both extensional and flexural waves was treated in [40, 41]. Gardonio and Elliot [42] investigated active control of flexural and extensional waves on a beam with a termination that coupled the two wave types.

2.3 Deriving an active junction

2.3.1 Wave formulation

The theoretical investigations presented in this chapter are based on a travelling wave solution to the Euler-Bernoulli bending wave equation. The Euler-Bernoulli bending wave equation describes the bending motion on a beam structure, neglecting rotational inertia and shear deformation. Euler-Bernoulli theory describes the low-frequency motion of a beam relatively well. Figure 2.2 shows a measured and

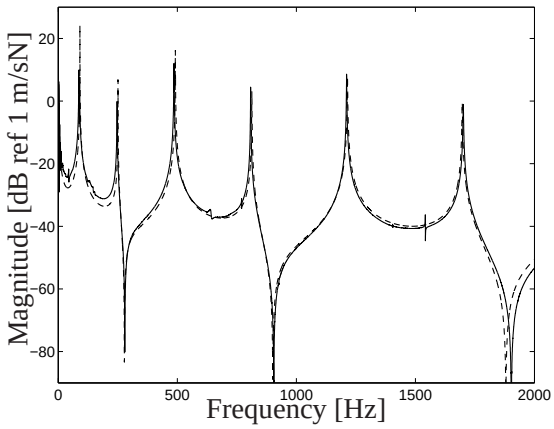

Figure 2.2: The transfer mobility of a 0.4 m long free-free aluminium beam. The beam is excited at one end and the velocity is measured at the midpoint. −: measurement; ·····: theory.

a calculated transfer mobility of a 0.4 m long, free-free aluminium beam. The beam is excited at one end and the acceleration is measured at the midpoint, i.e. 0.2 m from each end. The velocity is obtained by dividing the measured acceleration by $\mathrm{j}\omega$.

When considering a wave approach to the Euler-Bernoulli wave equation, the vibration field is composed of four wave components: two travelling wave components and two evanescent wave components also referred to as near-fields. Consider a wave and a near-field propagating towards a beam junction; see figure 2.3. The junction is in this case a connection between two beams where one is semi-infinite, and with a characteristic impedance which differs from the first beam. The difference in impedance between the beams could be due to differences in the geometry and/or the material properties. As the two wave components reach the junction, they will be transmitted and reflected according to

$$\mathbf{b}^+ = \mathbf{t}\mathbf{a}^+, \qquad \mathbf{a}^- = \mathbf{r}\mathbf{a}^+. \tag{2.1}$$

where

$$\mathbf{a}^+ = \left\{ \begin{array}{c} a_p^+ \\ a_N^+ \end{array} \right\}, \mathbf{a}^- = \left\{ \begin{array}{c} a_p^- \\ a_N^- \end{array} \right\}, \mathbf{b}^+ = \left\{ \begin{array}{c} b_p^+ \\ b_N^+ \end{array} \right\},$$

where the elements in the vectors represent wave amplitudes and are illustrated in Figure 2.3. The matrices $\mathbf{t}$ and $\mathbf{r}$ are referred to as the transmission and reflection matrix respectively, and can be calculated to give

$$\mathbf{t} = \frac{2}{\Delta} \left[\begin{array}{cc} (1+\gamma)(\alpha-1) & (1-\mathrm{j}\gamma)(1-\alpha) \\ (1+\mathrm{j}\gamma)(\alpha-1) & (1+\gamma)(1+\alpha) \end{array} \right], \tag{2.2}$$

and

$$\mathbf{r} = \frac{1}{\Delta}\begin{bmatrix} 2\alpha(1-\gamma^2) - \mathrm{j}\gamma(1-\alpha)^2 & \gamma(1+\mathrm{j})(1-\alpha^2) \\ \gamma(1-\mathrm{j})(1-\alpha^2) & 2\alpha(1-\gamma^2) + \mathrm{j}\gamma(1-\alpha)^2 \end{bmatrix}, \tag{2.3}$$

where

$$\alpha = \frac{EI_b k_b^2}{EI_a k_a^2}, \quad \gamma = \frac{k_b}{k_a}, \quad \Delta = 2\alpha(1+\gamma^2) + \gamma(1+\alpha)^2, \tag{2.4}$$

where EI_a and EI_b are the are the bending stiffnesses and k_a and k_b are the wavenumbers in the respective beams. The subscript on the bending stiffness, EI, means that both the Young's modulus (E) and the moment of inertia (I) may arbitrarily change; however, it is their product which is important to the scattering matrices. The reflection and transmission matrices were derived in [43]. By introducing a force at the junction, (see Figure 2.3), the reflection and transmission matrices can be derived, including the external force. By assuming that the junction is located several wavelengths from the primary excitation, the incident near-field can be neglected and thus only the first column of the scattering matrices is non-zero. Calculating the non-zero elements of the transmission and reflection matrices yields

$$r_p^{\text{act}} = r_p^{\text{pass}} + \frac{F^{\text{act}}}{2k_a^3 EI_a a_p^+} \frac{-\gamma(1+\mathrm{j}) + \alpha\gamma(1-\mathrm{j}) - 2\mathrm{j}\alpha}{\Delta}, \tag{2.5a}$$

$$r_N^{\text{act}} = r_N^{\text{pass}} + \frac{F^{\text{act}}}{2k_a^3 EI_a a_p^+} \frac{(\mathrm{j}-1)(\alpha(1+\gamma) + \mathrm{j}(\alpha+\gamma))}{\Delta}, \tag{2.5b}$$

$$t_p^{\text{act}} = t_p^{\text{pass}} + \frac{F^{\text{act}}}{2k_a^3 EI_a a_p^+} \frac{-\alpha(1+\mathrm{j}) + (1-\mathrm{j}) - 2\mathrm{j}\gamma}{\Delta}, \tag{2.5c}$$

$$t_N^{\text{act}} = t_N^{\text{pass}} + \frac{F^{\text{act}}}{2k_a^3 EI_a a_p^+} \frac{(\mathrm{j}-1) - \alpha(1+\mathrm{j}) + 2\gamma}{\Delta}. \tag{2.5d}$$

The external force at the junction has been given the superscript 'act' in order to indicate the intention to use it for active control. The scattering factors are also superscripted by 'act' and are here referred to as active scattering factors. Detailed derivation of these scattering factors can be found in *Paper* I. The scattering properties of the junction may be altered by putting constraints on the active scattering factors and deriving the force which is required to fulfil the constraints. In *Paper* I non-reflective, non-transmissive and power-absorbing junctions are studied. Parameter studies are conducted by varying the properties of the beams, and the power flow across the junction and control effort is calculated. Some key findings from *Paper* I are discussed in the final section of this chapter. The theory presented in *Paper* I is confined to semi-infinite beams and just a point force at the junction. In the following section, a more general approach based on an impedance formulation of the junction is developed in order to overcome these limitations.

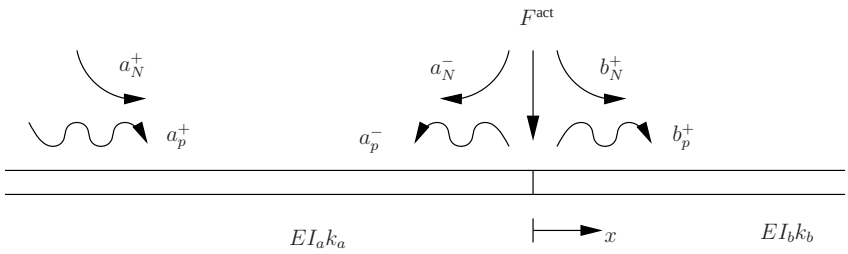

Figure 2.3: The waves present on two connected beams of different properties, where the right-side beam is semi-infinite. An active force is located at the junction.

2.3.2 Impedance formulation

A more general way to express the reflection matrix at a structural junction is through an impedance formulation. The structure on the right side of the junction (receiving system) can be treated as an arbitrary termination impedance, $\hat{\mathbf{Z}}$, seen by the left-side beam; see figure 2.4. The termination impedance relates the deflection and rotation to the internal force and moment at the junction. The reflection matrix can be expressed according to

$$\mathbf{r} = \left(\mathbf{C}^-\right)^{-1} \left(\tilde{\mathbf{Z}}^- - \hat{\mathbf{Z}}\right)^{-1} \left(\hat{\mathbf{Z}} - \tilde{\mathbf{Z}}^+\right) \mathbf{C}^+, \tag{2.6}$$

where

$$\mathbf{C}^- = \begin{bmatrix} 1 & 1 \\ \mathrm{j}k & k \end{bmatrix}, \quad \mathbf{C}^+ = \begin{bmatrix} 1 & 1 \\ -\mathrm{j}k & -k \end{bmatrix}.$$

The matrices $\tilde{\mathbf{Z}}^+$ and $\tilde{\mathbf{Z}}^-$ represent the characteristic impedance matrices defined in [44] and derived in *Paper* II. Note how equation 2.6 resembles the reflection factor for longitudinal waves. In fact, if the matrices in equation 2.6 are replaced by their scalar equivalents, the expression reduces to the scalar reflection factor for longitudinal waves. Using equation 2.6 the reflection matrix for any type of junction can be calculated, under the requirement that the termination impedance matrix is known. Appendix B presents the impedance matrix and corresponding reflection matrix for some examples of junctions.

Using the impedance formulation, active control may be introduced at the junction by splitting the termination impedance matrix into an active and a passive part according to

$$\hat{\mathbf{Z}} = \hat{\mathbf{Z}}^{\text{pass}} + \hat{\mathbf{Z}}^{\text{act}} \tag{2.7}$$

where $\hat{\mathbf{Z}}^{\text{act}}$ is the active impedance matrix representing an external impedance load and $\hat{\mathbf{Z}}^{\text{pass}}$ is the passive impedance matrix of the junction. The active impedance

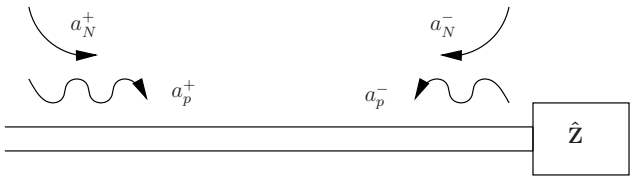

Figure 2.4: The waves present on an Euler-Bernoulli beam connected to an arbitrary junction impedance.

matrix, $\hat{\mathbf{Z}}^{\text{act}}$, relates a sensing vector (translational and rotational velocities) to an actuation vector (force and moment) according to

$$\mathbf{Q}^{\text{act}} = \mathbf{Z}^{\text{act}}\mathbf{u}, \tag{2.8}$$

where

$$\mathbf{Q}^{\text{act}} = \left\{ \begin{array}{c} F^{\text{act}} \\ M^{\text{act}} \end{array} \right\}, \qquad \mathbf{u} = \left\{ \begin{array}{c} \dot{w} \\ \dot{\beta} \end{array} \right\},$$

The actuation vector thus has a linear dependence on the translational and rotational velocity at the junction, specified by the active impedance matrix. The actuation vector can thus be used to manipulate the reflection matrix at a junction of an Euler-Bernoulli beam and an arbitrary receiving structure. In *Paper* II the impedance formulation is e.g. used to study the influence of bending near-fields on a reflection cancelling controller.

2.4 Discussion of results from *Paper* I and *Paper* II

As mentioned in the preceding section, *Paper* I presents a parameter study investigating the effect of beam properties on the control effort and power flow of a junction between two semi-infinite beams. A non-reflective, a non-transmissive and an absorptive junction are studied. The results from the non-reflective junction show that if the properties of the beams have a certain relation the junction is always absorptive, i.e. the active force which is driven to cancel the reflection removes vibratory power from the junction; see Figure 3 in *Paper* I. However, the active force only absorbs a part of the incident wave power while the rest is transmitted to the receiving beam. This remaining transmitted wave power could possibly be passively dissipated in the receiving beam, thus forming a hybrid active-passive vibration control treatment. However, *Paper* I is limited to semi-infinite, non-dissipative beams. The more general impedance approach developed in *Paper* II can be used to study finite and dissipative receiving beams. This is developed further in *Chapter 3*.

The impedance approach presented in *Paper* II facilitates some understanding of the impedance which is required in order to achieve certain junctions. For example, introducing impedance control at a free end, all incident wave power can be absorbed by choosing the (1,1) element of the active impedance matrix in equation 2.8 to be half the complex conjugate of the corresponding element in the characteristic impedance matrix of the beam, as previously reported in [32]. However, this assumes that only an incident wave is present at the junction. An incident near-field may in fact reflect a propagating wave and thus diminish the performance of the controller. In *Paper* II it was shown that if the junction is close (in terms of wavelengths) to the primary excitation, the effect can be significant; see Figures 6 and 7 in *Paper* II. Still, this can be remedied by including additional elements in the active impedance matrix in the control law, such as moment actuation or rotation sensing.

Chapter 3
Hybrid junction control

Combining passive and active vibration control results in hybrid vibration control. In this chapter the concept of an active junction which was introduced in the previous chapter will be expanded upon. A highly dissipative beam will be connected at the junction. The aim is to use the active inputs to confine vibrational energy to the highly dissipative beam, thereby achieving efficient hybrid active-passive vibration control.

3.1 Hybrid active-passive vibration control

There are several types of hybrid vibration control treatments. The possible benefits of using hybrid approaches are several. As passive damping is mainly a high-frequency approach, and active control mainly a low-frequency approach, their combination may provide vibration control over a broad frequency range. Further, the passive damping may help to increase the stability margins of a feedback control system as well as providing fail-safe damping if the active control system fails.

A common hybrid approach is active constrained layer damping (ACLD). It is an expansion of the passive constrained layer (PCL) by using an actuator as the constraining layer. The ACL consists of a viscoelastic damping layer constrained by an actuator. The ACL does not only benefit from the purely active or purely passive damping effects of the treatment; there is also a combination effect due to the actuator motion. As the actuator works against the primary vibration of the host structure, additional shear losses are introduced in the viscoelastic layer; see Figure 3.1. Several studies have treated ACLD; see e.g. references [45, 46, 47, 48] for beams, and [49, 50] for plates.

Some studies point out limitations of ACLD as a hybrid damping treatment. E.g. using a piezoelectric polymeric film (PVDF) as the constraining layer yields a damping treatment which is sub-optimal in its passive state, as the constraining layer is

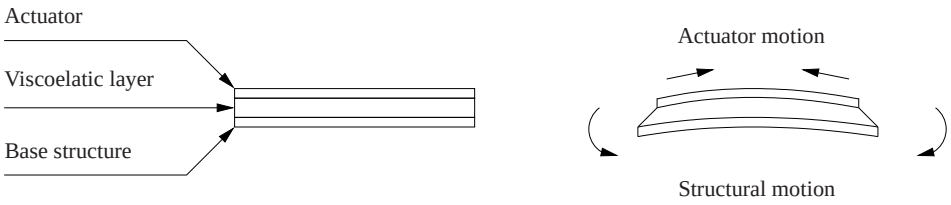

Figure 3.1: A schematic figure of an active constrained layer. To the left is the undeformed structure and to the right the deformed structure.

not stiff enough [51]. Lam [52] reported that the actuator action is reduced, compared to pure active control, because the actuator must act through the viscoelastic layer. An approach to overcome the insufficient stiffness of the constraining layer is to combine passive and active materials; see e.g. references [53, 54]. Another way to increase the efficiency of ACL has been to connect the active elements directly to the host structure through edge elements forming an enhanced active constrained layer (EACL) [55], which may increase the control authority of the configuration [56]. Studies have also been presented where the ACL is split into pure active control (AC) and a PCL; see e.g. references [52, 56, 51, 57]. Illaire [51] reports that the difference in control efficiency between ACL and AC-PCL is negligible, but the AC-PCL treatment requires less control effort as the actuator does not have to work through a viscoelastic layer.

3.2 Active junction with a sandwich beam

As hybrid treatments have many potential benefits compared to pure passive damping or active control the approach of active junction control - presented in the previous chapter - is here expanded upon to include also passive damping. The purpose is to use active junction control to confine vibrational power to a part of the structure which is treated with passive damping.

Using the impedance approach presented in section *Section 2.3.2*, the reflection matrix of a junction between an Euler-Bernoulli beam and a sandwich beam may be derived; see Figure 3.2. The sandwich beam consists of a host beam treated with a PCL. The sandwich beam was modelled using the approach of Mead and Markus [58]. As the driving point impedance matrix of this sandwich beam is quite complicated to derive analytically, it was numerically calculated using appropriate values for the material properties and geometry. The considered sandwich beam is 0.35 m long and has a viscoelastic layer with high losses ($\eta = 0.7$) and a thickness which

is 1% of the base beam; see *Paper* II for more details.

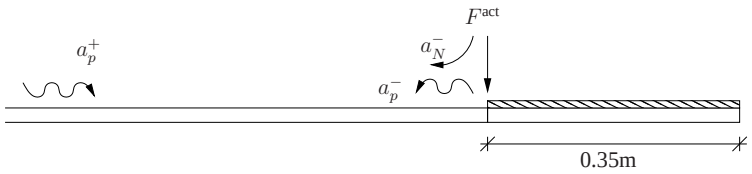

Figure 3.2: The hybrid configuration using impedance matching techniques. The beam to the right of the junction is a sandwich beam.

Figure 3.3 (a) shows the reflection efficiency of the junction without considering an incoming near-field. The figure shows that most of the power carried by an incident wave is reflected back from the junction and not much is lost in the sandwich beam. In fact, less than 1 dB of the incident wave power is absorbed in the considered frequency range of 1-2000 Hz; hence the sandwich beam in this case is not a very efficient damping treatment. Active junction control may be introduced to improve the damping efficiency of the sandwich beam. As no incident near-field is considered, a single force at the junction may be used to cancel the reflected wave. By cancelling the reflected wave all incident wave power is lost in the hybrid treatment, either passively in the sandwich beam or actively by the force.

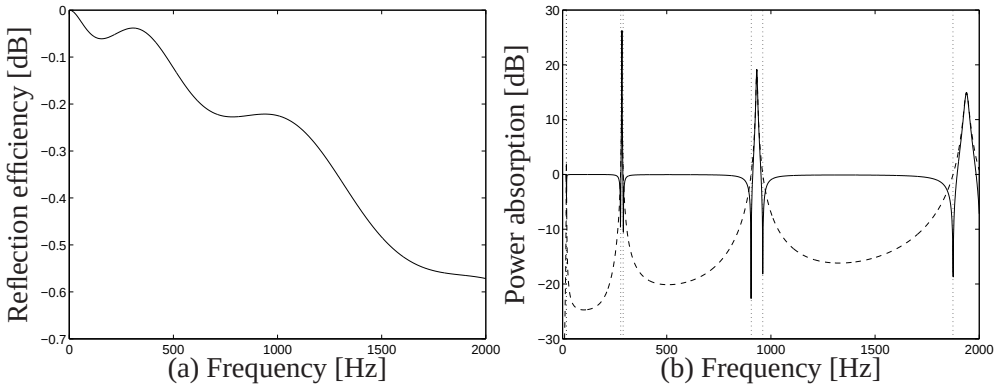

Figure 3.3: (a) The reflection efficiency of the junction of the Euler-Bernoulli and the sandwich composite, for the case of no active control at the junction. (b) The power absorbed by the hybrid treatment. −: active power ; - - -: passive power. The dotted line indicates the regions in between which the active power changes sign.

The power absorbed at the junction, normalized to the incoming wave power, is

plotted in Figure 3.3 (b). The figure shows how much of the incoming wave power is absorbed passively in the sandwich beam or actively by the force. It is evident that in between the resonance frequencies the active force absorbs most power, as the dashed line is 15-20 dB below the solid line. However, around the resonance frequencies where both the dashed and solid line has a peak, the active power changes sign. This means that the active force injects power into the sandwich beam. All incident wave power as well as power injected by the active force is absorbed in the sandwich beam. This is also associated with high control effort around the resonance frequencies, a control effort which is significantly higher than using a force to absorb all incoming wave power at a free end; see Figure 10 in *Paper* II. Thus this type of hybrid configuration is not optimal, as the control effort is considerably higher when the sandwich beam is present compared using the active force at a free end. This reveals the importance of a detailed knowledge of how the properties of the passive treatment of the hybrid configuration affect the active force and wether the properties of the passive treatment may be chosen in such a way that the active and passive treatments complement each other.

3.3 Parameter study of a highly damped beam

In order to investigate if the properties of the passive damping-treatment (the highly dissipative beam) can be chosen so that the active and passive parts complement each other, a parameter study was conducted. As mentioned in the previous section, an analytical expression for the driving point impedance matrix of the sandwich beam is difficult to obtain. Thus in order to gain some understanding of how the properties of the passive part of the hybrid treatment will affect the total hybrid configuration, the sandwich beam was replaced by a finite Euler-Bernoulli, which is simpler to treat analytically. As the beam to the left of the junction is non-resonant, the beam to the right is referred to as the resonant beam. The resonant beam had the length l, a rectangular cross-section, and arbitrary material properties. The driving point impedance matrix of this resonant beam can be found analytically as

$$\mathbf{Z}^{\text{dp}} = \frac{\mathrm{j}EI}{\omega} \frac{\cos kl \cosh kl}{\cos kl \cosh kl + 1} \begin{bmatrix} k^3(\tan kl + \tanh kl) & k^2 \tanh kl \tan kl \\ k^2 \tanh kl \tan kl & k(\tan kl - \tanh kl) \end{bmatrix}, \tag{3.1}$$

where kl is the product of the wavenumber and length. Internal losses are included in the model as a complex modulus, $E^* = E(1 + \mathrm{j}\eta)$, where E' is the Young's modulus and η is the loss factor. Inserting equation 3.1 into equation 2.6 yields

$$\mathbf{r} = \frac{1}{\Omega} \begin{bmatrix} r_{11} & r_{12} \\ r_{21} & r_{22} \end{bmatrix}, \tag{3.2}$$

where

$$r_{11} = -\mathrm{j}\chi^2 \det(\breve{\mathbf{Z}}) - \sqrt{2\chi}\,(\gamma\breve{z}_{11} - \beta\delta\breve{z}_{22}) + \chi\,(\breve{z}_{12} + \breve{z}_{21}) - \mathrm{j}, \quad (3.3a)$$

$$r_{12} = (1+\mathrm{j})\left(1 - \chi^2 \det(\breve{\mathbf{Z}})\right), \quad (3.3b)$$

$$r_{21} = (1-\mathrm{j})\left(1 - \chi^2 \det(\breve{\mathbf{Z}})\right), \quad (3.3c)$$

$$r_{22} = \mathrm{j}\chi^2 \det(\breve{\mathbf{Z}}) - \sqrt{2\chi}\,(\gamma\breve{z}_{11} - \beta\delta\breve{z}_{22}) - \mathrm{j}\chi\,(\breve{z}_{12} + \breve{z}_{21}) + \mathrm{j}, \quad (3.3d)$$

$$\Omega = \chi^2 \det(\breve{\mathbf{Z}}) + \sqrt{2\chi}\,(\gamma\breve{z}_{11} + \beta\delta\breve{z}_{22}) + \chi(\breve{z}_{12} + \breve{z}_{21}) + 1,$$

where $\det(\breve{\mathbf{Z}})$ denotes the determinant of $\breve{\mathbf{Z}}$ which is a dimensionless matrix and a function of kl. The parameters appearing in equations 3.3a through 3.3d are defined as

$$\beta^2 = \frac{EI_b}{EI_a}, \quad \gamma^2 = \frac{m'_b}{m'_a}, \quad \delta^2 = (1+\mathrm{j}\eta), \quad \chi = \beta\delta\gamma \quad (3.4a,b)$$

The subscripts a and b on EI and m' refer to the non-resonant and resonant beam respectively. The loss factor η is given no subscript as only the resonant beam in this case has internal damping. The dimensionless impedance matrix, $\breve{\mathbf{Z}}$, is a normalized version of the matrix $\mathbf{Z}^{\mathrm{dp}}$ in equation 3.1. The important parameters for the reflection matrix in equation 3.2 are the ratio of bending stiffnesses and masses between the beams, the loss factor and the product of the wave number and length, kl, of the resonant beam. By considering the case where both beams have the same mass and bending stiffness, the effect of the damping and the length of the resonant beam on the reflection matrix can be investigated.

Figure 3.4 shows the reflection efficiency of the junction for an incident bending wave as a function of the loss factor for different values of kl. The figure shows that as $kl = 1$ and $kl = 5$ the reflection efficiency decreases, i.e. the absorption increases, with an increasing loss factor in the range of $\eta = 0 - 0.5$. However, as $kl = 50$ and $kl = 100$ there is an optimal choice of loss factor which maximizes the absorption of incident wave power. A loss factor which is lower than this optimal value means that the wave power that enters the resonant beam is less dissipated, while a higher loss factor causes a greater impedance mismatch at the junction and thus a higher reflection efficiency. This highlights the fact that the highest loss factor does not always result in optimal absorption.

Figures 7-9 in *Paper* III present the results of a parameter study of the reflection efficiency of the junction, i.e. how much power is absorbed by the passive junction if only an incoming wave is considered. The loss factor of the resonant beam was chosen as $\eta = 0.3$ since the purpose of the study was to investigate a highly dissipative beam. The results show that a high passive absorption can be achieved

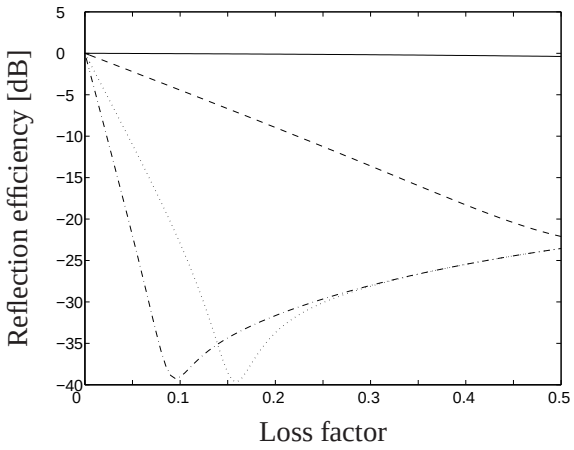

Figure 3.4: The reflection efficiency as a function of the loss factor, for the case $\beta^2 = \gamma^2 = 1$. $-$: $kl = 1$; - - -: $kl = 10$; $\cdots\cdots$: $kl = 50$; - $\cdot$ -: $kl = 100$.

if the beams have similar bending stiffness and mass, and the resonant beam is long in comparison to the bending wavelength. This seems natural, as there is a small difference in impedance between the beams and the wave will undergo several cycles in the dissipative, resonant beam. Figures 4 and 5 in *Paper* III show that, for the case where the beams have identical bending stiffness and mass, the junction impedance matrix approaches the characteristic impedance matrix of the wave travelling towards the junction. The parameter study revealed that for most beam combinations, however, most of the incident wave power was reflected at the junction. Thus, active control could be used as a complement to the passive damping in order to impprove the overall damping efficiency.

An external force and moment can be introduced at the junction using the active impedance matrix described in *Section 2.3.2*. If there is only an incident wave and no near-field at the junction, a force or moment is sufficient to cancel the reflection and thereby absorb all incoming wave power, either passively in the resonant beam or actively by the force or moment. The force which is required to cancel the reflection at the junction can be derived by putting constraints in the reflection matrix. The control effort of the active force, as well as the amount of the power which is actively and passively absorbed respectively, is investigated in *Paper* III.

A parameter study was conducted by varying the properties of the resonant and non-resonant beam in relation to each other. The results were investigated in terms of control effort and the amount of power absorbed by the active force and resonant beam respectively. The magnitude of the force required to cancel the reflection at

the junction is compared to the magnitude of the force required to cancel the reflection at a free end - the latter representing pure active control. These investigations show that there exist combinations of beams where the active and passive treatments complement each other, and thus where a hybrid control solution may offer benefits compared to a pure passive damping or pure active control. This implies a control effort that is lower than cancelling the reflection at a free end, and a passive power absorption which is substantially improved by the presence of the active force.

One case where a hybrid system may be advantageous over pure passive damping or pure active control is described: consider the case where the resonant-beam has a bending stiffness which is 10 % of the non-resonant beam, a loss factor of $\eta = 0.3$ and where $kl = 0.5$. For this case the passive junction reflects about 30% of the power carried by an incident wave. Introducing the active force to cancel the reflection at the junction will result in all incident wave power being absorbed, about 35 % passively in the resonant beam and 65 % by the active force. The control effort for this case is around 75 % of that of actively absorbing the incident wave power at the free end. Thus, for this specific case the active and passive parts of the hybrid system seem to complement each other to a certain degree. However, this requires that the properties of the beams can be decided with high precision, which might be difficult in a real implementation situation. A more detailed discussion can be found in *Paper* III. It may be pointed out that even for cases where the passive damping does not absorb any of the incident power in the presence of the active force, it can still be valuable as it may provide fail-safe damping, and/or increase the stability margins if the active force was driven by a feedback control system.

Chapter 4

Piezoelectric shunt damping

The ability of piezoelectric materials to transform mechanical energy to electrical energy and vice versa makes them suitable as transducers for both active and passive vibration control. By shunting an electrical network to the piezoelectric element, it can provide passive structural damping, a technique referred to as shunt damping. This chapter provides the fundamental principles of this approach and some of the literature published on the subject. A simple and common approach of shunt damping is to connect an inductance and resistance to the piezoelectric element and tune this shunt to augment structural damping to a certain mode. The shunt is tuned using certain criteria based on e.g. interpreting the shunt as a tuned vibration absorber using the principles know from there. However, there is not much reported on how different inductive-resistive shunts affect a structure over a wide frequency range. Further, if the objective is to reduce the radiated sound power of the structure instead of the structural response the radiation properties of the structure needs to be considered. The chapter presents two analytical models of piezoelectric shunt damping, one beam model and one plate model. The beam model is used verify the modelling approach by comparing it with experimental data. The plate model is used for a comprehensive parameter study of how different inductuvive-resistive shunts affect the kinetic energy on the plate and radiated sound power. Results show that the optimal shunt treatment varies depending on if it is designed with respect to the kinetic energy or radiated sound power respectively .

4.1 The piezoelectric effect

When a piezoelectric material is stressed it produces a small electric charge on the material surface. This effect was discovered by Pierre and Jacques Curie in 1880 [59]. By attaching electrodes to the surfaces of the piezoelectric material, a voltage potential is created between the electrodes; see Figure 4.1. Later the transverse

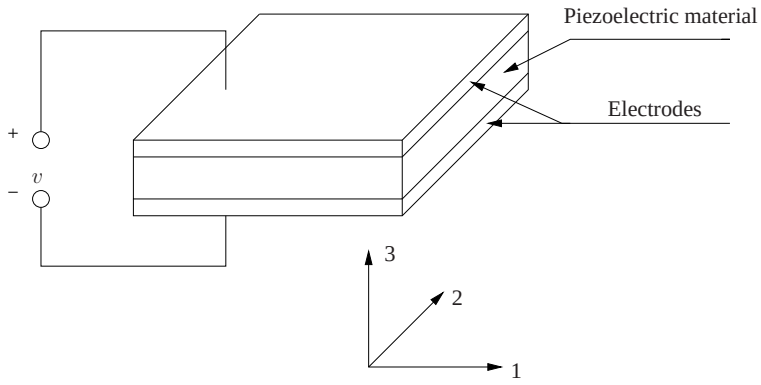

Figure 4.1: A schematic drawing of a piezoelectric material with electrodes attached at each surface

effect was also discovered, i.e. if an electric field is applied to the surfaces of the piezoelectric material it changes its size and shape. The piezoelectric effect can be found naturally in a number of different materials, e.g. quartz crystals, tourmaline and topaz [59]. However, it can also be artificially induced in certain materials during the manufacturing process. This is achieved by "poling" the material. In its unpolarized state, the material dipoles are arranged in random directions so that they cancel each other and no significant macroscopic effects are observable; see Figure 4.2 (a). If the material is heated above its Curie temperature, the dipoles in the solid phase material may change their location. By applying a large electric field the dipoles can all be arranged in a certain direction, referred to as the polarization direction; see Figure 4.2 (b). After the electric field is removed the dipoles remain in approximate alignment; see Figure 4.2 (c). Piezoelectric materials are used in a number of commercial products for sound and vibration sensing and actuation, e.g. accelerometers and ultrasonic transducers.

4.2 Shunted piezoelectric elements

4.2.1 Fundamental principles

The fundamental principle of piezoelectric shunt damping is to connect a passive electric impedance between the electrodes of a piezoelectric element attached to a host structure; see Figure 4.3. As the host structure vibrates, the piezoelectric element deforms and a voltage is created between the electrodes of the element. If an electrical network (impedance) is connected between the electrodes the voltage will drive a current through the network. Electrical energy will be lost as Joule heating

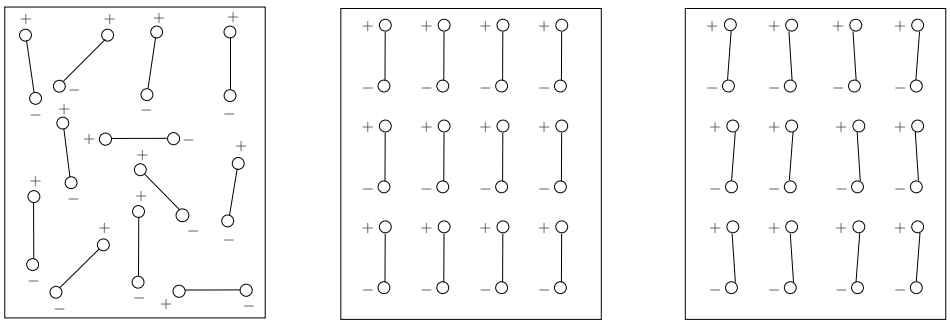

(a) (b) (c)

Figure 4.2: Electric dipole moments: (a) before polarisation, (b) during polarisation, (c) after polarisation.

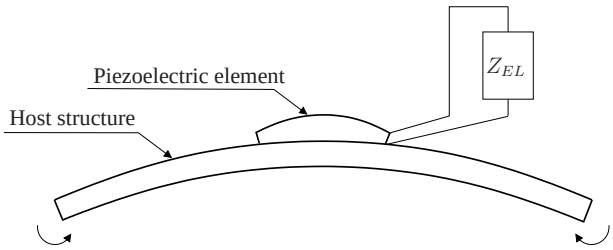

Figure 4.3: A schematic drawing of a piezoelectric element shunted by an electrical impedance and bonded to a host structure.

in the resistance of the electrical components. Thus, some vibrational energy is converted to electrical energy by the piezoelectric element, and some of the electrical energy is converted to heat in the electrical network, hence there is net loss of energy in the mechanical system. The damping efficiency of the shunted piezoelectric element is thus governed by the piezoelectric material's ability to transform mechanical energy into electrical energy. This property is characterized by the piezoelectric coupling factor, the definition of which can be found in standards on piezoelectricity [60].

The electrical network, i.e. shunt impedance, can be composed in a number of ways. In one of the first research articles on shunted piezoelectric elements, Forward [61] proposed shunting an inductance to the piezoelectric element. The inductive element together with the inherent capacitance of the piezoelectric material will have an electrical resonance frequency. By tuning the electrical resonance frequency to coincide with a structural eigenfrequency, modal suppression could be

achieved. Since no resistance was added in the electrical circuit, the purpose of the treatment was not to add structural damping but merely to suppress the vibrational response around the frequency for which the shunt network was tuned, in a fashion very similar to a tuned vibration neutralizer; see e.g. references [62, 63]. Hagood and von Flotow [64] extended the approach of Forward by also including a resistive element in the shunt circuit, thereby dissipating energy. The resonant network was compared to a purely resistive one, i.e. a non-resonant network which adds broadband damping in a fashion similar to a viscoelastic material [64]. In order to tune the components of the shunt network, Hagood and von Flotow developed an analogy to the tuned vibration absorber, which is here differentiated from the tuned vibration neutralizer mentioned earlier because it dissipates energy. By this analogy the components of the shunt network could be tuned by either minimizing the mechanical system transfer function or using pole placement techniques.

Although resonant shunts are very common, other types have also been investigated. Lesieutre [65] summarized different kinds of shunting networks in four basic categories. These four are:

- *Inductive shunt*: since the piezoelectric element behaves electrically as a capacitor, shunting an inductive element will result in a resonant LC circuit. This works in practice as a vibration neutralizer and the inductive element is tuned so that the electrical resonance frequency coincides with a mechanical resonance frequency. This is the type of shunt network proposed by Forward [61].

- *Resistive shunt*: shunting a resistive element to the piezoelectric element means that some of the electrical energy is lost in the circuit through Joule heating. This virtually works as augmenting the structural damping, and can be interpreted in terms of a loss factor [64].

- *Capacitive shunt*: a capacitive element in the shunt network will change the apparent stiffness of the piezoelectric element without affecting the damping properties of the structure. However, as a stiffer structure has the potential to store more energy, capacitive shunting may help increasing inherent material losses. A capacitive shunting could also be used to shift the eigenfrequencies of a mechanical system. Davis and Lesiture [66] presented an approach to alter the natural frequency of a single degree-of-freedom system by actively tuning a capacitance of a shunted piezoelectric element. This effectively minimized the structural response at a narrow frequency band given by the tuned

electric circuit.

- *Switched shunt*: a switched network can change its characteristics rapidly based on the state of the mechanical system. This enables a control of the energy transfer. There are several different types of switching shunts, e.g. switching the shunt between a high-stiffness state (open circuit) and low-stiffness state (short circuit or resistive shunt). The high-stiffness state is kept while the structural motion is large so that energy is stored in the shunted piezoelectric element. When the structural motion is reducing (close to its equilibrium state) so that it may receive the energy back from the shunted piezoelectric element, the shunt is switched to the low-stiffness state and energy is dissipated [67]. Other studies concerning switched shunts include [68, 69]. A switched shunt may also be used to harvest energy from vibrating structures, i.e. to store the energy which is dissipated from the mechanical system; see e.g. [70]

4.2.2 Resonant shunt tuning

The electrical resonance frequency ω_e of an inductive-resistive (LC) network is given by

$$\omega_e = \frac{1}{\sqrt{LC}}, \tag{4.1}$$

where L and C are the inductance and capacitance respectively. Since the capacitance is an inherent property of the piezoelectric element, the inductance can be chosen so that the electrical resonance frequency coincides with the eigenfrequency of a structural mode. In the RL shunt proposed by Hagood and von Flotow [64] the shunted piezoelectric element was interpreted as a tuned vibration absorber. The principles know from tuning a vibration absorber was applied to the tuning of the inductance and resistance. The optimal tuning parameter and damping ratio are then given by [64]:

$$\delta^{\text{opt}} = \sqrt{1 + K_{ij}^2}, \qquad r^{\text{opt}} = \frac{\sqrt{2} K_{ij}}{1 + K_{ij}^2}, \tag{4.2a, b}$$

where K_{ij} is the generalized electromechanical coupling coefficient, which is proportional to the fraction of the system strain energy that is converted to electrical energy. The indices i, j refer to the electrical and mechanical material axes respectively; see figure 4.1. The optimal shunt components are then calculated according to

$$L = \frac{1}{(\omega_n \delta^{\text{opt}})^2 C_p^{\varepsilon}}, \qquad R = r_{\text{opt}} \frac{1}{C_p^{\varepsilon} \omega_n} \tag{4.3a, b}$$

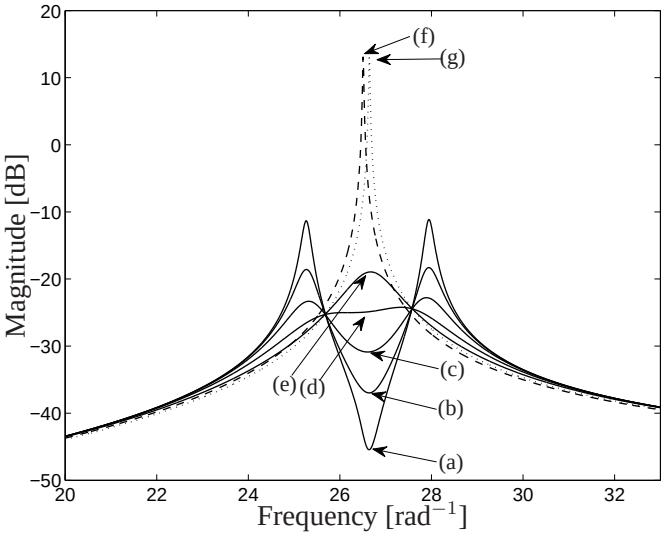

Figure 4.4: The calculated response of a piezoelectric element-structural plate composite for different values of the resistance: (a). $0.1 \cdot r^{\text{opt}}$; (b). $0.25 \cdot r^{\text{opt}}$; (c). $0.5 \cdot r^{\text{opt}}$; (d). r^{opt}; (e). $2 \cdot r^{\text{opt}}$; (f). short circuit; (g). open circuit

where C_p^{ε} is the capacitance under constant strain. The shunt is designed to damp the mode with eigenfrequency ω_n.

Figure 4.4 shows the magnitude of the first mode for a plate treatment with piezoelectric shunt damping. The results are calculated with the model presented in section 4.3.3. The inductance is tuned according to equation 4.3a and the resistance is varied in order to see the effect on the damping performance. The figure shows that as the resistance is reduced from its optimal value, the vibration at the modal eigenfrequency is more efficiently suppressed, while the response just below and just above the eigenfrequency is amplified, analogous to a tuned vibration neutralizer. Increasing the resistance amplifies the response again. Making the resistance infinite will give an open circuit condition and the eigenfrequency is slightly shifted compared to the short circuit case.

Since the early work of Hagood and von Flotow numerous research articles have treated piezoelectric shunt damping. Several papers have treated the issue of how to tune the components of a resistive-inductive (LR) shunt network. Behrens and Moheimani [71] determined the optimal resistive element by minimizing the 2-norm of a system transfer function, and Kim et al [72] propose a shunt tuning technique based on measuring the electrical impedance.

A problem associated with resonant shunt damping is the sensitivity to slight changes in the electrical and/or mechanical resonance frequencies. A slight shift of the modal eigenfrequency, e.g. due to temperature variations, will severely diminish the damping performance of the shunt. In a similar fashion, temperature variations can cause changes in the inherent capacitance of the piezoelectric element, which will detune the shunt. Such problems can be overcome by adaptively updating the shunt inductance. The inductance may be updated in different ways such as minimizing the RMS voltage [73] or controlling the relative phase shift between the velocity of the host structure and the current in the shunt network [74]. Some additional literature on adaptive shunt damping is presented in *Section 5.1.1*.

4.2.3 Virtual and synthetic shunt impedances/admittances

A problem which has generally been associated with shunt damping is the large inductance needed in order to tune the shunt to typical bending mode eigenfrequencies. As an example it can be mentioned that, in order to tune the shunt inductance to a mode with an eigenfrequency of 50 Hz using a piezoelectric element with a capacitance of 100 nF, an inductance of around 100 H is needed. Such an inductance normally needs to be synthesized with electronic circuitry, commonly using operational amplifiers (op-amps). A common virtual inductance consists of four resistances (R_1, R_2, R_3, R_5), a capacitance (C) and two op-amps; see Figure 4.5 and [75]. The inductance of the circuit is given by

$$L_{\text{vir}} = \frac{R_1 R_3 R_5}{R_2} C. \tag{4.4}$$

Due to the high voltage created by the stressed piezoelectric, element high-voltage components are normally necessary to implement such a virtual inductance.

Fleming et al. [76] proposed another approach using a synthetic admittance to create an arbitrary shunt impedance. The synthetic admittance consists of two voltage followers, a signal filter and a voltage-controlled current source. The voltage across the electrodes of the piezoelectric element, u_z, is used to determine the applied current, i_z, via the signal filter $Y(s)$; see Figure 4.6. The signal filter is implemented digitally on a DSP. The controlled current source can be made to synthesize an arbitrary impedance according to

$$i_z(s) = Y(s) v_z(s), \tag{4.5}$$

where s is the Laplace parameter and the impedance is given by $Z(s) = 1/Y(s)$. A synthetic impedance circuit can be also be utilized by applying a controlled voltage

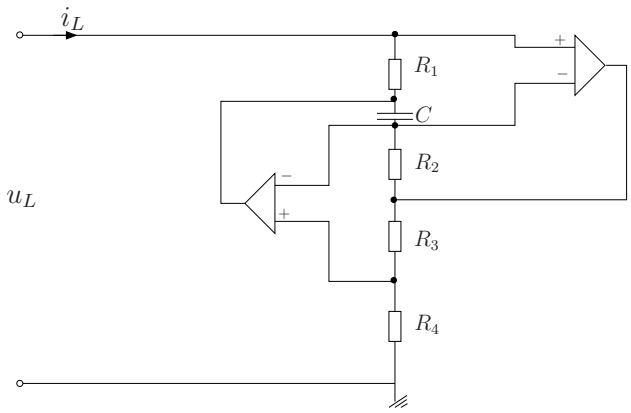

Figure 4.5: A virtual inductance implemented using gyrator circuits.

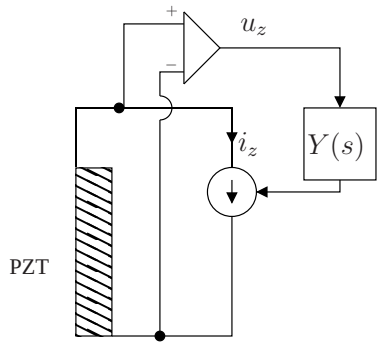

Figure 4.6: A synthetic impedance used to implement the shunt impedance

based on the measured current in the circuit. As the shunt is digitally implemented on the DSP there are no constraints on the value of the inductance.

4.2.4 Multimodal shunt damping

The structural damping provided by a piezoelectric element shunted by a LR circuit is usually confined to a single vibrational mode. A straightforward approach to damp several structural modes is to attach a number of shunted piezoelectric elements to the host structure. However, using one shunted piezoelectric element for each vibrational mode seems fairly unattractive due to the finite amount of space on a structure in which a large number of modes are excited. Another approach is to adapt the shunt for multimodal damping by expanding the electrical network.

Hollkamp [77] suggested adding one parallel RCL branch to the single RL branch for each additional mode which is targeted by the damping treatment; see Figure 4.7 (a). For a single mode this circuit would be equivalent to the one proposed by Hagood and von Flotow [64]. No closed-form optimal solution for choosing the electrical components was presented, but instead the components were tuned using a numerical optimisation scheme. An obvious problem with this type of strategy is the increasingly complex optimisation scheme as the number of considered modes (and thus RCL branches) increase.

Wu et al. [78, 79] proposed a shunt based on LR circuits (in series or parallel) to damp each vibrational mode together with blocking LC circuits. The blocking circuits have the purpose of blocking the current at all frequencies except the tuning frequency. Figure 4.7 (b) shows a two-mode current-blocking shunt circuit. LR circuits L_1, R_1 and L_2, R_2 are tuned to the eigenfrequencies of modes one and two respectively, while $\hat{L}_1, \hat{C}_1$ are tuned to block the current at the second eigenfrequency and $\hat{L}_2, \hat{C}_2$ to block the current at the first eigenfrequency. As the number of targeted vibrational modes increases, the networks grows quite rapidly, which is a drawback of such a configuration.

Behrens et al. [80] proposed a current-flowing circuit for multimodal damping. A branch containing one LC-pair and one RL-pair is introduced for each structural mode to be damped. The LC-pair is tuned to approximate a short circuit condition at the target frequency and an open circuit condition at adjacent target frequencies; see Figure 4.7 (c). This type of circuit has a clear advantage compared to the current-blocking circuit, since the network does not grow as rapidly with each new mode targeted by the shunt. This is especially important when op-amps are required in order to implement large inductances. In general $2n+4n(n-1)$, where n is the total number of structural modes, op-amps are required for a current-blocking multimodal shunt, while $2n$ op-amps are required for a current-flowing multimodal shunt [81].

4.2.5 Shunt damping for sound transmission and radiation

Shunted piezoelectric elements have also been used on structures in order to suppress the radiated sound field. Kim et al. [82, 83] applied their shunt design based on the measured electrical impedance to reduce sound transmission through piezoelectric smart panels. Ozer and Royston [84] compared the classical method for choosing the inductance and resistance of the shunt network, based on the work of Hagood and von Flotow [64], to a method based on the Sherman-Morrison matrix

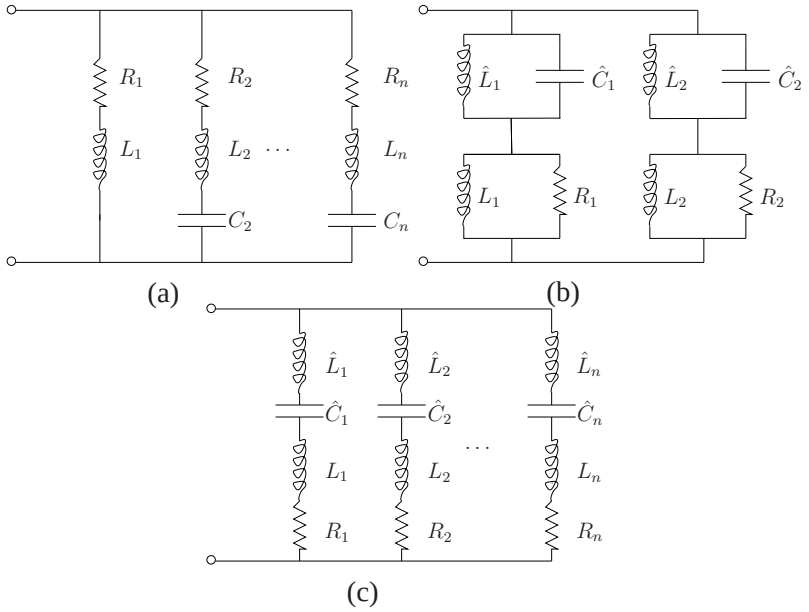

Figure 4.7: (a) The Hollkamp circuit. (b) A two-mode current-blocking shunt circuit of Wu et al. [79] (c) The current-flowing circuit.

inversion theorem. Their results were evaluated in terms of both structural response and radiated field. They recognized the limitations for tuning the inductance and resistance values for multi-modal systems. As the radiated field from a structure is combined by the response of several modes, which might overlap, the inductance based on the work of Hagood and von Flotow may be suboptimal. By using the Sherman-Morrison matrix inversion theorem, they showed that an optimal inductance could be found by minimizing the radiated sound power (or pressure at a certain point). Other studies concerning shunted piezoelectric materials for reduction of sound transmission or radiation include negative-capacitance shunts (explained more in *Section 5.1.2*) [85], switched shunts [86], tuned LR shunts [87, 88] or multimodal shunts [89].

4.2.6 Shunted constrained layer damping

Using shunted piezoelectric elements to constrain a viscoelastic layer has also been investigated. Edberg and Bicos [90] presented a configuration where one piezoelectric element was embedded in the structure and another was used to constrain a surface-bonded viscoelastic layer. The embedded piezoelectric element was connected to the constraining one with reversed polarity. As the structure deforms, the

constraining piezoelectric element works against this and extra shear losses are induced in the viscoelastic layer. This damping mechanism is also utilized in ACLD; see e.g. [47]. Ghoneim [91] reported that this technique performed better than a conventional PCL in suppressing the first bending and twisting modes of a plate.

4.2.7 Brief literature summary and motivation for study

Several papers treating resonant shunt damping have been presented during the last 20 years. Most studies concern damping of one vibrational mode by tuning the shunt according to some predefined criterium. A few studies have presented shunt damping to reduce the sound power radiated from- or transmitted through a structure, also mostly around a single mode. However, in many practical situation the vibration field of a structure is composed of several vibrational modes. Further, as the radiated sound field is composed of a weighted sum of several modes, in order to design the shunt to reduce the sound it is important to have knowledge of the radiation properties of the structure. Resonant shunts which targets more than one mode by expanding the electrical network have been proposed. However, due to the complexity of tuning the shunt consisting of several resonant branches the analysis is often confined to two vibrational modes. Reducing one or two modes on a plate where the vibrational field is composed of several modes does not always lead to a significant decrease of the kinetic energy or the radiated sound power. A question that arises is therefore, is it optimal to tune the shunt to a specific mode if the purpose is to reduce the kinetic energy or radiated sound power.

This chapter presents a parameter study of a plate with a piezoelectric element which is shunted by an resonant (LR shunt). The inductance and resistance is varied and the result is evaluated in terms of both the kinetic energy of the plate and the radiated sound power. An analytical model is developed by considering a perfectly bonded piezoelectric element. Two cases are studied: both when the modes have there eigenfrequencies well below the critical frequencies; and where the eigenfrequencies are in the same order as the critical frequencies. The results are presented in *Paper* IV and some key results are included in this chapter. A model of a beam with a piezoelectric element is also developed and compared with measurement in order to verify the modelling approach.

4.3 Modelling of piezoelectric shunt damping

4.3.1 The constitutive relations

The general constitutive equations, in matrix form, for a piezoelectric material are given by [64]:

$$\left\{ \begin{array}{c} \boldsymbol{\varepsilon} \\ \mathbf{D} \end{array} \right\} = \left[\begin{array}{cc} \mathbf{S}^E & \mathbf{d}^t \\ \mathbf{d} & \boldsymbol{\xi}^\sigma \end{array} \right] \left\{ \begin{array}{c} \boldsymbol{\sigma} \\ \mathbf{E} \end{array} \right\}, \tag{4.6}$$

where the vectors $\boldsymbol{\varepsilon}$ and $\boldsymbol{\sigma}$ contain the mechanical variables of stress and strain respectively, and vectors $\mathbf{D}$ and $\mathbf{E}$ contain the electric variables of electric displacement (or charge per unit area) and electric field respectively. The matrices $\mathbf{S}^E, \mathbf{d}$ and $\boldsymbol{\xi}^\sigma$ contain the materials' elastic compliance, piezoelectric strain constants and dielectric constants respectively. The superscript E and σ indicates that the quantity is measured under a constant electric field and constant stress respectively. The superscript t represent a matrix transpose. Equation 4.6 is explained in more detail in *Appendix A.*

4.3.2 Various modelling approaches

Several different models of piezoelectric element-structure composites can be found in the literature. Early works by Forward [61] proposed modelling the host structure around a modal eigenfrequency by its analogue electrical circuit. The piezoelectric element is then connected through a transformer to the analogue circuit. The resulting circuit can then be expanded by additional components describing the shunt network.

Hagood and von Flotow [64] included the effect of the shunt in the elastic compliance of the piezoelectric element according to

$$s_{jj}^{SU} = s_{jj}^{E}(1 - k_{ij}^2 \bar{Z}_i^{EL}), \tag{4.7}$$

where k_{ij} is the piezoelectric coupling factor and the superscript SU denotes the material's elastic compliance with the shunted electric network. $\bar{Z}_i^{EL}$ is the normalized electrical impedance which is found by normalising the electrical impedance with the impedance of the inherent capacitance of the piezoelectric element. The electrical impedance is the total impedance of the shunt network and inherent capacitance, where the shunt is parallel to the piezoelectric element's inherent capacitance [64]. For an inductive-resistive shunt the normalized electrical impedance is given by

$$\bar{Z}_i^{EL} = \frac{(R + Ls)c_p s}{1 + (R + Ls)c_p s}, \tag{4.8}$$

where R and L is the shunt inductance and resistance respectively and c_p the inherent capacitance of the piezoelectric element. A non-dimenisonalized mechanical impedance can be defined by considering the ratio of the shunted stiffness to the open circuited stiffness of the piezoelectric element according to

$$Z_{jj}^{M}(s) = \frac{(1 - k_{ij}^2)}{(1 - k_{ij}^2)\bar{Z}(s)_i^{EL}}, \tag{4.9}$$

The non-dimensional mechanical impedance may be frequency-dependent and complex. The impedance can be interpreted as a complex modulus according to

$$Z_{jj}^{M}(s) = E_{jj}(\omega)(1 + \mathrm{j}\eta_{jj}(\omega)), \tag{4.10}$$

where E_{jj} is the stiffness ratio of the shunted stiffness to the open circuit stiffness, and η_{jj} is a loss factor. They are defined as

$$E_{jj}(\omega) = \Re\{Z_{jj}^{M}(s)\}, \qquad \eta_{jj}(\omega) = \frac{\Im\{Z_{jj}^{M}(s)\}}{\Re\{Z_{jj}^{M}(s)\}}. \tag{4.11a, b}$$

Thus using this approach the shunt network can be included in modelling the stiffness of the piezoelectric element.

Other studies have presented different approaches to model the shunt network. Law et al [92] described the damping of a resistively shunted piezoelectric element by using energy considerations. In general the constitutive relation in equation 4.6 is considered to derived the coupled electromechanical equations for a shunted piezoelectric element bonded to a host structure. The coupled electromechanical equations can be solved by e.g. a Ritz method [93] or finite elements [94, 86].

4.3.3 Plate model

In this section a Kirchhoff plate model is presented, this model is used to conduct a parameter study on the effect of an inductive-resistive shunt on the kinetic energy and radiated sound power of a plate structure over a wide frequency range. The Kirchoff plate is the two-dimensional equivalent of the Euler-Bernoulli beam, and is based on the same assumption of no rotational inertia. The mass of the piezoelectric element is neglected in the plate model. Neglecting the mass may in some situations be erroneous, especially at higher frequencies were the inertial effects are significant [95]. However, the purpose of this model was not to closely resemble reality for all masses of piezoelectric elements. Importantly, though, the conclusions which can be drawn from a parameter study of the shunt circuit will not be significantly affected by neglecting the mass. A thin plate-like structure can

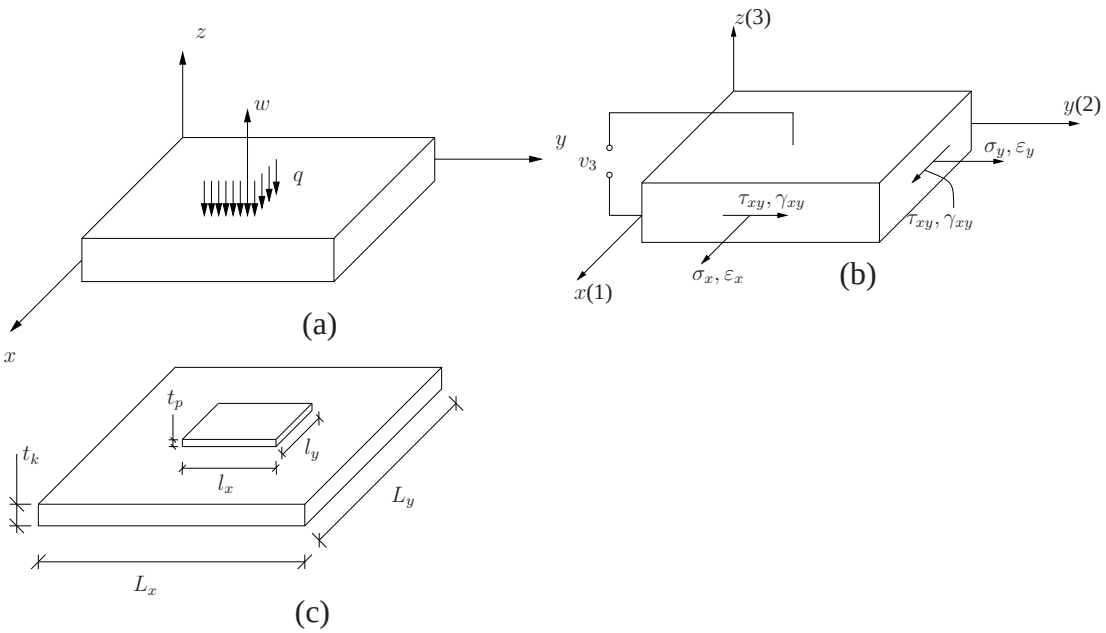

Figure 4.8: (a) Definition of load (q) and deflection directions (w) on the plate. (b) Definition of stresses and strains on the piezoelectric element with its material axes aligned with a Cartesian coordinate system. σ_x, ε_x and σ_y, ε_y are the extensional stresses and strains in the x and y and directions respectively and τ_{xy}, γ_{xy} are the shear stress and strain in the x-y plane. The voltage in the 3-direction is given by v_3. (c) The dimensions of the composite plate.

for low frequencies be modelled quite accurately by using Kirchhoff's plate theory. The modified Kirchhoff plate equation is given by

$$D\nabla^4 w(x,y,t) + m'' \frac{\partial^2}{\partial t^2} w(x,y,t) + \Gamma^{w,\Omega} = q(x,y,t), \tag{4.12}$$

where w is the deflection, D and m'' are the plate's flexural rigidity and mass per unit area respectively, q is a function describing an external loading, x, y, t are the space and time coordinates, and ∇ is the nabla operator. The definitions of load and deflection are defined in Figure 4.8 (a). The flexural rigidity is given by $D = \frac{E_k t_k^3}{12(1-\nu_k^2)}$, where E_k, t_k and ν_k are the plate's Young's modulus, thickness and Poisson's ratio respectively, where the subscript k is to denote Kirchhoff plate. The term $\Gamma_{w,\Omega}$ includes the stiffness du to the piezoelectric element and is derived by assuming a linear stress distribution which is continuous across the material borders. $\Gamma^{w,\Omega}$ is derived and explained in *Paper* IV. This stiffness is complex and contains the effect of the shunt network using the approach in reference [64].

Assuming a modal approach, a solution to equation 4.12 under harmonic excitation is given by

$$w(x,y,\omega) = \sum_n^\infty \sum_m^\infty a_{n,m}(\omega)\phi_{n,m}(x,y), \tag{4.13}$$

where $a_{n,m}$ and $\phi_{n,m}$ are the modal amplitude and modal shape function respectively. A more detailed derivation of equation 4.16 is given in *Paper* IV. For a rectangular plate which is simply supported along its edges, the modal shape function of the n, m:th mode is given by

$$\phi_{n,m}(x,y) = \sin(k_n x)\sin(k_m y), \tag{4.14}$$

where

$$k_n = \frac{n\pi}{L_x}, \quad k_m = \frac{m\pi}{L_y}, \tag{4.15a, b}$$

n and m are natural numbers and L_x, L_y are the plate dimensions; see figure 4.8 (c). The modal shape function are found by disregarding the piezoelectric element. By inserting equation 4.13 into equation 4.12 and following the standard approach, the deflection field on the plate is given as

$$w(x,y,\omega) = \sum_n^\infty \sum_m^\infty \frac{Q_{n,m}^{\text{ext}}}{M_{n,m}\left(\omega_{n,m}^2 - \omega^2\right) + K_{n,m}^{\text{pzt}}} \sin(k_n x)\sin(k_m y), \tag{4.16}$$

where the eigenfrequencies $\omega_{n,m}$ represent the plate without the piezoelectric element and are given by

$$\omega_{n,m} = \sqrt{\frac{D}{m''}}\left(k_n^2 + k_m^2\right). \tag{4.17}$$

The modal eigenfrequencies are found by considering the homogenous differential equation, i.e. without external loading. The modal mass is given by

$$M_{n,m} = \iint_S \rho t_k \phi_{n,m}^2 \mathrm{d}\mathbf{S} = \frac{1}{4}\rho t_k L_x L_y, \tag{4.18}$$

and the modal force due to the external disturbance and modal stiffness due to the piezoelectric element respectively are given by

$$Q_{n,m}^{\text{ext}} = \iint_S q(x,y,\omega)\phi_{n,m}\mathrm{d}\mathbf{S} = F^{\text{ext}} \sin(k_n x_e)\sin(k_m y_e), \tag{4.19}$$

$$\begin{aligned} K_{n,m}^{\text{pzt}} &= \iint_S \Gamma_{n,m}^{w,\Omega}\phi_{n,m}\mathrm{d}\mathbf{S} \\ &\approx l_x l_y D_{p11}^{SU}(k_n^4 + k_m^4 + 2\nu_p k_n^2 k_m^2)\sin^2(k_n x_c)\sin^2(k_m y_c) \\ &+ l_x l_y D_{p44}^{D} k_n^2 k_m^2 \left(\sin^2(k_n x_c) - \cos(2k_n x_c)\right)\left(\sin^2(k_m y_c) - \cos(2k_m y_c)\right), \end{aligned} \tag{4.20}$$

where ν_p is the Poisson's ratio of the piezoelectric element and $\Gamma_{n,m}^{w,\Omega}$ comes from inserting equation 4.13 into $\Gamma^{w,\Omega}$. F^{ext} is the amplitude of a harmonic point force at $(x_y; y_e)$. The approximation in equation 4.20 is based on the assumption that the size of the piezoelectric element is much smaller than the bending wavelength, i.e. $k_n l_x \ll 1$ and $k_m l_y \ll 1$. The cross-modal coupling terms are small and were therefore neglected. The dimensions of the plate and piezoelectric element are illustrated in Figure 4.8 (c).

As can be seen in equation 4.20 the modal stiffness due to the shunted piezoelectric element is divided into two parts containing two different flexural rigidities D_{p11}^{SU} and D_{p44}^{D}. They represent the flexural rigidity due to the shunted piezoelectric element and due to only the mechanical stiffness of the piezoelectric element respectively and are defined as

$$D_{p11}^{SU} = \frac{t_c}{S_{11}^{SU}(1-\nu_p^2)}, \qquad D_{p44}^{D} = \frac{t_c}{4S_{44}^{D}(1-\nu_p^2)}, \tag{4.21a, b}$$

where S_{11}^{SU} is the shunted compliance according to equation 4.7, and S_{44}^{D} is the open circuit compliance in the 4-direction. The term t_c is given by

$$t_c = \frac{t_k^2 t_p}{4} + \frac{t_k t_p^2}{2} + \frac{t_p^3}{3}, \tag{4.22}$$

where t_p is the thickness of the piezoelectric element. The second part of equation 4.20 may in fact be neglected without significant effects. In fact many models of a structure with surface bonded piezoelectric element neglect the mechanical stiffness due to the piezoelectric element; see e.g. reference [59].

4.3.4 Beam model

A beam model based on Euler-Bernoulli theory is developed for a shunt piezoelectric element surface bonded to a host beam. This model is based on the same assumptions as the plate model and is used to verify the modelling approach. The beam model is compared against measurements in *Section 4.5*. The modal mass due to the piezoelectric element is included in the beam model as the mass of the piezoelectric element used in the measurements cannot be neglected. The modified Euler-Bernoulli bending wave equation is given by

$$\begin{aligned} &EI\frac{\partial^4}{\partial x^4}w(x,t) + m'\frac{\partial^2}{\partial t^2}w(x,t) \\ &+ E_p b_p t_c \left(\frac{\partial^4 w}{\partial x^4}\Omega(x) + 2\frac{\partial^3 w}{\partial x^3}\Omega'(x) + \frac{\partial^2 w}{\partial x^2}\Omega''(x)\right) \\ &+ m'_p\frac{\partial^2}{\partial t^2}w(x,t)\Omega(x) = q(x,t), \end{aligned} \tag{4.23}$$

where w is the displacement, m' the mass per unit length and EI the bending stiffness of the beam, and m'_p the mass per unit length and E_p the Young's modulus of the piezoelectric element, t_c is given in equation 4.22. The function $\Omega(x)$ is given by

$$\Omega(x) = \left[\Theta(x - x_1) - \Theta(x - x_2)\right], \tag{4.24}$$

where Θ is the Heaviside step function. The primes denote differentiation with respect to x. The length and width of the piezoelectric element are given by $l_a = x_2 - x_1$ and b_p, x and t the length and time coordinate respectively. The force distribution loading the structure is given by $q(x,t)$ and Θ is the Heaviside step function. A detailed derivation of the two-dimensional equivalent of equation 4.23 can be found in *Paper* IV. Assuming harmonic excitation, a solution to equation 4.23 is given by

$$w(x,\omega) = \sum_n^\infty a_n(\omega)\phi_n(x), \tag{4.25}$$

where a_n and ϕ_n are the modal amplitude and modal shape function respectively. A free-free boundary condition is considered as this is easy to achieve experimentally. The modal shape function for a free-free beam is given by

$$\phi_n = \cosh(k_n x) + \cos(k_n x) - \gamma_n\left(\sinh(k_n x) + \sin(k_n x)\right), \tag{4.26}$$

where

$$\gamma_n = \frac{\cosh(\alpha_n) - \cos(\alpha_n)}{\sinh(\alpha_n) - \sin(\alpha_n)}, \tag{4.27}$$

where

$$\alpha_n \approx \left(n + \frac{1}{2}\right)\pi, \qquad k_n = \frac{\alpha_n}{L}. \tag{4.28a, b}$$

Inserting equation 4.25 into equation 4.23 and following the standard approach yields the modal amplitudes. These can be inserted back into equation 4.25 to give the vibration field of the beam according to

$$w(x,\omega) = \sum_n^{\infty} \frac{Q_n^{\text{ext}}}{M_n\left(\omega_n^2 - \omega^2\right) + \left(K_n^{\text{pzt}} - \omega^2 M_n^{\text{pzt}}\right)} \phi_n(k_n x), \tag{4.29}$$

where the modal mass and the modal disturbance force are given by

$$M_n = \rho b t_b \int_0^L \phi_n^2 \mathrm{d}x = \frac{L b t_b \rho}{2}, \tag{4.30}$$

$$Q_n^{\text{ext}} = \int_0^L F_e \delta(x - x_e)\phi_n \mathrm{d}x = F_e \phi_n(k_n x_e), \tag{4.31}$$

where ρ and b is the density and the width of the beam respectively. The external disturbance force is a harmonic point force at $x = x_e$ with amplitude F_e. The modal eigenfrequencies ω_n are considering the beam without the piezoelectric element and are given by

$$\omega_n = \sqrt{\frac{m'}{EI}} k_n^2. \tag{4.32}$$

The modal eigenfrequencies are found by considering the homogenous differential equation, i.e. with no external loading.

Assuming that the bending wavelength is much larger than the length of the piezoelectric element, i.e. $k_n l_a \ll 1$, and that cross-modal coupling terms can be neglected the modal mass and stiffness of the piezoelectric element is given by

$$M_n^{\text{pzt}} = \rho_p b_p t_p \int_{x_1}^{x_2} \phi_n^2 \mathrm{d}x \approx \rho_p t_p b_p l_a \zeta_n(x_c), \tag{4.33}$$

$$\begin{aligned} K_n^{\text{pzt}} &= E_p b_p t_c \int_0^L \left(k_n^4 \phi_n \Omega + 2\phi_n''' \Omega' + \phi_n'' \Omega''\right) \phi_n \mathrm{d}x \\ &\approx k_n^4 t_c b_p l_a E_p^{SU} \zeta_n(x_c), \end{aligned} \tag{4.34}$$

where ρ_p is the density of the piezoelectric element. The expression $\zeta_n(x_c)$ in equations 4.33 and 4.34 describes the location of the piezoelectric element in relation to the mode shape, and they are derived and defined in *Appendix A*. The effect of the shunt is included in compliance of the piezoelectric element according to equation 4.7. Thus $E_p^{SU} = 1/S_{11}^{SU}$, which is then complex and frequency-dependent.

4.3.5 Sound radiation from a baffled plate

Suppressing the vibrational field is not necessarily the primary objective of vibration control treatments; instead it might be minimizing the radiated sound field. Further, as the suppression of one or two structural modes does not necessarily reduce the radiated sound field it is important to consider the radiation properties of the structure. Fuller et al. [96, 97, 98] introduced the concept of active structural acoustic control (ASAC), which means using active structural inputs to reduce the radiated sound. As reported by Fuller et al., reducing the radiated acoustic field may under certain conditions actually lead to an increase of the plate's vibration field.

The radiated sound power can be calculated from the modal amplitudes of the structure. Although the structural modes are orthogonal in terms of the plate's vibrational response, they are not in terms of sound radiation. Thus, the modes influence each other's radiation efficiencies. This is especially important under the critical frequency of the mode. The fluid loading of the plate is neglected, and the plate is assumed to be in a rigid baffle. The radiated sound power, Π^{rad}, in terms of the structural modes can be expressed according to [12]:

$$\Pi^{\text{rad}} = \dot{\mathbf{a}}^H \mathbf{M} \dot{\mathbf{a}}, \tag{4.35}$$

where the matrix $\mathbf{M}$ is given by

$$\mathbf{M} = \frac{\omega \rho_0}{8\pi^2} \Re \left\{ \iint_{k_x^2+k_y^2 \leq k_0^2} \frac{\boldsymbol{\phi}^*(k_x,k_y)\boldsymbol{\phi}^T(k_x,k_y)}{\sqrt{k_0^2-k_x^2-k_y^2}} \mathrm{d}k_x \mathrm{d}k_y \right\}, \tag{4.36}$$

where the integration is done over the real-valued wavenumber components. The vectors $\dot{\mathbf{a}}$ and $\boldsymbol{\phi}$ contain the modal velocity amplitudes and the wavenumber representation of the modal shape functions according to

$$\dot{\mathbf{a}}^T = [\dot{a}_{1,1} \;\; \dot{a}_{1,2} \;\; \ldots \;\; \dot{a}_{n,m}], \tag{4.37}$$

$$\boldsymbol{\phi}^T(x,y) = [\phi_{1,1}(x,y) \;\; \phi_{1,2}(x,y) \;\; \ldots \;\; \phi_{n,m}(x,y)]. \tag{4.38}$$

The dimensions of these vectors depend on how many modes are considered in the calculations.

4.4 Numerical results

4.4.1 The efficiency of resonant shunt damping

The potential of any piezoelectric shunt damping treatment is governed by the piezoelectric material's ability to convert mechanical to electrical energy. The gen-

eralized electromechanical coupling factor is proportional to the fraction of the strain energy of the composite system, which is converted to electrical energy. The generalized electromechanical coupling factor for each mode can be defined as

$$K_{ij}^2 = \left(\frac{K_{jj}^E}{K_{jj}^E + K} \right) \left(\frac{k_{ij}^2}{1 - k_{ij}^2} \right), \tag{4.39}$$

where K is the modal stiffness of the host structure and K_{jj}^E the modal stiffness of the piezoelectric element under a short circuit condition. The generalized electromechanical coupling factor may be determined from experimental data by measuring the relative shift of the resonance frequency under a short and an open circuit condition respectively, according to

$$K_{ij}^2 = \left(\frac{(\omega_n^D)^2 - (\omega_n^E)^2}{(\omega_n^E)^2} \right), \tag{4.40}$$

where superscripts E and D denote short and open circuit respectively. Equation 4.39 shows that as long as the structural stiffness is larger than the piezoelectric modal stiffness the generalized electromechanical coupling coefficient increases if the piezoelectric stiffness increases. Hence, so does also the potential of more efficient shunt damping.

The reduction in modal peak amplitude for different values of the generalized electromechanical coupling factor, and different internal damping values of the host structure, is presented in Table 4.1. The numerical values are calculated with the model presented in *Section 4.3.3* using an inductive-resistive shunt.

The left column in the table shows that quite significant damping of the modal peak magnitude is achieved for reasonable values of K_{ij} for a lightly damped host structure, i.e. $\eta = 0.001$. For a host structure with very low internal damping, even small counteracting forces from passive shunt treatments can significantly increase the system damping [99]. However, many practical structures have considerable internal damping. If the loss factor of the host structure is increased, the reduction in the structural response which can be achieved by adding shunt damping is significantly decreased. The right column in Table 4.1 shows the reduction in peak magnitude if the internal damping of the host structure is increased 10 times, i.e. $\eta = 0.01$. It is clear that as the internal damping of the host structure is increased, the additional reduction due to the shunt is significantly decreased.

Table 4.1: The reduction in peak amplitude of the first mode for different values of the generalized electromechanical coupling factor and different loss factors (η) of the host structure. The reduction is given in dB relative to the short circuit case.

K_{ij}^2	$\eta = 0.001$	$\eta = 0.01$
0.01 %	-17.1 dB	-3.9 dB
0.11 %	-27.4 dB	-10.0 dB
0.53 %	-34.1 dB	-15.4 dB
1.02%	-37.2 dB	-18.3 dB

4.4.2 Parameter study of LR shunts

The reduction in modal peak magnitudes presented in table 4.1 have been all been based on tuning the shunt to a specific mode according to the design approach presented by Hagood and von Flotow [64]. However, the response of a structure often consists of several modes with different amplitudes. Further, if the shunt ought to be designed to reduce the radiated sound power, a weighted sum of several modes needs to be considered. In fact, at a particular frequency it may not be the mode with the closest eigenfrequency which is driving the radiation, at least below the critical frequencies where the radiation efficiencies of the modes may differ substantially. *Paper* IV presents a comprehensive parameter study, calculated with the model presented in *Section 4.3.3,* of how different inductive-resistive shunts affect the kinetic energy and sound radiation of a plate. The shunts which minimize the kinetic energy of the plate and the sound radiation respectively are compared and discussed. The position of the piezoelectric element is also varied so that it is either optimally located to damp the efficiently radiating odd-odd modes and no other modes, or so that it may provide some damping for all modes. The key results from *Paper* IV are summarized here.

Figure 4.9 shows the total sound power (TSP) as a function of different LR shunts. The total sound power is calculated by summing the spectral components of the sound power over the considered frequency range. The TSP is given in dB relative to the short circuit case. In the left figure the piezoelectric element is located at the centre point of the plate where all odd-odd modes suffer maximum strain, while the other modes suffer no strain. This location is optimal for damping the odd-odd modes but provide no damping for the other modes. In the right figure the piezoelectric element is collocated with the primary disturbance at a location where all modes could be damped some. The first nine eigenmodes are included in the model, and the primary disturbance force is positioned so that all modes are excited with similar peak amplitudes. The geometry and material properties of the

host structure and piezoelectric element are given in Tables 1 and 2 in *Paper* IV. In Figures 4.9 are also marked the shunts which minimize the response of the first mode and the total kinetic energy (TKE), referred to as the modal shunt and TKE shunt respectively. The TKE is defined analogously to TSP.

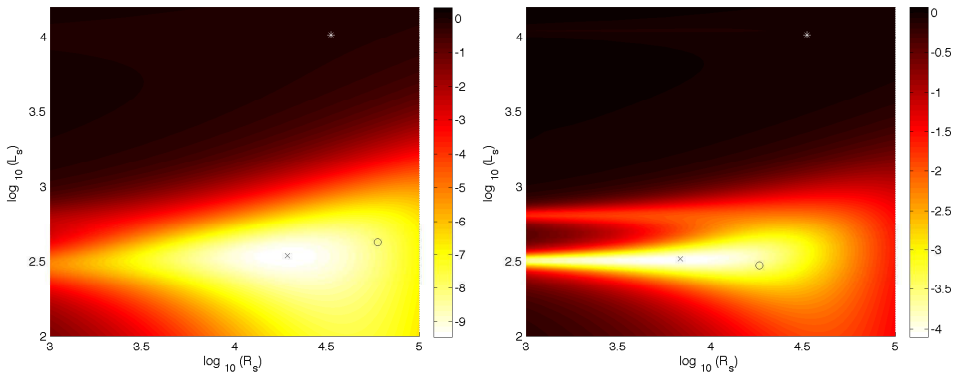

Figure 4.9: The total sound power (TSP) normalized to the short-circuited case as a function of the inductance and resistance. The $\times$, $\circ$, $*$ mark the inductance and resistance of the TSP, TKE and modal shunts respectively. Left: The piezoelectric element centered on the plate. Right with the piezoelectric element collocated with the primary disturbance force

Figures 4.9 (left) and (right) shows that the TSP and TKE shunts are relatively similar, while the modal shunt differs from them quite a lot. The TKE shunt has a larger resistance than the TSP shunt, which gives less efficient but more broadband damping. The TSP shunt gives about 9 dB and 4 dB reduction of the TSP respectively if is centered on the plate or collocated with the primary disturbance. The relatively broad region of a TSP around negative 8-9 dB shows that the TSP shunt is relatively insensitive to small changes in the inductance and resistance. Small parameter variations will not degrade the reduction of the TSP in a significant wave. This is contrary to modal shunt damping where the shunt is very sensitive to small parameter variations. The inductance of the TSP shunt is insensitive to the location of the piezoelectric element. This can be expected because the stiffness added by the piezoelectric element does not shift the modal eigenfrequencies significantly. The TSP shunt is more efficient if the piezoelectric element is centered on the plate. With this location the odd-odd modes can be well damped and these modes are the most efficient radiators below the critical frequency. The shunt which minimizes the TSP in this case is not tuned to any specific mode. In fact the inductance of this shunt is tuned somewhere in between the eigenfrequencies of mode (3,1) and (1,3).

Figure 4.10 shows the sound power as function of frequency for the TSP, TKE- and modal shunt compare to the short circuit case. The figure shows that the TSP shunt effectively reduces the sound power around the eigenfrequencies of modes (3,1) and (1,3). A similar behaviour is shown for the TKE shunt. It is important to mention that these results are calculated for a plate with very low inherent losses, a loss factor of 0.1% ($\eta = 0.001$). If the loss factor of the plate is increased to damping performance of these shunt are severely diminished. As the TSP shunt is not tuned to a specific mode it is relatively insensitive to small changes in the inductance or resistance; see figures 4.9 (left) and (right). The modal shunt is efficient at reducing the sound power around the eigenfrequency of the first mode, but simply shifts the eigenfrequencies of the higher modes; see Figure 4.10. As the modal eigenfrequencies are under the critical frequency, this will increase the radiation at these frequencies. However, as can be seen in Figure 4.10 (b) this effect is not significant.

Table 3 in *Paper* IV sumarizes the results from figure 4.9, that below the critical frequency placing the piezoelectric element in the centre of the plate is more advantageous for the TSP shunt. However if the objective is to reduce the TKE it is better to place the piezoelectric at a point where several modes can be effected by the shunt. If the eigenfrequencies appear above the critical frequencies though it is more efficient to place the piezoelectric at a point where all modes can be effected, in terms of reducing both the TSP and the TKE; see table 4 in *Paper* IV. This highlights the fact that the optimal shunt location does not only depend on the purpose of the damping treatment but also on the properties of the structure. Thus when implementing shunt damping it is vital to have proper knowledge of the physical behavior of the structure as well as the shunted piezoelectric element.

4.5 Experimental implementation of LR shunt damping

4.5.1 Untreated beams

An experimental investigation of shunt damping applied to a beam is presented here. These experiments are conducted in order to verify the beam model presented in *Section 4.3.4*. Ast he plate model is constructed based on the same principles as the beam model, it can be assumed to be quite accurate if the beam model is experimentally validated. The beam used in the experiments was of aluminium, 0.4 m long and suspended by a soft spring in one end to simulate a free-free condition. The primary disturbance force was given by an electrodynamic shaker at one of the

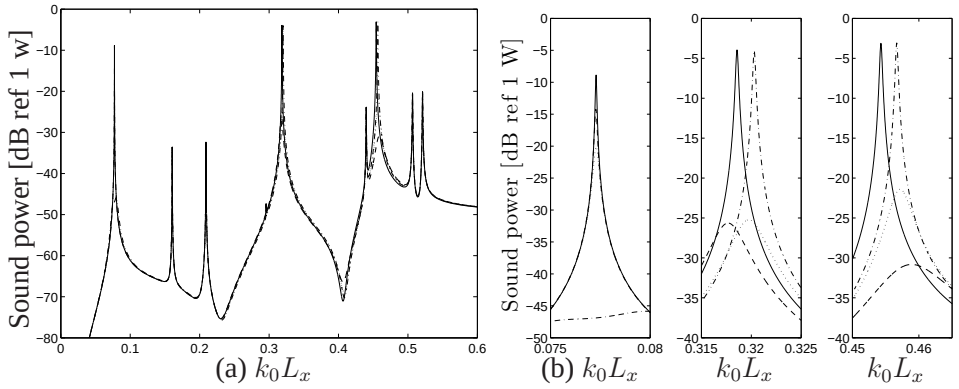

Figure 4.10: (a) The radiated sound power. (b) The radiated sound power around the eigenfrequencies of the odd-odd modes (1,1);(3,1);(1,3). $-$: short-circuit; - - -: the TSP shunt; $\cdots\cdots$: the TKE shunt; - $\cdot$ -: the modal shunt. The piezoelectric element is centered on the plate.

beam ends, and the acceleration was measured at the same location. A photo of the set-up is shown in Figure 4.11.

Figure 4.12 shows the measured and calculated driving point mobility of the beam. The mobility was calculated with the model presented in *Section 4.3.4*, excluding the piezoelectric element, i.e. setting $K_n^{\text{pzt}} = M_n^{\text{pzt}} = 0$ in equation 4.29. The properties of the beam are given in Table 4.2.

Table 4.2: The properties and geometry of the beam used in the experiments.

E_b	ρ	L	b	t
73 GPa	2800 kg/m^3	400 mm	30 mm	2.7 mm

4.5.2 Effect of bonding

In the theoretical models, the piezoelectric element was assumed to be perfectly bonded to the host structure. In practice, though, the piezoelectric element needs to be attached to the host structure by using an adhesive. Two different types of adhesives were used to attach the piezoelectric element, one electrically insulating (EPO-TEK 301-2) and one electrically conducting (EPO-TEK E4110). Four composite beams were constructed, two using the insulating adhesive (referred to as beams i1 and i2) and two using the conductive adhesive (c1 and c2). The conductive adhesive has the advantage that no connector had to be placed between the

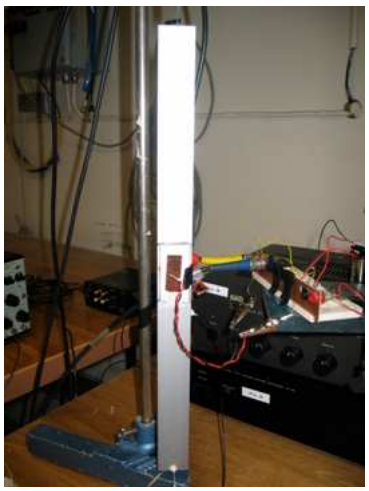

Figure 4.11: A photograph of the experimental set-up.

piezoelectric element and the host structure. The purpose of this was to create a better bonding surface. Table 4.3 shows the effect of the adhesive on the generalized electromechanical coupling factor, calculated with equation 4.40, for the odd modes for the different beams. The piezoelectric element was centred on the beam and thus only the odd modes could be significantly affected. The table shows that there are some variations between the different beams. The difference between the beams with the same adhesive is just as large as, or larger than, the difference between the beams with different adhesives. However, the sample is too small to draw any statistically significant conclusions.

Table 4.3: Measured generalized electromechanical coupling factor for the different beams.

Mode:	K_{31} mode 1	K_{31} mode 3	η mode 1	η mode 3
bare:	-	-	0.36 %	0.36 %
i1:	0.060	0.085	2.8 %	1.1 %
i2:	0.071	0.068	1.5 %	1.0 %
c1:	0.085	0.068	1.2 %	1.0 %
c2:	0.074	0.085	3.1 %	0.6 %

Figures 4.13 (a) and (b) show the measured point mobilities of the four different beams. Figure 4.13 (a) shows that the point mobility of the different beams are

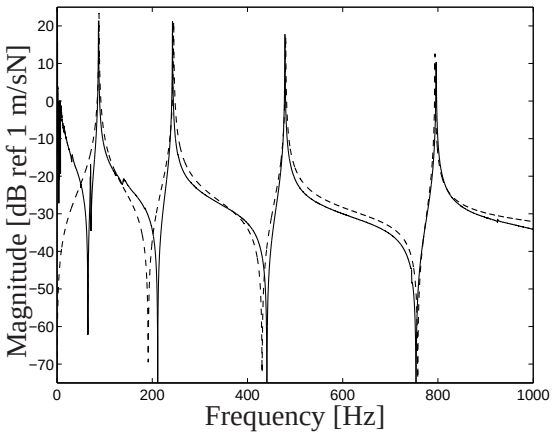

Figure 4.12: The driving point mobility of a 0.4 m long free-free aluminium beam. −: measurement; ·····: model.

very similar, but Figure 4.13 (b) reveals that there are are small differences in amplitude and frequency at the first resonance. Bonding the piezoelectric element to the structure adds damping due to the adhesive layer which effects the amplitude at the resonance frequency. The treatment will in practice work as a passive constrained layer and augment structural damping due to shear losses in the adhesive bond. Due to the location of the piezoelectric element, it is mainly the odd modes which are affected. The modal loss factors were calculated from the measured mobilities by using modal circle fitting. By calculating the modal loss factors of the first and third modes of the untreated beam and the beam with the bonded piezoelectric element, the additional losses due to the adhesive layer could be estimated; see Table 4.3. The modal loss factors are substantially increased by the bonded piezoelectric element. Just as for the generalized electromechanical coupling factors, there is a large spread between the beams. The small differences in resonance frequencies suggest that there are also individual differences in stiffness and/or mass in the beams and piezoelectric elements.

4.5.3 Open and short circuit conditions

The driving point mobility of the beam was measured under a short circuit and an open circuit condition respectively in order to derive the generalized electromechanical coupling factor according to equation 4.40. The properties of the piezoelectric patch are given in Table 4.4. The measured driving point mobility under a short circuit condition compared to the results calculated with the beam model is shown in Figure 4.14. The figure shows that the model agrees well with the measurements. The piezoelectric coupling factor k_{31} in the model was tuned so

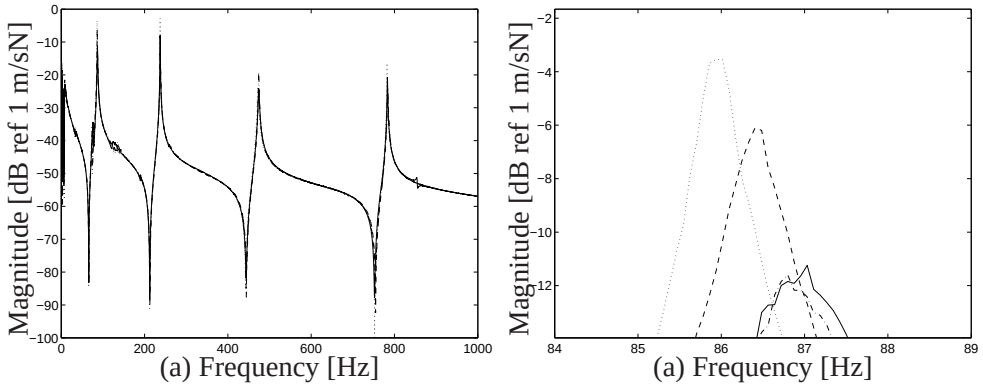

Figure 4.13: The driving point mobility of the four beams under a short circuit condition: (a) 0-1000Hz, (b) a zoom around the first resonance frequency. −: I1; - - -: I2; ·····: C1; - · -: C2

that the generalized electromechanical coupling factor in the model agrees with the measured one. The reason that this tuning is needed is because the piezoelectric element is not perfectly bonded as assumed in the model. The figure shows that it works well to model the piezoelectric-beam composite by using equation 4.29, if the additional damping due to the adhesive layer is accounted for and the piezoelectric coupling factor k_{31} is tuned. Comparing Figure 4.14 with Figure 4.12 one can se that the most obvious difference between the bare beam and the beam with a bonded piezoelectric element is the damping effect due to the bond. Although, closer inspection reveals small shifts in the resonance frequencies of the odd modes. It may be mentioned that modelling approaches exist where the adhesive layer is included; see e.g. reference [100].

The discrepancy between model and measurements at low frequencies is most likely due to a rigid body mode appearing in the measurement due to the suspension of the beam.

Table 4.4: The properties and geometry of the piezoelectric element used in the experiments.

E_p	ρ_p	l_a	b	t_p	C_p^{ε}
58.8 GPa	7200 kg/m^3	50 mm	25mm	1mm	18.06 nF

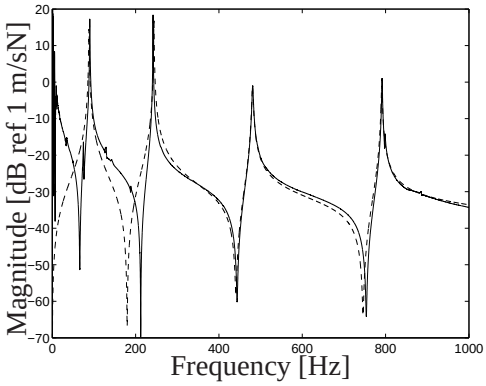

Figure 4.14: The driving point mobility under a short circuit condition. −: measurement; - - -: model

4.5.4 Shunt damping of the first and third bending modes

The experimental set-up was used to implement modal shunt damping. The shunt circuit was implemented by using the synthetic admittance concept proposed by Fleming et al. [76] which was briefly explained in *Section 4.2.3*. The schematic figure of the synthetic shunt circuit is shown in Figure 4.15. The synthetic shunt was implemented on the digital signal processor (DSP) as an admittance transfer function according to

$$Y(s) = \frac{1}{Ls + R}, \tag{4.41}$$

where L and R are the shunt inductance and resistance respectively. The DSP was a *dspace* system with a sampling frequency of $F_s = 4000Hz$. The resistor R_g in Figure 4.15 sets the transconductance gain as $1/R_g$ A/V. The resistor was chosen as $R_g = 1000\,\Omega$, and a corresponding gain was set on the DSP. The input to the DSP was highpass filtered and the output was lowpass filtered to remove access frequencies from the signal.

Figure 4.16 shows the measured and modelled driving point mobility around the first and third resonance frequencies when shunt damping was implemented, compared to the measured driving point mobility under a short circuit condition. The optimal resistance and inductance were chosen according to the design concept of Hagood and von Flotow [64] (*Section 4.2.2*), and are shown in Table 4.5. Figure 4.16 shows that the amount of damping which can be achieved in practice is very well predicted by the model, although the model slightly overestimates the damping. The first and third modes were damped by about 15 dB and 20 dB respectively at their eigenfrequencies. The experimental results shows that the beam model

presented in *Section 4.3.4* works well in describing damping by a surface bonded shunted piezoelectric element. This also suggest that the plate model presented in *Section 4.3.3* is accurate, as it is derived using the same principles.

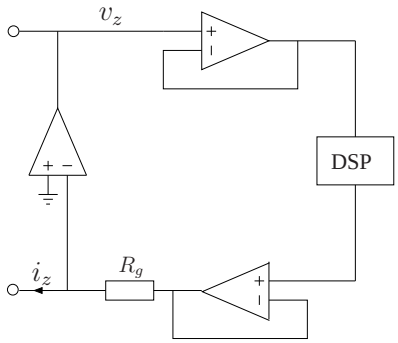

Figure 4.15: A schematic figure of the implementation of the synthetic admittance circuit.

Table 4.5: The shunts which were implemented to damp the first and third modes respectively on the beam.

Mode:	L	R
1	172 H	9830 Ω
3	6 H	1749 Ω

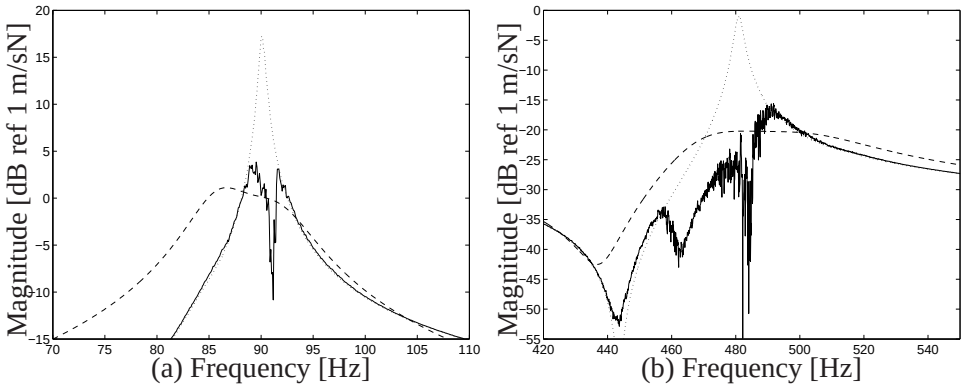

Figure 4.16: The driving point mobility: (a) zoomed around the first resonance frequency; (b) zoomed around the third resonance frequency. —: measurement; - - -: model; ·····: measured under a short circuit condition.

Chapter 5

Active shunts and hybrid piezoelectric vibration control

Shunt damping as presented in the previous chapter have some limitations such as shunt detuning due to temperature changes or the relative narrowband damping characteristics. Some of the limitations can be overcome by allowing the shunt to be active. Adding a voltage or current source in the electrical network of the shunted piezoelectric element forms a hybrid active-passive vibration control system. This approach has proved to have several advantages over conventional active vibration control, e.g. reduced control effort or improved fail-safe characteristics. Similarly to passive shunt damping most studies on piezoelectric hybrid damping have focused on one single vibration mode. This chapter provides a model of a plate with surface bonded piezoelectric element which is connected to an external voltage source in series with an inductive-resistive shunt. The piezoelectric hybrid damping treatment is evaluated in terms of both the plate's structural response and radiated sound power including several structural modes. The model is used to identify particular situations where hybrid damping can provide advantages compared to pure active control or pure passive damping. Compared to active control a hybrid system may for example help reduce spillover effects, i.e. energy leakage into uncontrolled modes, and/or reduce the control effort.

5.1 Active or semi-active shunt damping

There are several techniques for improving the performance of passive shunts. Two common approaches are to adaptively updating the shunt in order to avoid detuning, and to use a negative-capacitance shunt in order to improve the broadband damping of the shunt. Updating the shunt circuit is here considered as and active or semi-active technique as it requires variable components and possibly additional sensors. A negative capacitance cannot be constructed by using passive components only. They are usually implemented using op-amp which require power supply and are

therefore here regarded as active shunts. The following two subsections briefly explain adaptive shunts and negative-capacitance shunts.

5.1.1 Adaptive shunt tuning

As was mentioned in the previous chapter, a major disadvantage with resonant shunt damping is the sensitivity to slight variations in the capacitance of the piezoelectric element or in the eigenfrequencies of the host structure, as this will detune the shunt. Moheimani and Fleming [81] report that the damping performance of a resonant shunt circuit diminished from 14 dB to only 4 dB due to a 40-degree temperature change. However, by adaptively updating the shunt, detuning can be prevented and the damping performance ensured. As briefly mentioned in *Section 4.2.2* there are different ways of updating the shunt components in order to ensure the damping performance of the shunt.

Hollkamp and Starchville [101] presented a self-tuning shunt based on the RMS voltage across the shunt. They used an adjustable resistor in the form of a motorized potentiometer to adjust the value of a virtual inductance. Fein and Gaul [102] used a digital potentiometer to adjust the resistance of a purely resistive shunt. Fleming and Moheimani [73] used a synthetic shunt impedance and a reconstructed estimate of the RMS strain. They experimentally implemented a two-mode current-flowing adaptive shunt circuit to damp the second and third modes of a pinned-pinned beam. The shunt provided 22 dB and 19 dB reduction of the response around the second and third eigenfrequencies [73].

Niederberger et al. [74] made an electrical equivalent model of the host structure and recognized that the phase shift between the host structure velocity and the current in the shunt circuit can be used to tune a LR shunt. At the tuning frequency, i.e. $\omega = 1/\sqrt{LC}$, this phase shift was exactly $\pi/2$. The adaptive shunt circuit was tested experimentally on a cantilever beam. The adaptation proved successful in compensating both temperature variations in the piezoelectric element and changes in the eigenfrequency of the host structure. Simulation results showed that the adaptive shunt based on the relative phase was faster in tuning to changes in structural eigenfrequencies than an adaptive technique based on the RMS strain [74]. However, the approach requires a sensor on the host structure to monitor the velocity. Niederberger also developed this approach for adaptive electromagnetic shunt damping [103].

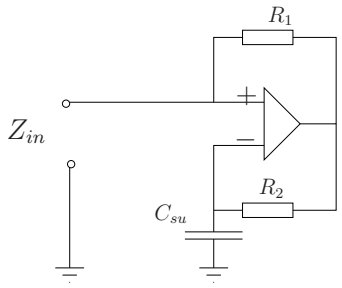

Figure 5.1: A negative-capacitance converter. The impedance seen from the terminal is equivalent to a negative capacitance, $Z_{in} = -\frac{R_1}{R_2}C_{su}$

5.1.2 Negative capacitor shunt impedances

If the internal voltage produce by the stressed piezoelectric element is interpreted as a power supply and the shunt impedance as a load, the maximum power transfer concept may be used [81] to convert a maximum amount of structural energy into electrical energy. The electrical energy can than be dissipated by resistive elements. This can add broadband damping to a structure. The optimal shunt impedance should then be equal in magnitude to the source impedance but opposite in phase. As the piezoelectric element electrically behaves as a capacitance, a negative capacitance is required as shunt impedance. A negative capacitance cannot be constructed by using only passive components, and can thus be regarded as an active or semi-active technique. However, it is in principle an easy circuit to construct and no additional sensors are needed. An example of a negative-capacitance converter is shown in Figure 5.1. The implementation requires an op-amp and does therefore need a power supply. The maximum power transfer principle does not apply to circuits with internally dependent sources, thus derivation of the shunt impedance needs to be modified [81]. Moheimani and Fleming [81] presented a technique for a negative-capacitance shunt based on their concept of synthetic impedances; see *Section 4.2.3*. They notice that choosing the shunt impedance as a negative copy of the impedance of the piezoelectric element is equal to making the closed loop dynamics zero. However, they point out that this is equivalent to a strain feedback controller of infinite gain and therefore not realizable. As a consequence, the synthetic shunt capacitance is made slightly greater than the inherent capacitance of the piezoelectric element. The negative-capacitance shunt was successfully implemented in experiments [104, 81]. Other studies of negative-capacitance shunts include [105, 85, 106].

5.2 Hybrid piezoelectric control

Hybrid piezoelectric control is here defined as connecting both a passive electric network and an active source to the piezoelectric element. Thus, though such a configuration, energy can be passively dissipated in the electrical network, and the piezoelectric element may be driven like an actuator by the active source. The active source can e.g. be a voltage or a current source.

Adachi et al. [107] presented an investigation of hybrid piezoelectric damping using an active voltage source in series with a tuned LR shunt. The shunt circuit was treated as a filter and the control gains and shunt components were determined using linear quadratic (LQ) control theory. They showed that the control effort of the hybrid system was decreased, compared to a purely actively driven piezoelectric element. Agnes [108] investigated the difference in driving an LR shunted piezoelectric element with a charge or current source. He pointed out that the purpose of the shunt, other than reducing the modal response, was to increase the effectiveness of the actuator close to its tuning frequency. He also reported that, in the case of voltage driving, the shunt works as a filter causing a faster roll-off at high frequencies, which could reduce the risk off control spillover [108].

Tsai and Wang [109] also pointed out that the shunt of a piezoelectric hybrid system could improve the control authority of the actuator close to the tuning frequency. In order to determine the control gains and optimal shunt, they formed a quadratic cost function of the weighted control effort and control performance. They investigated how the optimal shunt varied with different weightings and showed that, if the weighting on the control effort is reduced, the shunt approaches a short circuit and the hybrid system approaches a purely active system; and if the weighting on control effort was increased, the shunt approached the optimal passive shunt as the hybrid system approached a purely passive shunt.

Tang and Wang [110] investigated the influence of the generalized electromechanical coupling coefficient (see equation 4.39) on the passive damping performance and control authority of a hybrid system where a resonant shunt was optimally tuned for passive damping. They also showed that the generalized electromechanical coupling coefficient could be increased by using a negative capacitance circuit. Ozer and Royston [111] extended their approach of using the Sherman-Morrison matrix inversion theorem for choosing the shunt to piezoelectric hybrid damping. Just as for their study on the passive shunt [84], it was pointed out that the standard method for shunt tuning based on the work by [64] has limitations, since it neglects the system's inherent damping and the response from adjacent modes.

Using the synthetic impedance or admittance approach described in section 4.2.3, the system of host structure with a bonded shunted piezoelectric element may be interpreted as a feedback control problem. The shunt impedance can then be determined by using standard regulator design approaches such as LQG, $\mathcal{H}_2$ and $\mathcal{H}_\infty$ control synthesis [112, 99, 81]. As the shunt impedance is no longer confined to being passive, the shunt can be much more effective in control structures with significant inherent damping [112].

The mentioned studies consider only one or possibly two vibration modes. Further, the shunt is often designed using some predefined design criterium. Thus, it is not straightforward to draw conclusions on how different shunts will affect e.g. the control performance or control effort of a hybrid system over a wide frequency range. This chapter presents a model of hybrid piezoelectric damping where an active voltage source is connected in series with an inductive-resistive shunt. The piezoelectric element is assumed perfectly bonded on a structural plate. The purpose is to identify and investigate situation where hybrid damping might be advantageous compared to pure active control. A parameter study is performed in order to find the shunt which e.g. gives the lowest control effort over a wide frequency range including four structural modes. A beam model is developed in order to verify the modelling approach. The beam model is compared against measurement for active driving of the piezoelectric element.

5.3 Modelling piezoelectric actuation

5.3.1 Various modelling approaches

Several studies have presented models of piezoelectric elements bonded to structures and used for sensing vibrations and/or actuating vibrations. Crawley and de Luis [113] showed that the influence on a beam-like structure by the piezoelectric element driven by an external voltage could be included as edge moments at the boundaries of the piezoelectric element. The same approach was presented for plate-like structures by Dimitriadis et al. [114]. These models are based on static relations, i.e. the inertial forces due to the mass of the piezoelectric element are neglected. They also neglect the local increase in stiffness due to the mechanical stiffness of the piezoelectric element. Recently models including both the inertia and increased local stiffness have been developed [95].

5.3.2 Hysteresis

The constitutive relation in equation 4.6 as well as the models presented in the succeeding sections are all based on considering the piezoelectric elements as being governed by linear relations. This is generally true for many applications, but for high driving-volatges the piezoelectric elements may experience hysteresis, i.e. the relationship between the mechanical stress or strain and the electric field or displacement is no longer linear; see e.g. references [115, 116]. Non-linear effects may severely degrade the damping performance and control stability of control systems with piezoelectric transducers [117]. Several techniques have been presented to decrease the non-linear effects, e.g. the hysteresis effect is reduced when the piezoelectric element is driven by charge or current instead of voltage. Both current and charge driving have been successfully implemented in experiments [118].

5.3.3 Plate model

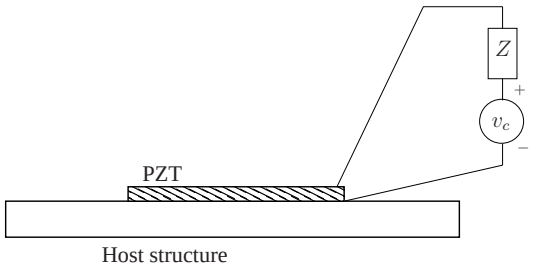

Figure 5.2: A host structure with a surface-bonded piezoelectric element (PZT) which is shunted by a passive impedance (Z) and an active voltage source v_c.

The plate model presented in this section is similar to the one presented in the previous chapter. However, in addition to shunting a piezoelectric element by a passive electrical network, a voltage source is added in series to the shunt; see Figure 5.2. This forms a hybrid active-passive vibration control system. In order to model the hybrid damping treatment, the shunt network is not included in the material compliance as in the previous chapter. Instead and electrical model of the piezoelectric element, the shunt and the voltage source is used; see Figure 5.3. The voltage source is assumed to drive the piezoelectric element at moderate voltages, hence linear relations for the piezoelectric element can be used. Considering the piezoelectric element as a voltage source in series with a capacitance, as in reference [81], an expression for the terminal voltage (v_3) can be found as

$$v_3(s) = \frac{v_c(s) - Z_s(s)v_p(s)c_p s}{1 + Z_s(s)c_p s} = g_c v_c + g_{su} v_p, \tag{5.1}$$

where s is the Laplace variable, and where $g_c = 1/(1 + Z_s C_p s)$ and $g_{su} = -Z_s c_p s/(1 + Z_s c_p s)$. The voltages v_c and v_p describe the control voltage and voltage produced by the stressed piezoelectric element respectively, Z_s describes the shunt impedance and c_p the inherent capacitance of the piezoelectric element. The voltage produced by the stressed piezoelectric element, v_p, is found by integrating the charge over the area of the piezoelectric element and can be expressed as

$$v_p = \frac{d_{31}}{c_p} \iint_a (\sigma_1 + \sigma_2) \mathrm{d}\mathbf{a}, \tag{5.2}$$

where a is the area of the piezoelectric element.

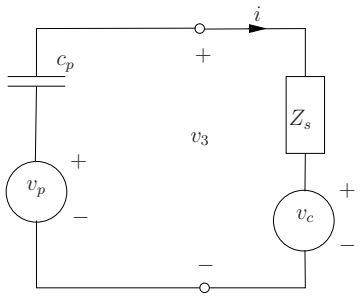

Figure 5.3: The electrical model of the piezoelectric element, shunt impedance (Z_s) and external voltage source (v_c). v_p and c_p is the voltage produced by the stressed piezoelectric element and its inherent capacitance respectively, and v_3 is the terminal voltage and i is the current.

By including a voltage across the piezoelectric element in the derivations, equation 4.12 is replaced by

$$D\nabla^4 w(x,y,t) + m'' \frac{\partial^2}{\partial t^2} w(x,y,t) + \Gamma_{w,\Omega} = q(x,y,t) + q_{\text{pzt}}(x,y,t), \tag{5.3}$$

where

$$q^{\text{pzt}} = v_3 d_{13} D_{pc} (1 + \nu_p) \nabla^2 \Omega(x,y), \tag{5.4}$$

where d_{31} is the piezoelectric strain constant. The term D_{ps} is defined as

$$D_{pc} = \frac{E_p t_{pc}}{1 - \nu_p}, \tag{5.5}$$

where $t_{pc} = \frac{t_k + t_p}{2}$. The derivation of equation 5.3 can be found in *Paper* V. The term $\Gamma_{w,\Omega}$ in equation 5.3 does here only include the mechanical stiffness of the

piezoelectric element and no shunt effects, and is derived and explained in *Paper V*. This term is often neglected and is only included here to be coherent with the model in *Chapter 4*. For the purposes of this study, it has no significant effects. Excluding this term will simply shift the eigenfrequencies slightly downward in the spectrum as the composite structure becomes less stiff. Equation 5.3 is solved by a modal approach, for a simply supported rectangular plate, and gives the deflection field according to

$$w(x,y,\omega) = \sum_{n}^{\infty}\sum_{m}^{\infty} \frac{Q_{n,m}^{\text{ext}} - Q_{n,m}^{\text{pzt}}}{M_{n,m}\left(\omega_{n,m}^2 - \omega^2\right) + K_{n,m}^{\text{pzt}} + \Xi_{n,m}^{\text{pzt}}} \sin(k_n x)\sin(k_m y). \tag{5.6}$$

The term $K_{n,m}^{\text{pzt}}$ does here only describe the mechanical stiffness of the piezoelectric element and does not include the shunt effects. The modal complex stiffness due to the shunt is instead included in $\Xi_{n,m}^{\text{pzt}}$. The force due to the voltage driving of the piezoelectric element is given by

$$\begin{aligned} Q_{n,m}^{\text{pzt}} &= \iint_S g_c v_c d_{13} D_c (1+\nu_p) \nabla^2 \Omega(x,y) \phi_{n,m} \mathrm{d}\mathbf{S} \\ &\approx g_c v_c d_{13} D_c (1+\nu_p)(k_n^2 + k_m^2) l_x l_y \sin(k_n x_c)\sin(k_m y_c). \end{aligned} \tag{5.7}$$

The modal stiffness due to the shunt is given by

$$\begin{aligned} \Xi_{n,m}^{\text{pzt}} &= \iint_S g_{su} v_p d_{13} D_c (1+\nu_p) \nabla^2 \Omega(x,y) \phi_{n,m} \mathrm{d}\mathbf{S} \\ &\approx g_{su} \frac{k_{13}^2}{1-k_{13}^2} D_{pc} (k_n^2 + k_m^2)^2 a \sin^2(k_n x_c)\sin^2(k_m y_c). \end{aligned} \tag{5.8}$$

The modal mass, disturbance force and modal stiffness due to the shunted piezoelectric element are defined in equations 4.18, 4.20 and 4.19 respectively. The approximation in equations 5.7 and 5.8 comes again from assuming that the piezoelectric element is small compared to the bending wavelength.

5.3.4 Beam model

A beam model is derived using the same modelling approach as for the plate. The beam model is used in order to verify the model against measurements. The model is derived for pure driving of the piezoelectric element and not hybrid damping. The beam model with a surface bonded piezoelectric element, presented in *Section 4.3.4*, can be extended to including an external electric field. By including an external electric field (in this case a voltage) in the derivations of the differential

equation an additional term appears and equation 4.23 is replaced by

$$\begin{aligned} &EI\frac{\partial^4}{\partial x^4}w(x,t) + m'\frac{\partial^2}{\partial t^2}w(x,t) \\ &+ E_p b_p t_c \left(\frac{\partial^4 w}{\partial x^4}\Omega(x) + 2\frac{\partial^3 w}{\partial x^3}\Omega'(x) + \frac{\partial^2 w}{\partial x^2}\Omega''(x)\right) \\ &+ m'_p\frac{\partial^2}{\partial t^2}w(x,t)\Omega(x) = q(x,t) + q_{pzt}, \end{aligned} \tag{5.9}$$

where

$$q_{pzt}(x,t) = v_3 d_{13} E_p t_c \left[\delta'(x-x_1) - \delta'(x-x_2)\right], \tag{5.10}$$

where δ' is the derivative of the Dirac function. Equation 5.9 is similar to the standard equation for modelling piezoelectric driving as found in reference [12]. However, equation 5.9 includes mass- and stiffness effects of the piezoelectric element. Inserting equation 5.10 into equation 5.9 using a modal approach to solve for the deflection field yields

$$w(x,\omega) = \sum_n^\infty \frac{Q_n^{\text{ext}} + Q_n^{\text{pzt}}}{M_n\left(\omega_n^2 - \omega^2\right) + \left(K_n^{\text{pzt}} - \omega^2 M_n^{\text{pzt}}\right)}\phi_n(k_n x). \tag{5.11}$$

Equation 5.11 contains an extra terms compared to equation 4.29, describing the actuation by the control voltage (Q_n^{pzt}). The modal force due to the external voltage source can be expressed as

$$Q_n^{\text{pzt}} \approx v_c k_n^2 t_{pzt} b_p l_a E_p d_{31}\phi_n(x_c). \tag{5.12}$$

The modal shape functions ϕ_n for a free-free beam are given by equation 4.26. Equation 5.11 describes a free-free beam with a surface bonded piezoelectric element.

Figure 5.4 shows the transfer function between the terminal voltage and the velocity at one end of the beam. The figure shows that the model describes the beam motion well, especially around the eigenfrequencies of the first and third modes. The piezoelectric element is centred on the beam. However, as the second and fourth modes are weakly excited the piezoelectric element is slightly off-centre. The beam and piezoelectric element have the same properties and geometry as in *Section 4.5*. The model has been tuned some in order to get the correct level of the transfer function. This is due to that the piezoelectric element is not perfectly bonded as assumed in the model.

Including the mass and stiffness in equation 5.9 was done in order to be coherent with the previous chapter. However, neglecting these will lead to very similar results except a slight increase in magnitude of the transfer function. As the model

is anyway slightly tuned in order to get the correct level of the transfer function magnitude, in practice the mass and stiffness in equation 5.9 could have been neglected. Aoki et.al. showed that including the stiffness effects of the piezoelectric element bonded to a plate results in a transfer function between driving voltage and plate response which decreased compared than when these effects are excluded [95]. However, the frequency behavior of the transfer functions with and without the stiffness effects were very similar, as long as the bending wavelength was significantly larger than the size of the piezoelectric element. They also showed that including the mass of the piezoelectric element only affected the transfer function for high frequencies.

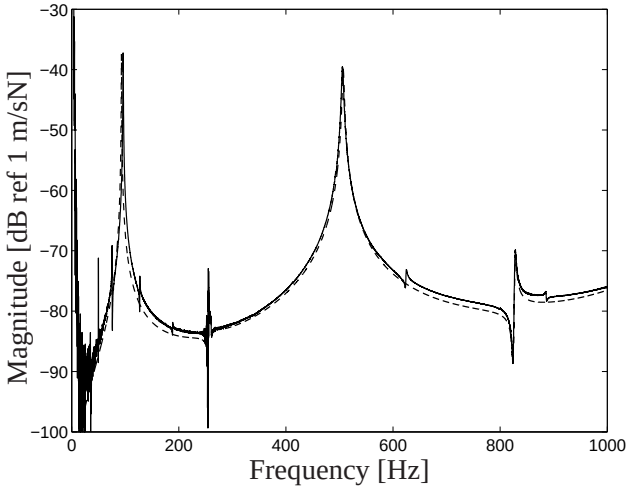

Figure 5.4: The transfer function between voltage applied to the terminals of the piezoelectric element and the velocity at one end of the beam. −: measurements; - - -: model

5.3.5 Control law for the active voltage source

The control voltage may be determined in several ways, e.g. by measuring the current in the shunt circuit; as in the case of the synthetic impedance [81]; or by a structural sensors [115]. A control law is defined, based on what is desirable to achieve for the specific case. In order to ensure global vibration control of the plate, a straightforward control law is to minimize the kinetic energy. The kinetic energy can be expressed in terms of the structural modes according to [12]:

$$E_k(\omega) = \frac{M\omega^2}{4}\mathbf{a}^H\mathbf{a}. \tag{5.13}$$

The modal amplitudes can be written as a sum of the contribution of the primary excitation and control voltage respectively according to

$$\mathbf{a} = \mathbf{a}_p + \mathbf{b}v_c, \tag{5.14}$$

where $\mathbf{a}_p$ is a vector containing the modal amplitudes in the presence of only the primary disturbance, and $\mathbf{b}$ is a vector of transfer functions which relate the control voltage to the modal amplitudes. Substituting 5.14 into 5.13 gives

$$E_k(\omega) = |v_c|^2\mathbf{b}^H\mathbf{b} + v_c^*\mathbf{b}^H\mathbf{a}_p + v_c\mathbf{a}_p^H\mathbf{b} + \mathbf{a}_p^H\mathbf{a}_p. \tag{5.15}$$

E_k is a quadratic function which has a unique minimum given by

$$E_{k,0}(\omega) = \frac{M\omega^2}{4}\left(\mathbf{a}_p^H\mathbf{a}_p - \frac{\mathbf{b}^H\mathbf{a}\mathbf{a}_p^H\mathbf{b}}{\mathbf{b}^H\mathbf{b}}\right), \tag{5.16}$$

for the control voltage given by

$$v_{c,0}(\omega) = -\frac{\mathbf{a}_p^H\mathbf{b}}{\mathbf{b}^H\mathbf{b}}. \tag{5.17}$$

This control law requires that the primary disturbance is known. This may be unrealistic in many practical cases but serves the purpose of the investigation well, i.e. identify situations where hybrid piezoelectric sound and vibration control can be advantageous compared to pure active control or passive damping. The kinetic energy of the plate and the radiated sound power with and without active control are shown in Figures 5.5 (upper) and 5.5 (lower) respectively. The piezoelectric element was collocated wit the primary disturbance at $(x_c; y_c) = (L_x/4; L_y/4)$. The figures show that the energy of the plate is efficiently reduced over the entire considered frequency range. Reducing the kinetic energy of the plate naturally leads to a reduction in the radiated sound power.

The results in Figure 5.5 are calculated with the optimal frequency domain results given by equation 5.17; thus there are no guarantees that the filter is realizable. Further, this controller requires that modal amplitudes can be exactly measured, something which is hard to achieve in practice. However, it has been shown that the kinetic energy can be efficiently reduced by considering the sum of responses at several spatial points; see references [12, 51] for minimizing the kinetic energy on a beam or [119] for minimising the far field sound pressure.

5.3.6 Parameter study of LR-shunt for hybrid piezoelectric damping

This section will provide examples of some cases where hybrid active-passive piezoelectric damping might be advantageous compared to pure active control.

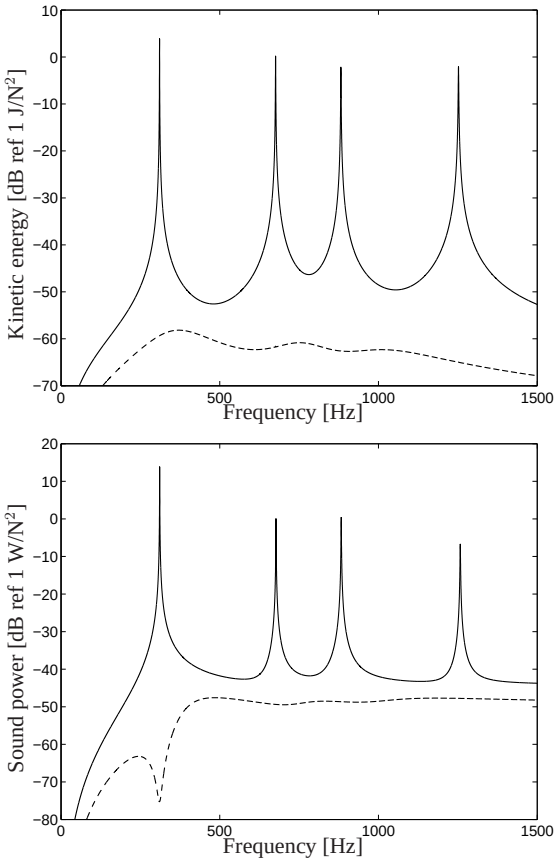

Figure 5.5: Upper: The kinetic energy of the composite plate. Lower: The sound power of the composite plate. No control (−) compared to active control (- - -) .

Previous literature have identified positive effects of having and inductive-resistive shunt together with active driving of the piezoelectric element, e.g. an improved control authority around the tuning frequency.

The control law presented in the preceding section for active voltage driving efficiently reduces the kinetic energy of the plate; see Figure 5.5. Thus, in this ideal case, additional damping provided by a shunt network may not be very interesting. However, there are other advantages that the shunt network can contribute. Passive damping will provide fail-safe damping in case the active control fails due to e.g. loss of power. Furthermore, the control law proposed in the preceding section is the optimal frequency domain controller and may not be realizable in the time domain. In fact, the control law is non-causal and thus the controller needs to predict the future behaviour of the disturbance signal. This might be possible in some cases but is generally not. Thus, the causal controller may not be as efficient, and in that case the shunt may provide additional reduction of the sound and/or vibrations.

Further, as only a finite number of modes can be included in the controller, there may be some control spillover, i.e. the controller excites residual modes. As reported in reference [108] a LR shunt causes a roll-off of the control authority above the tuning frequency of the shunt. This will in practice work similar to a lowpass filter which will reduce the spillover effect.

Figure 5.6 shows the energy contained in each mode for the case of no control (black), active control (dark grey) and hybrid control (light grey). The modal energy is calculated by summing the response of each mode in the frequency range where the mode is dominant. The control law in this case is to minimize the kinetic energy of only the first mode, i.e. the vectors in equation 5.14 reduce to scalars. The figure shows that the pure active control efficiently controls the first mode. As the simulations consider ideal conditions, the kinetic energy in the first mode is reduced to virtually zero, i.e. negative infinity dB. However, energy is leaked into the other modes, which are amplified compared to the case of no control. Introducing a passive LR-shunt reduces the effect of control spillover and the energy in the higher modes is less or equal to the uncontrolled case. The shunt is chosen from a parameter study to give the lowest total kinetic energy of the plate in the case of the controller only including the first mode. The parameter space was chosen to include optimal damping according to reference [64] for all considered modes, and the total kinetic energy was calculated by summing the spectral components of the kinetic energy over the considered frequency range. The "optimal" shunt in this case was tuned to a frequency in between the third and fourth mode. Thus, the (2,1) and (2,2) modes are slightly damped due to the passive damping provided by

the shunt. In the passive configuration this shunt give about a 3.5 dB reduction for the kinetic energy. Thus proving fail-safe damping to the structure.

It may also be mentioned that, in case of a feedback control, control spillover in combination with observation spillover - i.e. residual modes observed by the sensors - can lead to instabilities [120, 121]. In that case, passive damping can help improve the stability margins.

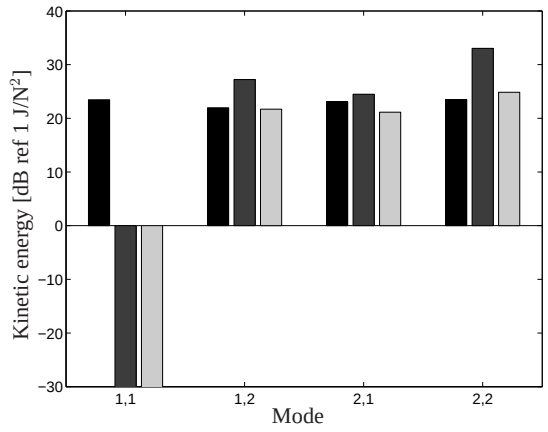

Figure 5.6: Modal energy. No control (black), active control (grey), hybrid control (light grey)

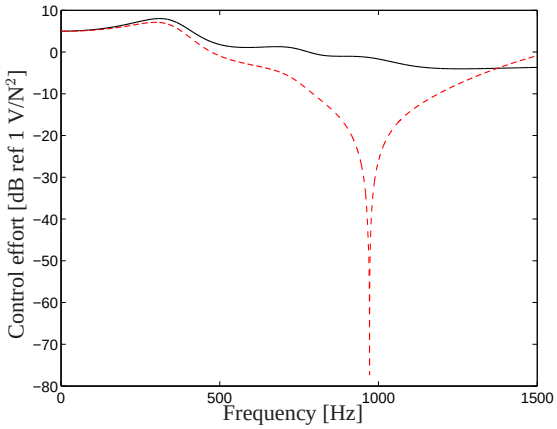

Figure 5.7: The control effort using only active control (−) compared to using hybrid control (- · -)

The magnitude of the voltage which is needed to fulfil the control law describes the control effort. The control effort will in turn set the requirement on the hardware which is needed to implement the controller, e.g. the amplifier which is needed to provide the voltage and the tolerance of the actuator. References such as [108, 110] report that the shunt may increase the control authority around the tuning frequency of the LR-shunt which will reduce the control effort around this frequency. Figure 5.7 shows the control effort of pure active control compared to hybrid control. The figure shows that there is a significant reduction of the control effort around the tuning frequency of the shunt, which is approximately at 970 Hz. The shunt is in this case chosen from the parameter space explained above in order to minimize the total control effort. The total control effort is the sum of the spectral components of the control effort over the considered frequency range. The shunt which gives this "optimal" results in terms of control effort is a purely inductive shunt. Such a shunt does not dissipate any vibrational energy in the passive configuration and does not offer any of the fail-safe damping which is normally associated with hybrid control. Therefore it might be advantageous to introduce a resistive element in the shunt. This gives a trade-off between control effort and passive damping.

The figure also shows that at the upper end of the considered frequency range the control effort is increased for hybrid control compared to pure active control. This is due to the lowpass filtering effect explained above. Thus a hybrid system may cause an increased control effort if modes included in the controller appear above the tuning frequency of the shunt. This phenomenon was also reported in [111].

Chapter 6

Implementation of shunt damping on an oil pan

This section presents an experimental investigation of implementing piezoelectric shunt damping on a car structure. The chosen structure was the oil pan. Studies have revealed that the oil pan is responsible for a major part of the radiated sound from the engine and power train. Bending modes of the oilpan are identified and shunt damping is implemented to reduce the modal response. Experimental reduction of around 10 dB is achieved.

6.1 Car structure

The structure which was chosen in order to implement the shunt damping technique on was an oil pan from a passenger car; see Figure 6.2. The oil pan has been identified as a major contributor of engine noise emission, both for cars [122] and trucks [123]. The oil pan was mounted in a wooden wall in order to give it a relatively stiff mounting as well as significant damping. This is not a mounting condition which will reflect the actual mounting of the oil pan inside the car engine. However, it captures two important features: firstly the stiff mounting can be expected also in the car engine, as the oil pan is screwed to the gearbox; secondly the high damping can also be expected because of viscous damping from the oil inside the oil pan. The measurement set-up is shown in Figure 6.1.

An electromechanical shaker was used to excite the oil pan. The stinger was mounted as indicated by the arrow in Figure 6.1. The shaker is not mounted in order to resemble the real excitation when the oil pan is mounted in the engine, but merely to try to excite some potentially efficiently radiating modes. The transfer function (accelerance) between the force input and the acceleration at various points on the oil pan was measured. The mobility can be calculated by integrating

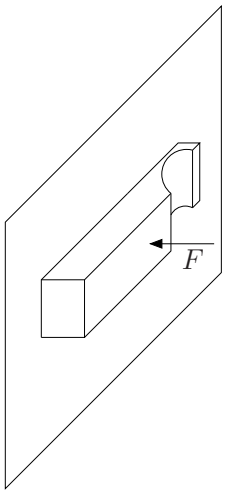

Figure 6.1: A schematic drawing of the oil pan mounted on a wooden frame. The arrow indicates where on the top plate the force was applied by the shaker.

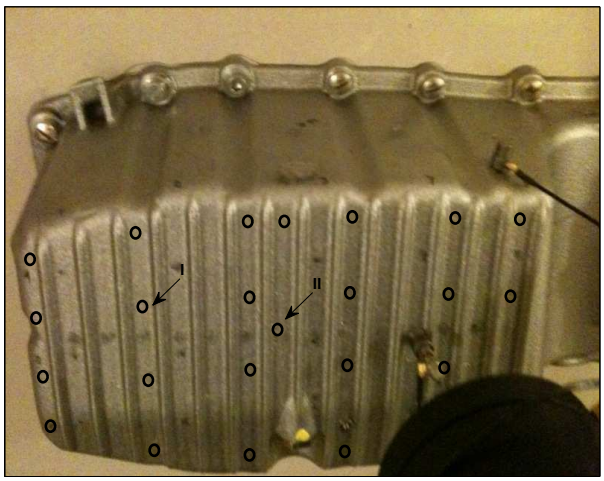

Figure 6.2: A photo of the oil pan; the circles indicate the measurement points.

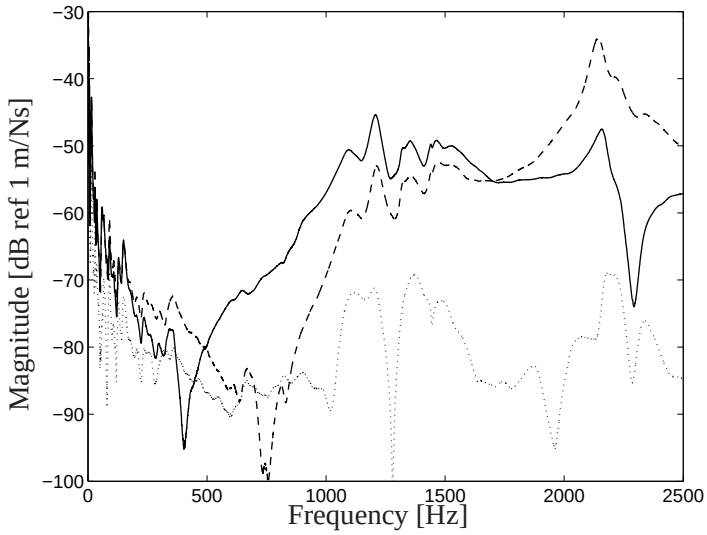

Figure 6.3: Measured transfer mobilities between the force input and velocity at three different points. −: the velocity at point I; - - -:the velocityat point II; ·····: the velocity at a control point not located on the top plate.

the accelerance, which in the case of harmonic oscillations corresponds to a division with $j\omega$. The transfer mobilities between the input force and velocity at the points indicated by the arrows in Figure 6.2 are shown in Figure 6.3. The figure also includes the transfer mobility between force input and a point on the oil pan outside the top plate. There seem to be two distinct peaks in the mobility functions, one at approximately 1200 Hz and one at approximately 2150 Hz. Plotting the vibrational response at these frequencies may indicate wether any particular mode is driving the response. Figures 6.4 show the velocity distribution of the oil pan at the two mentioned frequencies. The figures indicate that, at the first and second resonance frequencies the velocity fields look like they are dominated by the first and second bending modes, respectively, of a simply supported plate. Thus the model presented in the previous section may be used to gain some insight into the possibility of applying piezoelectric damping to the oilpan.

6.2 Engineering model

The transfer functions measured on the oil pan can be roughly estimated with the plate model described in *Section 4.3.3*. The simply supported plate model can approximately describe the top plate of the oil pan. The material data of the oil pan may be difficult to find by looking in standard tables. However, the product of the

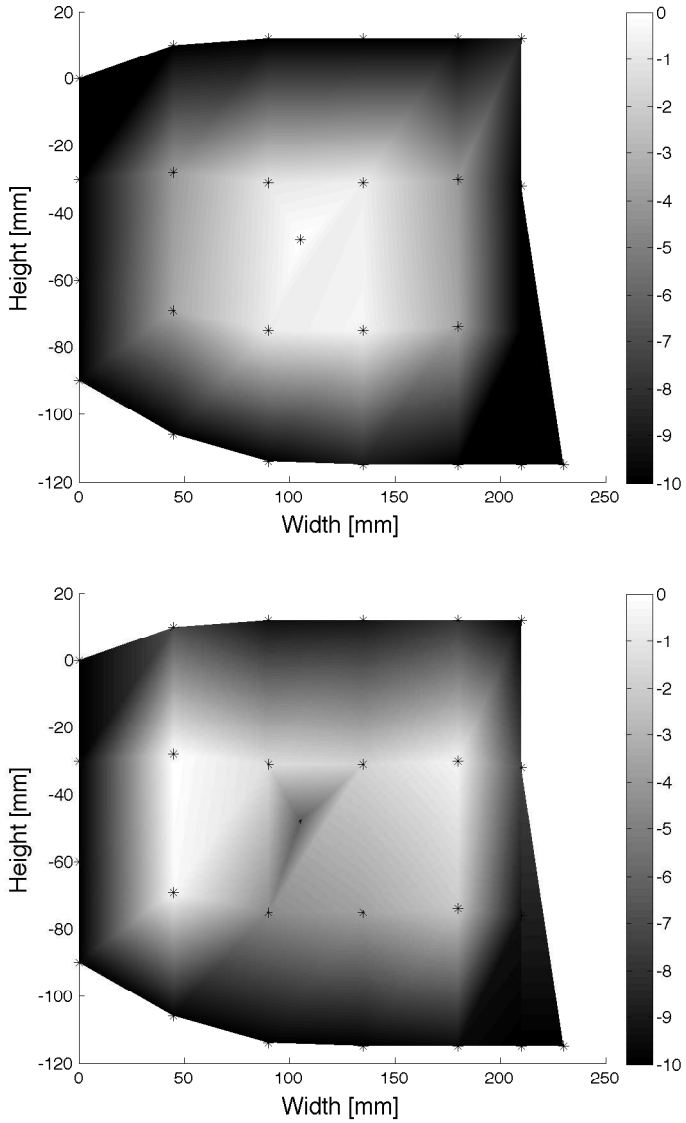

Figure 6.4: Upper: The velocity field at 1207 Hz. Lower: The velocity field at 2157 Hz. The asterisks ($*$) indicate the measurements positions.

Table 6.1: The material properties and geometry used in the plate model.

Young's modulus	Density	Width	Height	Thickness
158 MPa	3000 kg/m^3	220 mm	130 mm	4.5 mm

mass per unit area and bending stiffness can be found by finding the level of the plate mobility. The mobility of an infinite plate is given by

$$Y_{inf} = \frac{1}{8\sqrt{m''B}}, \tag{6.1}$$

where m'' and B are the mass per unit area and bending stiffness respectively. The dimensions of the top plate of the oil pan can be roughly measured, and by choosing the density as that of casting iron the stiffness can be determined by finding the proper level of the infinite plate mobility. The properties and dimensions of the plate are given in Table 6.1. The modal damping of the plate was determined by finding the correct level of the resonance peaks. The mobilities of the plate model are compared to the measured mobilities in Figures 6.5. The first seven bending modes are included in the model, the highest with an eigenfrequency of around twice the upper considered frequency limit. The plate model can be used to estimate the potential damping that a shunted piezoelectric element would augment to the oil pan. The model can also assist in choosing the properties, geometry and location of the piezoelectric element.

6.2.1 Prediction of shunt damping efficiency

The shunted piezoelectric element can be designed to provide optimal damping according to [64] of either of the two modes which have their eigenfrequencies in the considered frequency range. A common piezoceramic material with the properties given in Table 6.2 was used in the simulation. The model was used to investigate the effect of the thickness of the piezoelectric element on the efficiency of the shunt damping treatment. Figure 6.6 (a) shows the plate's centre point velocity per unit force zoomed around the first resonance frequency for three different thicknesses. The piezoelectric element was placed in the centre of the plate, as this is the point of maximum strain for the first mode. As the thickness of the piezoelectric element increases (i.e. the bending stiffness increases) the shunt damping becomes more efficient. A piezoelectric element 1 mm thick can only provide a reduction of the velocity of less than 3 dB, while a 3 mm thick element can provide almost 5 dB reduction. Figure 6.6 (b) shows the plate velocity at $x = L_x/2$, $x = L_y/4$ per unit force zoomed around the second resonance frequency for three different thicknesses. The piezoelectric element was placed at the point of maximum strain for

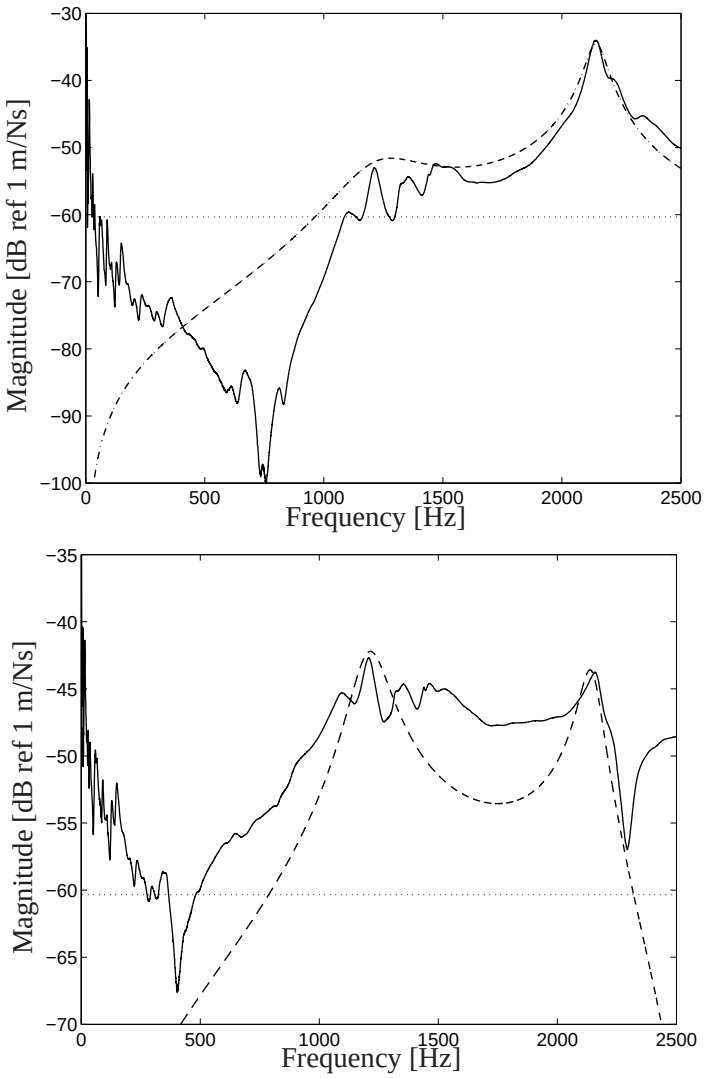

Figure 6.5: Upper: Measured and calculated mobilities at point I. Lower: Measured and calculated mobilities at point II. −: measured mobility; - - -: calculated mobility; ·····: mobility of an infinite plate.

Table 6.2: The material properties and geometry for the piezoelectric element.

S_{11}^E	l_x	l_y	k_{31}	C_p
$1.7 \cdot 10^{-11}$ m^2/N	0.05m	0.025m	0.327	25 μF

the second mode. A piezoelectric element 1 mm thick can provide a reduction of the velocity of approximately 10 dB, while a 3 mm thick element can provide about 15 dB reduction. Piezoelectric shunt damping is thus more efficient in damping the second mode compared to the first mode, due to that the piezoelectric element in this case is larger compared to the bending wavelength. Increasing the thickness of the piezoelectric element is one way to increase the generalised electromechanical coupling coefficient, thereby increasing the efficiency of shunt damping. Another way would be to increase the area. However, increasing the thickness is more efficient than increasing the area, as the thickness has a larger effect on the total modal stiffness of the shunted piezoelectric element.

6.3 Experimental implementation of shunt damping

Inductive-resistive shunt damping of the second bending mode on the oil pan was experimentally implemented. The shaker was placed in the position shown in Figure 6.2, which is the position where the second bending mode is most easily excited. An accelerometer was placed at the point where the second bending mode has maximum strain. The shunt was implemented on the DSP board as described in *Section 4.5*. The optimal resistance and inductance were calculated to be $R = 344\,\Omega$ and $L = 0.23$ H respectively. Figure 6.7 shows the measured transfer mobility with the piezoelectric element shorted and shunted respectively. The figure shows that the peak amplitude could be reduced by approximately 10 dB. This is approximately the reduction which was predicted by the plate model. The measurement with shunt damping is quite noisy. This is due to the fact that the piezoelectric element is exciting the structure at other frequencies except the tuning frequency. This was most likely due to poor electrical circuitry.

Figure 6.8 shows the sound pressure level in the direct field of the radiating oil pan. It is clear that the sound pressure level is reduced in the frequency range of approximately 1900 Hz to 2100 Hz. In the one-third octave band with a centre frequency of 2000 Hz the sound pressure level is reduced by approximately 3 dB.

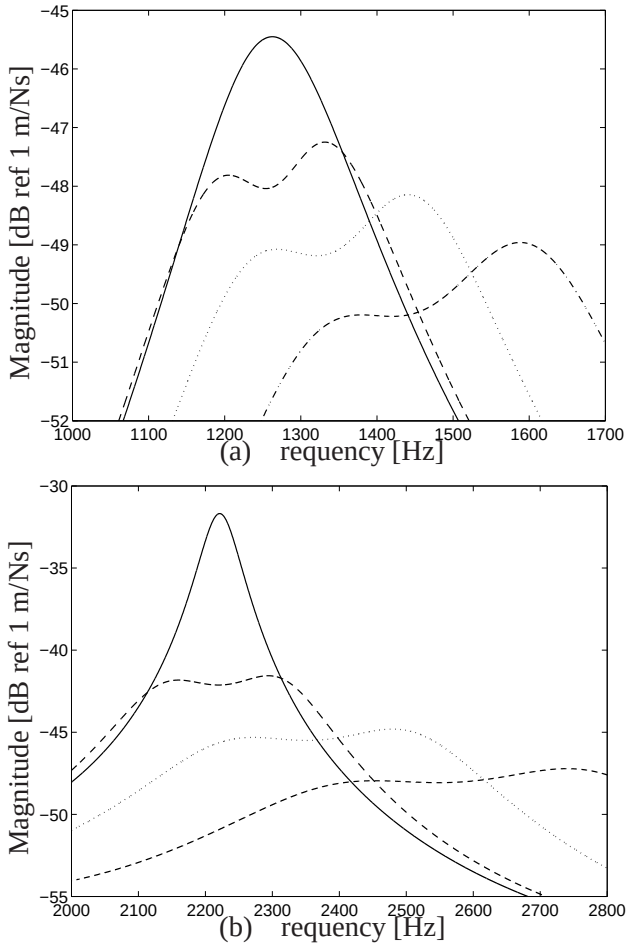

Figure 6.6: (a) The normalised velocity at the centre point of the plate, zoomed around the first resonance frequency. (b) The normalised velocity at $x_c = L_x/2; y_c = L_y/2$, zoomed around the second resonance frequency. $-$: $t_p = 0.001m$ short circuit, - - -: $t_p = 0.001m$ LR shunt; $\cdots\cdot$: $t_p = 0.002m$ LR shunt; $t_p = 0.003m$ LR shunt.

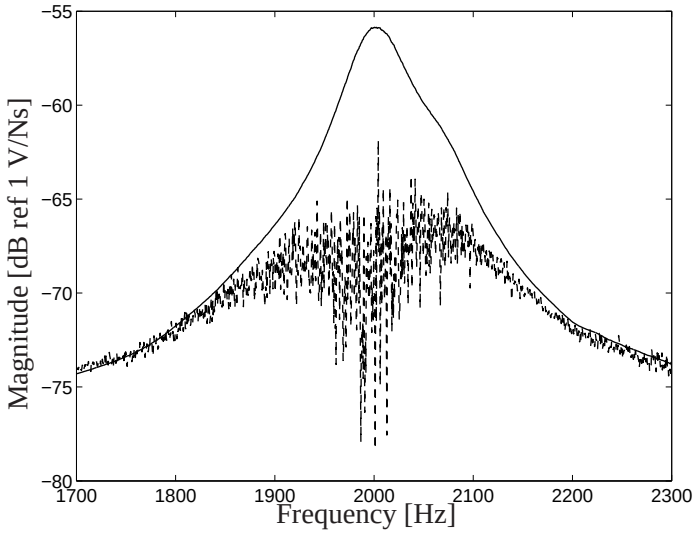

Figure 6.7: The measured transfer mobility under an open circuit condition (−) and with shunt damping (- - -).

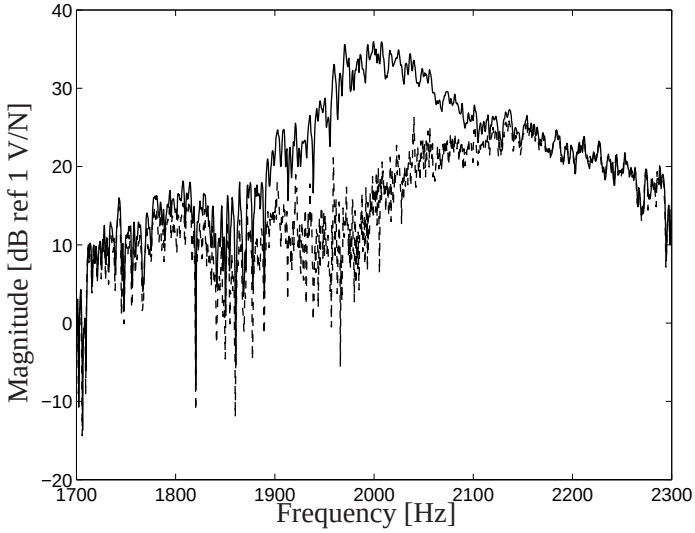

Figure 6.8: The sound pressure level in the direct field of the oil pan, under and open circuit condition (−) and with shunt damping (- - -).

Chapter 7
Discussion and conclusions

7.1 General discussion

This thesis has presented approaches to passive, active and hybrid active-passive vibration control for lightweight vehicle structures. Mathematical models describing beam- and plate-like structures were developed to theoretically evaluate the vibration damping treatments, and experiments were conducted to verify the models.

Referring back to the introduction, the outcome of the first part of the thesis - investigating the potential of controlling propagating waves in structures in order to confine vibratory energy in structural components with high inherent passive damping - can be summarized as follows:

The concept of active scattering factors (*Section 2.3.1*) enabled simple derivations of control laws to alter the scattering properties at a structural junction of two semi-infinite, non-dissipative beams. Results from a parameter study (*Paper* I) showed that if an active force is driven to cancel the reflection at the junction, the properties of the beams can be chosen so that the force always absorbs a part of the incident wave power. This result inspired a hybrid active-passive damping treatment, as passive damping could be introduced to possibly dissipate the remaining wave power transmitted across the junction.

By developing an impedance approach to active junction control (*Section 2.3.2*), more general beams could be treated, such as finite and dissipative beams. By introducing a highly dissipative sandwich beam at the junction, with the force driven to cancel the reflection of a wave, all incident wave power could be absorbed, either actively by the force or passively in the sandwich composite. However, studying this junction reveals that, at resonance frequencies of the sandwich beam ,the required control effort is substantial. Furthermore, at these frequencies the active force injects power, which is naturally unfortunate for a hybrid damping treatment (*Section 3.2* and *Paper* II).

Paper III presented a detailed parameter study of a hybrid damping treatment consisting of an active force driven to cancel the reflection at a structural junction and a beam with high inherent losses with the purpose of dissipating wave power transmitted across the junction. The study revealed that the properties of the highly dissipative beam can be chosen in a way so that the hybrid system may offer advantages compared to pure active control (i.e. a lower control effort), and pure passive control (i.e. an improved efficiency). However, this requires that the properties of the passive damping treatment can be chosen with high precision, which will severely limit the possibility of experimental implementation. Moreover, this investigation assumed that exact measurements of the bending wave amplitudes, or deflection and rotation, could be obtained as well as having actuators applying ideal point forces and moments. This would further complicate actual implementation.

Furthermore, as this approach requires structural components with specific properties, it could imply a structure with high mass, which is evidently not acceptable. These results motivated the second part of the thesis, replacing the structural components with electrical components to provide passive damping.

Piezoelectric shunt damping can be used to augment structural damping to a structure by introducing electrical losses (*Chapter 4*). Analytical models of a plate and a beam with a surface-bonded, shunted piezoelectric elements were developed for investigating shunt design based on both structural response and radiated sound power (*Section 4.3.4*, *Section 4.3.3* and *Paper* IV). For very lightly damped structures, piezoelectric shunt damping using an LR network which was detuned from any structural eigenfrequency could be used to influence the kinetic energy and radiated sound power over a wider frequency range than just a single mode (*Chapter 4.4.2* and *Paper* II). Detuning the LR shunt gives the potential to reduce the total-kinetic energy and/or sound power (i.e. the sum of respective spectral components), and makes the shunt less sensitive to changes in structural eigenfrequencies and/or piezoelectric capacitance.

If the eigenfrequencies of the first structural modes of the plate appear under their critical frequencies the shunt treatment which is optimal from the viewpoints vibration and sound radiation respectively may differ substantially - in terms of both the inductance and resistance of the shunt as well as the location of the piezoelectric element (*Paper* IV). The analytical model of the beam with a surface-bonded, shunted piezoelectric element agreed very well with measurement and could be used to predict the efficiency of modal shunt damping (*Section 4.5*).

Shunt damping was also successfully implemented on an oil pan of an automotive

vehicle. The oil pan has been recognized as a major contributor of external noise emission. Experiments showed that the amplitude of the second bending mode could be reduced by approximately 10 dB by implementing a simple inductive-resistive shunt, although the measurements were very noise.

Combining voltage driving of the piezoelectric element with a passive LR shunt may offer certain advantages over pure active driving (*Chapter 5* and *Paper* V). E.g. in cases where the active controller excites residual uncontrolled modes, a passive shunt can help to provide passive damping of these modes. Further studies are needed in order to clarify in which situations hybrid damping is advantageous and how it can be designed. However, initial results reveal the potential of a piezoelectric hybrid damping. Previous studies have reported that a passive shunt can be used to increase the control authority of the active controller; see e.g. [108, 107].

In general it can be said that when designing passive, active, or hybrid damping treatments it is vital to have knowledge of the specific circumstances for which the treatment is intended, as this may significantly influence the optimal design. This is clearly shown in the results from the study of piezoelectric shunt damping, where the shunt varies significantly when optimized on the basis of different criteria.

7.2 Future work

Based on the results from the studies presented in this thesis, several points in the discussion could be used as topics of subsequent studies. However, the most natural extension of this work would be to experimentally implement the piezoelectric hybrid active-passive control system, for broadband control. Control laws for designing the control filter and principles for shunt designing could be studied with respect to vibration levels, radiated sound and fail-safe damping, thereby investigating wether there are any general design principles which can be applied to piezoelectric hybrid damping treatments.

Appendix A

Mathematical derivations

Here follows some mathematical derivation which are not included in the main body of the thesis or in the appended papers.

A.1 The piezoelectric constitutive relations

The general constitutive relation for a linear piezoelectric material is given by equation 4.6 in *Chapter 4*. The stress and strain vectors given in equation 4.6 are defined as

$$\boldsymbol{\varepsilon} = \left\{ \begin{array}{c} \varepsilon_1 \\ \varepsilon_2 \\ \varepsilon_3 \\ \varepsilon_4 \\ \varepsilon_5 \\ \varepsilon_6 \end{array} \right\} = \left\{ \begin{array}{c} \varepsilon_x \\ \varepsilon_y \\ \varepsilon_z \\ \gamma_{xy} \\ \gamma_{xz} \\ \gamma_{yz} \end{array} \right\}, \quad \boldsymbol{\sigma} = \left\{ \begin{array}{c} \sigma_1 \\ \sigma_2 \\ \sigma_3 \\ \sigma_4 \\ \sigma_5 \\ \sigma_6 \end{array} \right\} = \left\{ \begin{array}{c} \sigma_x \\ \sigma_y \\ \sigma_z \\ \tau_{xy} \\ \tau_{xz} \\ \tau_{yz} \end{array} \right\}, \tag{A.1}$$

where it is assume that the material axes (1,2,3) of the piezoelectric plate are aligned with the coordinate axes (x, y, z) of a Cartesian coordinate system; see figure **??**. σ and τ represent extensional stress and shear stress respectively, and ε and γ extensional strain and shear strain respectively. Thus, the material axes 4,5,6 represents shear around the x, y, z-axes respectively. The electrical field and the electrical displacement vectors are defined as

$$\mathbf{E} = \left\{ \begin{array}{c} E_1 \\ E_2 \\ E_3 \end{array} \right\}, \quad \mathbf{D} = \left\{ \begin{array}{c} D_1 \\ D_2 \\ D_3 \end{array} \right\}. \tag{A.2}$$

The elastic compliance matrix is given by

$$\mathbf{S}^E = \begin{bmatrix} S_{11}^E & S_{12}^E & S_{13}^E & 0 & 0 & 0 \\ S_{21}^E & S_{22}^E & S_{23}^E & 0 & 0 & 0 \\ S_{31}^E & S_{32}^E & S_{33}^E & 0 & 0 & 0 \\ 0 & 0 & 0 & S_{44}^E & 0 & 0 \\ 0 & 0 & 0 & 0 & S_{55}^E & 0 \\ 0 & 0 & 0 & 0 & 0 & S_{44}^E \end{bmatrix}. \tag{A.3}$$

As the electric field can only contribute to electric charge in the same direction as the field is applied the matrix $\boldsymbol{\xi}^\sigma$ is diagonal according to

$$\boldsymbol{\xi}^\sigma = \begin{bmatrix} \xi_1^\sigma & 0 & 0 \\ 0 & \xi_2^\sigma & 0 \\ 0 & 0 & \xi_3^\sigma \end{bmatrix}. \tag{A.4}$$

The electromechanical coupling matrix is given by

$$\mathbf{d} = \begin{bmatrix} 0 & 0 & 0 & 0 & d_{15} & 0 \\ 0 & 0 & 0 & d_{15} & 0 & 0 \\ d_{31} & d_{31} & d_{33} & 0 & 0 & 0 \end{bmatrix}. \tag{A.5}$$

A.2 Modal forces by a shunted piezoelectric element on a free-free beam

The contribution by the piezoelectric element in equation 4.23 is given by the term

$$E_p b_p t_c \left(\frac{\partial^4 w}{\partial x^4}\Omega(x) + 2\frac{\partial^3 w}{\partial x^3}\Omega'(x) + \frac{\partial^2 w}{\partial x^2}\Omega''(x) \right) + m_p' \frac{\partial^2}{\partial t^2} w(x,t). \tag{A.6}$$

Inserting the modal solution approach gives for the n:th mode

$$E_p bt \left(k_n^4 \phi_n \Omega + 2\phi_n''' \Omega' + \phi_n'' \Omega'' \right) a_n - \omega^2 m_p' a_n \phi_n \Omega \tag{A.7}$$

Multiplying this expression by ϕ_m and integrating over the length of the beam gives

$$\left(E_p bt k_n^4 - \omega^2 m_p' \right) a_n \int_{x_1}^{x_2} \phi_n \phi_m dx + 2E_p bt a_n \int_0^L \phi_n'' \phi_m \Omega' dx + E_p bt a_n \int_0^L \phi_n'' \phi_m \Omega'' dx \tag{A.8}$$

Solving this integral and assuming orthogonality of the modes, i.e. $\phi_n \phi_m = 0$ if $n \neq m$ yields the modal mass and stiffness due to the piezoelectric element according to

$$M_n^{\text{pzt}} = \rho_p t_p b_p l_a \omega^2 \zeta_n(x) \tag{A.9}$$

$$K_n^{\text{pzt}} = E_p bt k_n^4 \zeta_n(x). \tag{A.10}$$

Assuming $k_n l_a \ll 1$ the function $\zeta_n(x)$ can be approximated as

$$\begin{aligned}\zeta_n(x_c) \approx & 1 + \frac{(1+\gamma_n^2)}{2}(\cosh^2(k_n x_c) - \sinh^2(k_n x_c)) \\ & + \frac{(1-\gamma_n^2)}{2}(\cos^2(k_n x_c) - \sin^2(k_n x_c)) \\ & - 2\gamma_n(\sinh(k_n x_c)\cosh(k_n x_c) + \cos(k_n x_c)\sin(k_n x_c)) \\ & + 2(\cosh(k_n x_c) - \gamma_n \sinh(k_n x_c))(\cos(k_n x_c) - \gamma_n \sin(k_n x_c)) \quad \text{(A.11)} \\ & \quad \text{(A.12)}\end{aligned}$$

Which is the expression found in equation 4.29.

Appendix B
Examples of beam junctions

This chapter presents some examples of passive and active junctions and how the impedance formulation, which was presented in 2.3.2, can be used to calculate the scattering properties of such junctions.

B.1 Passive junctions

Two examples of passive junctions are presented: A beam terminated by a deflection spring and a mass; and a junction where a semi-infinite beam with arbitrary cross-sectional area and material properties is connected.

B.1.1 Example I: *A beam terminated with a mass and deflection spring*

In order to derive the reflection matrix for an Euler-Bernoulli beam terminated by a mass and deflection spring at a free end, the impedance matrix for each component has to be derived and added. Thus the impedance matrix for a free end, a deflection spring and a point mass has to be known. Table B.1 gives the impedance matrices for a point-mass and a deflection spring respectively. The combined junction impedance matrix is given by

$$\hat{\mathbf{Z}}_{\text{tot}} = \hat{\mathbf{Z}}_{\text{free}} + \hat{\mathbf{Z}}_{\text{mass}} + \hat{\mathbf{Z}}_{\text{spring}} = \begin{bmatrix} \mathrm{j}(\omega m - \frac{K_d}{\omega}) & 0 \\ 0 & 0 \end{bmatrix}. \qquad \text{(A I)}$$

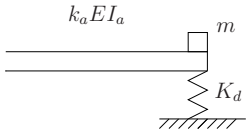

Figure B.1: *Figure depicts the junction in example A.*

Inserting this into equation 2.6 gives

$$\mathbf{r}^{mK_d} = \frac{1}{\sigma}\begin{bmatrix} -\mathrm{j}k^3EI - m\omega^2(1+\mathrm{j}) + K_d(1+\mathrm{j}) & k^3EI(1+\mathrm{j}) \\ k^3EI(1-\mathrm{j}) & \mathrm{j}k^3EI - m\omega^2(1+\mathrm{j}) + K_d(1+\mathrm{j}) \end{bmatrix}, \tag{A II}$$

where m and K_d represent mass and spring stiffness respectively and,

$$\sigma = k^3EI + m\omega^2(1+\mathrm{j}) - K_d(1+\mathrm{j}). \tag{B.1}$$

B.1.2 Example II: *A beam with an arbitrary change in Young's modulus, density or cross-sectional dimensions*

In this example the beam is connected to a semi-infinite beam with arbitrary cross-sectional dimensions material properties. The junction impedance matrix is thus the characteristic impedance matrix of a semi-infinite Euler-Bernoulli according to

$$\hat{\mathbf{Z}} = \tilde{\mathbf{Z}}_b^+ = \frac{EI_b}{\omega}\begin{bmatrix} (1+\mathrm{j})k_b^3 & k_b^2 \\ k_b^2 & (1-\mathrm{j})k_b \end{bmatrix}, \tag{B.2}$$

where the subscript b has been introduced in order to separate this matrix from the characteristic impedance matrix of the original beam. Inserting this into equation 2.6, the reflection matrix will turn into that of equation 2.3. Also the transmission matrix can for this case be stated with the impedance formulation according to,

$$\mathbf{t}^{\text{arb}} = \mathbf{C}_b^+\left(\mathbf{I} + \left(\tilde{\mathbf{Z}}^- - \hat{\mathbf{Z}}\right)^{-1}\left(\hat{\mathbf{Z}} - \tilde{\mathbf{Z}}^+\right)\right), \tag{B.3}$$

where $\mathbf{C}_b^+$ is just as $\mathbf{C}^+$ except with a discriminating wave number and bending stiffness, and $\mathbf{I}$ is a 2×2 unit matrix. By solving this equation the transmission matrix will be equal to the one in equation 2.2. Hence, the impedance formulation was here used to derive the scattering matrices matrices in equations 2.3 and 2.2, originally presented in [43].

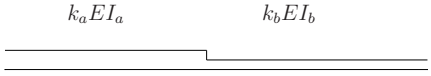

Figure B.2: *Figure depicts the junction in example B.*

Table B.1: *A few standard junction impedance matrices and the corresponding reflection matrix. m represents mass, K_d spring stiffness while EI and k represent the bending stiffness and the wavenumber respectively of he beam.*

Case	$\hat{\mathbf{Z}}$	$\mathbf{r}$
Free end	$\mathbf{0}$	$\begin{bmatrix} -\mathrm{j} & 1+\mathrm{j} \\ 1-\mathrm{j} & \mathrm{j} \end{bmatrix}$
Continuous beam	$\tilde{\mathbf{Z}}^{+}$	$\mathbf{0}$
Point mass	$\begin{bmatrix} -\mathrm{j}\omega m & 0 \\ 0 & 0 \end{bmatrix}$	$\frac{1}{\Gamma}\begin{bmatrix} (1+\mathrm{j})k^3EI - 2\omega^2 m & -2k^3EI \\ 2\mathrm{j}k^3EI & -(1+\mathrm{j})k^3EI - 2\omega^2 m \end{bmatrix}$
Deflection spring	$\begin{bmatrix} \frac{\mathrm{j}K_d}{\omega} & 0 \\ 0 & 0 \end{bmatrix}$	$\frac{1}{\Omega}\begin{bmatrix} -\mathrm{j}(k^3EI + K_d - \mathrm{j}K_d) & (1+\mathrm{j})k^3EI \\ (1-\mathrm{j})k^3EI & \mathrm{j}(k^3EI - K_d + \mathrm{j}K_d) \end{bmatrix}$
Constants		$\Gamma = 2\omega^2 m - k^3EI(1-\mathrm{j})$ $\Omega = K_d + K_d\mathrm{j} + k^3EI$

B.2 Active junctions

Constraints may be specified on the reflection matrix in equation 2.6 and the corresponding required active impedance load can be derived. Inserting equation 2.7 into equation 2.6 yields

$$\mathbf{r} = \left(\mathbf{C}^{-}\right)^{-1}\left(\tilde{\mathbf{Z}}^{-} - (\hat{\mathbf{Z}}^{\text{pass}} + \hat{\mathbf{Z}}^{\text{act}})\right)^{-1}\left((\hat{\mathbf{Z}}^{\text{pass}} + \hat{\mathbf{Z}}^{\text{act}}) - \tilde{\mathbf{Z}}^{+}\right)\mathbf{C}^{+}. \tag{B.4}$$

From this equation, $\hat{\mathbf{Z}}^{\text{act}}$ can be solved as

$$\hat{\mathbf{Z}}^{\text{act}} = \frac{\tilde{\mathbf{Z}}^{-}(\mathbf{T} + \mathbf{I}|\mathbf{T}|) + \tilde{\mathbf{Z}}^{+}(\mathbf{I} + \text{adj}(\mathbf{T}))}{|\mathbf{T}| + \text{trace}(\mathbf{T}) + 1} - \hat{\mathbf{Z}}^{\text{pass}}, \tag{B.5}$$

where

$$\mathbf{T} = \mathbf{C}^{-}\mathbf{r}(\mathbf{C}^{+})^{-1}, \tag{B.6}$$

and where adj denotes the adjugate matrix of $\mathbf{T}$. Almost any beam junction can be actively achieved by a correct choice of the active impedance matrix, e.g. a continuous beam can be modified to behave as a free end. Note, it is important to

remember that this reasoning is highly theoretical. For an actual implementation on a real beam a number of issues would complicate the matter, filter implementation, measurements and actuation.

The power injected or absorbed by the active impedance load is given by

$$W_{\text{in}} = \frac{1}{2}\text{Re}\left\{\left((\mathbf{C}^{+} + \mathbf{C}^{-}\mathbf{r})\mathbf{a}^{+}\right)^{H} \mathbf{Z}^{\text{act}}(\mathbf{C}^{+} + \mathbf{C}^{-}\mathbf{r})\mathbf{a}^{+}\right\}, \tag{B.7}$$

where H denote Hermitian transpose. An optimal power absorbing controller may be derived by choosing $\mathbf{Z}^{\text{act}}$ in a way that will minimise equation B.7.

Different control laws, for both force and moment actuation, are investigated in *Paper* II. A few examples are given here in order to facilitate understanding of actively manipulating beam junctions in this way.

B.2.1 Example III: *Making a continuous beam into a free end*

The active impedance matrix is here used in order to manipulate a continuos beam to have the reflection matrix of a free end. The reflection matrix for a free end is given by Table B.1

$$\mathbf{r}^{\text{free}} = \begin{bmatrix} -\text{j} & 1+\text{j} \\ 1-\text{j} & \text{j} \end{bmatrix}. \tag{B.8}$$

The passive junction matrix for a continuous beam is

$$\hat{\mathbf{Z}}^{\text{pass}} = \frac{EI}{\omega}\begin{bmatrix} (1+\text{j})k^3 & k^2 \\ k^2 & (1-\text{j})k \end{bmatrix}, \tag{B.9}$$

which is the characteristic impedance matrix for a wave and near-field traveling in positive x-direction. Inserting B.8 into equation B.6 and then together with equation B.9 into equation B.5 and yields

$$\hat{\mathbf{Z}}^{\text{act}} = \frac{EI}{\omega}\begin{bmatrix} -(1+\text{j})k^3 & -k^2 \\ -k^2 & -(1-\text{j})k \end{bmatrix} = -\tilde{\mathbf{Z}}^{+}. \tag{B.10}$$

In this case the choice of the active impedance matrix is obvious. Since the free end impedance matrix is the null matrix, according to equation 2.7 the active impedance load just has to be equal to the negative of the passive junction impedance matrix. However, in other cases the correspondence between the desired reflection matrix and the junction impedance matrix might be less obvious. This active impedance load will block any incident wave field from being transmitted across the junction. This could be helpful for isolating a part of a structure from a disturbance.

B.2.2 Example IV: *Avoid reflections at a junction with an arbitrary change in Young's modulus, density and/or cross-sectional dimensions.*

The reflection matrix for junction where the beam is connected to a semi-infinite beam with arbitrary cross-sectional dimensions material properties is given in equation 2.3. The active impedance load can be chosen so that the reflection matrix becomes zero and no reflection occurs at the junction despite the impedance mismatch between the beams. The desired reflection matrix is thus the null matrix, and the passive-junction impedance matrix is

$$\hat{\mathbf{Z}}^{\text{pass}} = \frac{EI_b}{\omega}\begin{bmatrix} (1+\mathrm{j})k_b^3 & k_b^2 \\ k_b^2 & (1-\mathrm{j})k_b \end{bmatrix} = -\tilde{\mathbf{Z}}_b^+, \tag{B.11}$$

where the subscript b denotes the difference in bending stiffness and bending wavenumber between the beam to the left and right side of the junction respectively. Inserting equation B.11 and $\mathbf{T} = \mathbf{0}$ into equation B.5 yields

$$\hat{\mathbf{Z}}^{\text{act}} = \frac{EI}{\omega\gamma}\begin{bmatrix} k^3(1+\mathrm{j})(\gamma-\alpha\gamma^2) & k^2(\gamma-\alpha\gamma) \\ k^2(\gamma-\alpha\gamma) & k(1-j)(\gamma-\alpha) \end{bmatrix}, \tag{B.12}$$

where α and γ are defined in equation 2.4. The active impedance load defined by the matrix in equation B.12 compensates for the impedance mismatch introduced by the step change in Young's modulus, density or cross-sectional dimensions, or any combination of these. If the beam is continuous, i.e. $\alpha = \gamma = 1$, equation B.12 becomes the null matrix. This is obvious, since in that case no active control is needed. If $\alpha = 1$ and $\gamma \to 0$, i.e. the right side beam vanishes and the junction turns into a free end, the matrix in equation B.12 turns into the matrix of equation B.11. Hence, to avoid any reflection at the free end the active impedance load has to be equal to the characteristics impedance matrix for a wave and near-field traveling in the positive x-direction. In this case the beam junction is matched. This has previously been reported by [29].

B.2.3 Example V: *Active absorber on an infinite beam.*

The last example treats an active absorber on an infinite beam. An infinite beam can be seen as two connected semi-infinite beams. Thus, the passive impedance matrix is equal to

$$\hat{\mathbf{Z}}^{\text{pass}} = \frac{EI}{\omega}\begin{bmatrix} (1+\mathrm{j})k^3 & k^2 \\ k^2 & (1-\mathrm{j})k \end{bmatrix}. \tag{B.13}$$

Here it is assumed that the control system consists of a translational velocity sensor which provides the reference for a force actuator, and thus only the (1,1) element of the active impedance matrix is non-zero. The impedance control law is thus scalar and equation B.7, which expresses the power injected or absorbed by the active impedance load, reduces to

$$W_{\text{in}} = \frac{1}{2}\text{Re}\left\{Z^{\text{act}}\right\}|v|^2, \tag{B.14}$$

where Z^{act} is a scalar active impedance and v is the velocity in the position where the force is applied. Further assume that only a wave and no near-field is incident at the junction, then minimising W_{in} gives

$$Z^{\text{act}} = 2\left(\tilde{Z}^{+}_{11}\right)^{*}, \tag{B.15}$$

where $\tilde{Z}^{+}_{11}$ is the (1,1) element in the characteristic impedance matrix of rightward travelling wave and near-field and $*$ denotes complex cnjugate. This control law gives a reflection factor and a transmission factor of 0.5. Thus, half the incident power absorbed while one quarter is reflected and one quarter transmitted, as reported in [32].

References

[1] Inventory of u.s. greenhouse gas emissions and sinks: 1990-2008. Technical report, U.S. Environmental Protection Agency, 2010.

[2] Övergripande statistik om transportsektorn, 1996.

[3] U. Sandberg. Tyre/road noise: myths and realities. In *Proceedings of Inter-noise, the Hague*, 2001.

[4] B. Berglund, T. Lindvall, and D. H. Schwela. Guidelines for community noise. Technical report, WHO, 2000.

[5] WHO. Night noise guidlines for europe.

[6] E. Öhrström and A. Skånberg. Longitudinal surveys on effects of road traffic noise: substudy on sleep assessed by wrist actigraphs and sleeplogs. *Journal of Sound and Vibration*, 272(3-5):1097–1109, 2004.

[7] B. Berglund. Health effects of community noise. *Acoustics Bulletin*, 1996.

[8] J. M. Finkelman, L. R. Zeitlin, J. A. Filippi, and M. A. Friend. Noise and driver performance. *Journal of Applied Psychology*, 62(6):713–718, 1977.

[9] P. Lueg. Us patent no 2043 416: granted june 9:th 1936, 1936.

[10] H.F. Olson. Electronic control of noise, vibration, and reverberation. *Journal of the Acoustical Society of America*, 28(5):966–972, 1956.

[11] T.H. Rockwell and J.M. Lawther. Theoretical and experimental results on active vibration dampers. *Journal of the Acoustical Society of America*, 36(8):1507–1515, 1964.

[12] C.R. Fuller, S.J. Elliot, and P.A. Nelson. *Active Control of Vibration*. Academic Press, 1996.

[13] C.H. Hansen and S.D. Snyder. *Active Control of Noise and Vibration*. E and FN Spon, 1997.

[14] R. Alkhatib and M. F. Golnaraghi. Active structural vibration control: a review. *The shock and vibration digest*, 35(5):367–383, 2003.

[15] W-H. Zhu, B. Tryggvason, and J-C. Piedboeuf. On active acceleration control of vibration isolation systems. *Control Engineering Practice*, 14(8):863–873, 2006.

[16] R. Shoureshi and T. Knurek. Automotive applications of a hybrid active noise and vibration control. *IEEE Control Systems Magazine*, 16(6):72–78, 1996.

[17] J.C. Sun, X.G. Wang, and F.J. Xi. Sliding mode active vibration contol of circular saws. In *Proceedings of the 2000 IEEE International Conference on Control Applications in Anchorage U.S.A*, pages 953–958, 2000.

[18] M.J. Cunningham, D.F.L. Jenkins, W.W. Clegg, and M.M. Bakush. Active vibration control and actuation of a small cantilever for applications in scanning probe instruments. *Sensors and Actuators A*, A50(1-2):147–150, 1995.

[19] J. Scheuren. Engineering applications of active sound and vibration control. *Noise Control Engineering Journal*, 53(5):197–210, 2005.

[20] J. Scheuren. Active attenuation of bending waves in beams. In *Proceedings of the Spring Conference of the Institute of Acoustics in Southampton*, 1990.

[21] C.R. Halkyard and B.R. Mace. Feedforward adaptive control of flexural vibration in a beam using wave amplitudes. *Journal of Sound and Vibration*, 254(1):117–141, 2002.

[22] C.R. Halkyard and B.R. Mace. Adaptive active control of flexural waves in a beam in the presence of near-fields. *Journal of Sound and Vibration*, 285(1-2):149–171, 2005.

[23] D.J. Pines and A.H. von Flotow. Active control of bending waves at acosutic frequencies. *Journal of Sound and Vibration*, 142(3):391–412, 1990.

[24] S.J. Elliot and L. Billet. Adaptive control of flexural waves propagating in a beam. *Journal of Sound and Vibration*, 162(2):295–310, 1993.

[25] N. Tanaka and Y. Kikushima. Optimal vibration feedback control of an Euler-Bernoulli beam: Toward realization of the active sink method. *Journal of Vibration and Acoustics*, 121(2):174–182, 1999.

[26] N. Tanaka and H. Iwamoto. Active boundary control of an euler-bernoulli beam for generating vibration-free state. *Journal of Sound and Vibration*, 304(3-5):570–586, 2007.

[27] H. Iwamoto and N. Tanaka. Feedforward control of flexural waves propagating in a rectangular panel. *Journal of Sound and Vibration*, 324(1-2):1–25, 2009.

[28] R.J. McKinnel. Active vibration isolation by cancelling bending waves. *Proceeding of the Royal Society of London*, 421(1861):357–393, 1989.

[29] A.H. von Flotow and B. Schäfer. Wave-absorbing controllers for a flexible beam. *Journal of Guidance*, 9(6):673–680, 1986.

[30] B.R. Mace. Active control of flexural vibrations. *Journal of Sound and Vibration*, 114(1):253–270, 1987.

[31] P. Audrain, P. Masson, and A. Berry. Investigation of active structural intensity control in finite beams: Theory and experiment. *Journal of the Acoustical Society of America*, 108(2):612–623, 2000.

[32] D. Guicking, J. Melcher, and R. Wimmel. Active impedance control in mechanical structures. *Acustica*, 69(2):39–52, 1989.

[33] J. Scheuren. Non-reflecting termination for bending waves in beams by active means. In *Proceedings of Internoise, Avignon*, 1988.

[34] W. Redman-White, P.A. Nelson, and A.R.D. Curtis. Experiments on the active control of flexural wave power flow. *Journal of Sound and Vibration*, 112(1):187–191, 1987.

[35] M.J. Brennan, S.J. Elliot, and R.J. Pinnington. Strategies for the active control of flexural vibration on a beam. *Journal of Sound and Vibration*, 186(4):657–688, 1995.

[36] D.W. Miller. *Modelling and active modification of wave scattering in structural networks*. PhD thesis, Massachussets Institute of Technology, 1988.

[37] D. Miller, A.H. von Flotow, and S Hall. Active modification of wave reflection and transmission in flexible structures. In *Proceedings of the 1987 American Control Conference*, 1987.

[38] D. Miller, S. Hall, and A. von Flotow. Optimal control of power flow at structural junctions. *Journal of Sound and Vibration*, 140(3):475–497, 1990.

[39] R.d.l.G.G. Gonzalez and F.O. Bustamente. Active control of the reflection of waves in beams. *Proceedings of SPIE - The International Society for Optical Engineering*, pages 587–596, 2001.

[40] C.R. Fuller, P. Gibbs, and R.J. Silcox. Simultaneous active control of flexural and extensional waves in beams. *Journal of Intelligent Material Systems and Structures*, 1(2):235–247, 1990.

[41] Jr. R.L. Clark, J. Pan, and C.H. Hansen. An experimental study of the active control of multiple-wave types in an elastic beam. *Journal of the Acoustical Society of America*, 92(2):871–876, 1992.

[42] P. Gardonio and S.J. Elliot. Active control of waves on a one-dimensional structure with a scattering termination. *Journal of Sound and Vibration*, 192(3):701–730, 1996.

[43] B.R. Mace. Wave reflection and transmission in beams. *Journal of Sound and Vibration*, 97(2):237–246, 1984.

[44] X. Pan and C.H. Hansen. Effect of end conditions on the active control of beam vibration. *Journal of Sound and Vibration*, 168(3):429–448, 1993.

[45] A. Baz. Active constrained layer damping. In *Damping'93 conference*, volume 3, pages IBB 1–23, San Francisco, CA, 1993.

[46] A. Baz and J.J. Ro. Partial treatment of flexible beams with active constrained layer damping. In *Conference of engineering science society*, volume ASME-AMD 67, pages 61–80, Charlottesville, VA, 1993.

[47] A. Baz and J.J. Ro. The concept and performance of active constrained layer damping treatments. *Sound and Vibration*, 2193:98–114, 1994.

[48] H. Illare and W. Kropp. Quantification of damping mechanisms of active constrained layer treatments. *Journal of Sound and Vibration*, 1-2(2005):189–217, 2005.

[49] A. Baz and J.J. Ro. Vibration control of plates with active constrained layer damping. *Smart Materials and Structures*, 5(3):272–280, 1996.

[50] M. Alvelind and M. Enelund. Modelling of constrained thin rubber layer with emphasis on damping. *Journal of Sound and Vibration*, 300(3-5):662–675, 2007.

[51] Hélène Illare. *A study of Active-Passice Damping Treatments*. PhD thesis, Chalmers University of Technology, 2004.

[52] M. Lam and D. Inman W. Saunders. Vibration control through passive constrained layer damping and active control. *Journal of Intelligent Material Systems and Structures*, 8(8):663–677, 1997.

[53] Y. Liu and K.W. Wang. Active-passive hybrid constrained layer for structural damping augmentation. *Journal of Vibration and Acoustics*, 122(3):254–262, 2000.

[54] Y. Liu and K.W. Wang. Distribution of active and passive constraining sections for hybrid constrained layer damping treatments. *Journal of Intelligent Material Systems and Structures*, 13(1):23–34, 2002.

[55] W. H. Liao and K.W. Wang. A new active constrained layer configuration with enhanced boundary actions. *Smart Materials and Structures*, 5(5):638–648, 1996.

[56] M. Lam, D. Inman, and W. Saunders. Variations of hybrid damping. In *Proceedings of SPIE - The International Society for Optical Engineering*, volume 3327, pages 32–43, 1998.

[57] C. M. A. Vasques and J. D. Rodriques. Numerical and experimental comparison of the adaptive feddforward control of vibration of a beam with hybrid active-passive damping treatments. *Journal of Intelligent Material Systems and Structures*, 19:805–813, 2008.

[58] D. J. Mead and S. Markus. The forced vibration of a three-layer, damped sandwich beam with arbitrary boundary conditions. *Journal of Sound and Vibration*, 10(2):163–75, 1969.

[59] S. O. R. Moheimani. A survey of recent innovations in vibration damping and control using shunted piezoelectric transducers. *IEEE TRANSACTIONS ON CONTROL SYSTEMS TECHNOLOGY*, 11(4):482–494, 2003.

[60] ANSI/IEEE Std-176-1987. *IEEE Standard on Piezoelectricity*. The Institute of Electrical and Electronics Engineers, Inc, 1987.

[61] R. L. Forward. Electronic damping of vibrations in optical structures. *Applied Optics*, 18(5):690–697, 1979.

[62] M.J. Brennan and J. Dayou. Global control of vibration using a tunable vibration neutralizer. *Journal of Sound and Vibration*, 232(3):585–600, 2000.

[63] J. Dayou and M. J. Brennan. Global control of structural vibration using a multiple-tuned vibration neutralizers. *Journal of Sound and Vibration*, 258(2):345–357, 2002.

[64] N. W. Hagood and A. von Flotow. Damping of structural vibrations with piezoelectric materials and passive electrical networks. *Journal of Sound and Vibration*, 146(2):243–268, 1991.

[65] G. A. Lesieutre. Vibration damping and control using shunted piezoelectric materials. *The shock and vibration digest*, 30(3):187–195, 1998.

[66] C. L. Davis and G. A. Lesiutre. An actively tuned solid-state vibration absorber using capacitive shunting of piezoelectric stiffness. *Journal of Sound and Vibration*, 232(3):601–617, 2000.

[67] W. W. Clark. Vibration control with state-switched piezoelectric materials. *Journal of Intelligent Material Systems and Structures*, 11:263–271, 2000.

[68] G. D. Larson K. A. Cunefare. Quarter-cycle switching control for switch-shunted dampers. *Journal of Vibration and Acoustics*, 126:278–283, 2004.

[69] D. Niederberger. *Smart Damping Materials using Shunt Control*. PhD thesis, Swiss Federal Institute of Technology (ETH) Zurich, 2005.

[70] G. A. Lesiutre, G. K. Ottman, and H. F. Hofmann. Damping as a result of piezoelectric energy harvesting. *Journal of Sound and Vibration*, 269(3-5):991–1001, Jan 2004.

[71] S. Behrens and S. O. R. Moheimani. Optimal resistive elements for multiple mode shunt damping of a piezoelectric laminate beam. In *Proceedings of the 39th IEEE Conference on Decision and Control*, 2000.

[72] J. Kim, Y-H. Ryu, and S-B. Choi. New shunting parameter tuning method for piezoelectric damping based on measured electrical impedance. *Smart Materials and Structures*, 9(868-877), 200.

[73] A. J. Fleming and S. O. R. Moheimani. Adaptive piezoelectric shunt damping. *Smart Materials and Structures*, 12(1):36–48, 2003.

[74] D. Niederberger, M. Morari, and S. Pietrzko. Adaptive resonant shunted piezoelectric devices for vibration suppression. *Smart Structures and Materials - Proceeding of SPIE*, 5056:213–224, 2003.

[75] A. Antoniou. Realisation of gyrators using operational amplifiers, and their use in rc-active-network synthesis. *Proceedings of IEEE*, 112(11):1838–1850, 1969.

[76] A. J. Fleming, S. Behrens, and S. O. R. Moheimani. Synthetic impedance for implementation of piezoelectric shunt-damping circuits. *Electronic letters*, 36(18):1525–1526, 2000.

[77] J. J. Hollkamp. Multimodal passive vibration suppression with piezoelectric materials and resonant shunts. *J Intel Mat Syst Str*, 5(1):49–57, Jan 1994.

[78] S. Y. Wu. Method for multiple mode piezoelectric shunting with single pzt transducer for vibration control. *J Intel Mat Syst Str*, 9(12):991–998, Jan 1998.

[79] S. Y. Wu. Method for multiple mode shunt damping of structural vibration using a single pzt transducer. *Proceedings of the SPIE - The International Society for Optical Engineering*, 3327:159–168, 1998.

[80] S. Behrens, S. O. R. Moheimani, and A. J. Fleming. Multiple mode current flowing passive piezoelectric shunt controller. *Journal of Sound and Vibration*, 266(5):929–942, 2003.

[81] S. O. R. Moheimani and A. J. Flemming. *Piezoelectric transducers for vibration control and damping*. Springer, 2006.

[82] J. Kim and J-K. Lee. Broadband transmission noise reduction of smart panels featuring piezoelectric shunt circuits and sound-absorbing materials. *Journal of the Acoustical Society of America*, 112(3):990–998, 2002.

[83] J. Kim and J. Kim. Multimode shunt damping of piezoelectric smart panel for noise reduction. *Journal of the Acoustical Society of America*, 116(2):942–948, 2004.

[84] M. B. Ozer and T. J. Royston. Passively minimizing structural sound radiation using shunted piezoelectric materials. *Journal of the Acoustical Society of America*, 114(4):1934–1946, 2003.

[85] J. Kim and Y-C. J. Broadband noise reduction of piezoelecetric smart panel featuring negative-capacitive-converter shunt circuit. *Journal of the Acoustical Society of America*, 120(4):2017–2025, 2006.

[86] M. Calmon, D. Guyomar, and R. Ohayon. Evaluation of an enhanced semi-passive technique for the reduction of structural noise and vibrations. *Smart Structures and Materials - Proceeding of SPIE*, 5386:381–392, 2004.

[87] M. Ahmadian and K. M. Jeric. On the application of shunted piezoceramics for increasing acoustic transmission loss in structures. *Journal of Sound and Vibration*, 243(2):347–359, 2001.

[88] M. A. Bassyiouni, B. Lester, B. Delon, S. Edmonds, S. Hoidra, and K. Wroblewski. Control of enclosed sound fields using shunted piezoelectric circuits. *Smart Structures and Materials - Proceeding of SPIE*, 6166, 2006.

[89] C. H. Nguyen and S. J. Pietrzko. Vibroacoustic fe analysis of an adaptive plate with pzt actuator/sensor pairs connected to a multiple-mode, electric shunt system. *Finite elements in analysis and design*, 43:1120–1134, 2007.

[90] D. L. Edberg and A. S. Bicos. Design and developmenet of passive and active damping concepts for adaptive space structures. In G. J. Knowles, editor, *Prceeding of the ADPA/AIAA/ASME/SPIE conference on active materials and adaptive structures*, 1992.

[91] H. Ghoneim. Application of the electromechanical surface damping to the vibration control of a cantilever plate. *Journal of Vibration and Acoustics*, 118:551–557, 1996.

[92] H. H. Law, P. L. Rossiter, G. P. Simon, and L. L. Koss. Characterization of mechanical vibration damping by piezoelectric materials. *Journal of Sound and Vibration*, 197(4):489–513, Jan 1996.

[93] D. A. Saravanos. Damped vibration of composite plates with passive piezoelectric-resistor elements. *Journal of Sound and Vibration*, 221(5):867–885, 1999.

[94] J. Becker, O. Fein, and M. Maess abd L. Gaul. Finite element-based analysis of shunted piezoelectric structures for vibration damping. *Computers and Structures*, 84:2340–2350, 2006.

[95] Y. Aoki, P. Gardonio, and S. J. Elliot. Modelling of a piezoceramic patch actuator fpr velocity feedback control. *Smart Materials and Structures*, 17(1):1–13, 2008.

[96] C. R. Fuller. Active control of sound transmission/radiation from elastic plates by vibration inputs: I. analysis. *Journal of Sound and Vibration*, 136(1):1–15, 1990.

[97] C. R. Fuller, C. A. Rogers, and H. H. Robertshaw. Control of sound radiation with active/adaptive structures. *Journal of Sound and Vibration*, 157(1):19–39, 1992.

[98] V. L. Metcalf, C. R. Fuller, R. J. Silcox, and D. E. Brown. Active control of sound transmission/radiation from elastic plates by vibration inputs: II. experiments. *Journal of Sound and Vibration*, 153(3):387–402, 1992.

[99] A. J. Fleming and S. O. R. Moheimani. Control orientated synthesis of high-performance piezoelectric shunt impedances for structural vibration control. *IEEE Transactions on control systems technology*, 13(1):98–112, 2005.

[100] Y. K. Kang, H. C. Park, J. Kim, and S-B. Choi. Interaction of active and passive vibration control of laminated composite beams with piezoceramic sensors/actuators. *Materials and Design*, 23:277–286, 2002.

[101] J. J. Hollkamp and T. F. Starchville. A self-tuning piezoelectric vibration absorber. *Journal of Intelligent Material Systems and Structures*, 5:559–566, 1994.

[102] O. Fein and L. Gaul. An adaptive shunted piezo approach to reduce structural vibrations. *Smart Structures and Materials - Proceeding of SPIE*, 5386:393–404, 2004.

[103] D. Niederberger, S. Behrens, A. J. Flemming, S. O. R. Moheimani, and M. Morari. Adaptive electromagnetic shunt damping. *IEEE/ASME Transactions on Mechatronics*, 11(1):103–108, 2006.

[104] S. Behrens, A. J. Fleming, and S. O. R. Moheimani. A broadband controller for shunt piezoelectric damping of structural vibration. *Smart Materials and Structures*, 12(18):18–28, 2003.

[105] S. Y. Wu. Broadband piezoelectric shunts for passive structural vibration control. *Smart Structures and Materials - Proceeding of SPIE*, 4331:251–261, 2001.

[106] M. Neubauer, R. Oleskiewicz, K. Popp, and T. Krzyzynski. Optimization of damping and absorbing performance of shunted piezo elements utilizing negative capacitance. *Journal of Sound and Vibration*, 298:84–107, 2006.

[107] K. Adachi, Y. Awakura, and T. Iwatsubo. Hybrid piezoelectric damping for structural vibration supression. *Journal of Intelligent Material Systems and Structures*, 15:795–801, 2004.

[108] G. S. Agnes. Development of a modal model for simultaneous active and passive piezoelectric vibration suppresion. *Journal of Intelligent Material Systems and Structures*, 6, 1995.

[109] M. S. Tsai and K. W. Wang. On the structural damping characteristics of active piezoelectric actuators with passive shunt. *Journal of Sound and Vibration*, 221(1):1–22, 1999.

[110] J. Tang and K. W. Wang. Active-passive hybrid piezoelectric networks for vibration control: comparisons and improvement. *Smart Materials and Structures*, 10:794–806, 2001.

[111] M. B. Ozer and T. J. Royston. Optimal passive and hybrid control of vibration and sound radiation from linear and nonlinear pzt-based smart structures. *Smart Structures and Materials - Proceeding of SPIE*, 4693:69–80, 2002.

[112] A. J. Fleming and S. O. R. Moheimani. Synthesis of optimal piezoelectric shunt impedances for structural vibration control. *Smart Structures and Materials - Proceeding of SPIE*, 5386:516–527, 2004.

[113] E. F. Crawley and J. de Luis. Use of piezoelectric actuators as elements of intelligent structures. *American Institue of Aeronautics and Astronautics Journal*, 25:1373–1385, 1987.

[114] E. K. Dimitriadis, C. R. Fuller, and C. A. Rogers. Piezoelectric actuators for distributed vibration excitation of thin plates. *Journal of Vibration and Acoustics*, 113:100–107, 1991.

[115] J. Tang and K. W. Wang. High authority and nonlinearity issues in active-passive hybrid piezoelectric networks for structural damping. *J Intel Mat Syst Str*, 11(8):581–591, Jan 2000.

[116] T. J. Royston and B. H. Houston. Modeling and measurement of nonlinear dynamic behavior in piezoelectric ceramics with application to 1-3 composites. *Journal of the Acoustical Society of America*, 104(5):2814–2827, 1998.

[117] J. A. Main and E. Garcia. Design impact of piezoelectric actuator nonlinearities. *Journal of Guidance, Control and Dynamics*, 20(2):327–332, 1997.

[118] A. J. Fleming and S. O. R. Moheimani. Improved current and chrage amplifiers for driving piezoelectric loads, ans issues in signal processing desugn for synthesis of shunt damping circuits. *Journal of Intelligent Material Systems and Structures*, 15:77–92, 2004.

[119] P.A. Nelson and S.J. Elliot. *Active Control of Sound*. Academic Press Limited, 1992.

[120] M. J. Balas. Feedback control of flexible systems. *IEEE Transactions on Automatic Control*, AC-23(4):673–679, 1978.

[121] M. J. Balas. Modal control of certain flexible dunamic systems. *SIAM Journal on Control and Optimization*, 16(3):450–462, 1978.

[122] T. Luft, S. Ringwelski, U. Gabbert, W. Henze, and H. Tschöke. Active noise and vibration control of a stripped car engine using different piezoelectric actuators. In *Proceedings of the Internoise, Lisbon*, 2010.

[123] O. Heintze and M. Rose. Active structural acoustic control for a truck oil pan: Actiator placemnet and efficiency estimation. *Noise Control Engineering Journal*, 58(3):291–301, 2010.